ISSN 2074-272X

науково-практичний журнал 2016/3

Електротехніка і Електромеханіка

Електротехніка. Визначні події. Славетні імена

Електричні машини та апарати

Електротехнічні комплекси та системи. Силова електроніка

Техніка сильних електричних та магнітних полів. Кабельна техніка

Електричні станції, мережі і системи

Ювілеї

За 2014р. журнал отримав індекс 79,35 від міжнародної наукометричної бази Index Copernicus

«ELECTRICAL ENGINEERING & ELECTROMECHANICS»

SCIENTIFIC & PRACTICAL JOURNAL

Journal was founded in 2002 by

National Technical University «Kharkiv Polytechnic Institute»

Co-Founder – State Institution «Institute of Technical Problems of Magnetism of the NAS of Ukraine»

Адреса редакції / Editorial office address:
Кафедра "Електричні апарати", НТУ "ХПІ", вул. Кирпичова, 21, м. Харків, 61002, Україна
Dept. of Electrical Apparatus, NTU "KhPI", Kyrpychova Str., 21, Kharkiv, 61002, Ukraine
тел. / phone: +380 57 7076281, +380 67 3594696, e-mail: a.m.grechko@gmail.com (**Гречко Олександр Михайлович / Grechko O.M.)**

ISSN (print) 2074-272X
ISSN (online) 2309-3404

Printed 27.06.2016. Format 60 x 90 ⅛. Paper – offset. Laser printing.
Edition 200 copies. Order no.66/172-03-2016.
Design of cover by Vyrovets L.P. e-mail: vsv_2007@ukr.net
Printed by Printing house «Madrid Ltd» (11, Maksymilianivska Str., Kharkiv, 61024, Ukraine)

ELECTRICAL ENGINEERING & ELECTROMECHANICS

Scientific and practical journal

2016/3

TABLE OF CONTENTS

Electrical Engineering. Great Events. Famous Names

Electrical Machines and Apparatus

Electrotechnical complexes and systems. Power Electronics

High Electric and Magnetic Field Engineering. Cable Engineering

Power Stations, Grids and Systems

UDC 621.3:537.311:910.4 **doi: 10.20998/2074-272X.2016.3.01**

M.I. Baranov

AN ANTHOLOGY OF THE DISTINGUISHED ACHIEVEMENTS IN SCIENCE AND TECHNIQUE. PART 32: ALTERNATIVE ENERGY: STATE AND PROSPECTS OF DEVELOPMENT

Purpose. Implementation of brief analytical review of the state and prospect of development in the modern world of alternative energy, including wind energy, sun energy, geothermal energy, biogas energy, flood-tide water energy, hydrogen energy and small water energy. Methodology. Scientific methods of collection, analysis and analytical treatment of scientific and technical information in area of the present state of world energy and ways of its further development. Results. A brief scientific and technical review is resulted about the state and prospects of world development of basic types of alternative energy. It is shown that, in spite of comparatively small stake (to 10 %) of this untraditional energy in general world balance of making of electric power, world association taking into account the necessary changing in the nearest 50 years of present oil-gas «foundation» of energy on other with large raw material, potential and ecological possibilities are forced to invest large financial means in development of the indicated directions of alternative energy. Originality. First on the basis of materials of separate magazine publications, scientific monographs and internet-reports on power problem the brief analytical review of the state and prospects of world development of basic types of alternative energy is executed. Practical value. Deepening and spread of the scientific and technical learnings in area of functioning and ways of development of modern energy. Scientific popularization of arising up before society claimed tasks from global and important for all of humanity of power problem. References 30, figures 28.

Key words: **alternative energy, state and prospects of world development, review.**

Приведен краткий научно-аналитический обзор о состоянии и перспективах мирового развития альтернативной энергетики, включающей ветроэнергетику, солнечную энергетику, геотермальную энергетику, биогазовую энергетику, приливную гидроэнергетику, водородную энергетику и малую гидроэнергетику. Библ. 30, рис. 28.

Ключевые слова: **альтернативная энергетика, состояние и перспективы мирового развития, обзор.**

Introduction. Energy, as we know, is that one of the main industrial sectors of the economy of any country in the world, in terms of development and the potential for that in a society is judged on the economic strength (power) of the country. Despite the continued leadership is currently in the global production of electric and thermal energy of its traditional high-power sources such as thermal, nuclear and hydroelectric power plants in recent years in the industrialized countries of the world their «momentum» is gaining ***alternative energy*** based on renewable energy sources of relatively small power [1]. These promising renewable energy sources should be classified based primarily on the use of [1-8]: wind energy, solar energy, heat of the Earth's core, biogas energy from waste, the potential energy of the water with the installed capacity of hydroelectric power plants (HPP) to (5-30) MW and energy from the use of hydrogen. Alternative energy, unlike traditional energy has almost unlimited source of raw materials and the potential for humanity. In addition, its practical use does not lead to negative environmental consequences for the nature around us. Given the urgency and the importance of energy issues for humanity, undeniable scientific and technical interest is the analytical summary of the latest achievements of scientists and experts around the world in addressing the urgent applications in the field of alternative energy.

Wind power. This type of alternative energy has become today one of the major scientific and technical «locomotives» in the promotion of renewable energy in the global energy market [2]. ***Wind power*** is that alternative energy industry, which specializes in the transformation of the kinetic energy of air masses moving in the lower layers of the Earth's atmosphere, in the electrical, mechanical, thermal, or other form of energy [2]. Wind energy is currently booming worldwide technical industry. So, in 2014 the amount of electrical energy that is produced by all wind turbines of the world amounted to 706 TW·hour (about 3 % of the produced electricity humanity annual volume) [2]. In 2014, 85 countries used wind energy on a commercial basis. It should be noted that some countries especially intensively develop wind power. For example, Denmark in 2014 with the help of wind turbines (if 4845 MW installed capacity) worked out to 39 % of its annual volume of electricity production [2]. According to the European Wind Energy Association Germany in 2005 it had an installed capacity of wind turbines (windmills) in the amount of 18 428 MW. In 2014, this installed capacity of wind turbines in Germany was already 34 250 MW [2]. As for Ukraine, then in 2005 the installed capacity of its wind turbine was 77 MW, and in 2014 – 498 MW [2]. For comparison, the Russian Federation (RF) has an installed capacity of its wind turbines of 14 MW in 2005, and in 2009 – 18 MW [2]. We mention the fact that in 2010 up to 44 % of all wind power plants constructed in the world were concentrated in Europe, in Asia – 31 %, and in North America – 22 % (the remaining 3 % were all other continental part of the globe) [2]. According to statistics from the World Wind Energy Council the total installed capacity of wind power plants on the planet at the beginning of 2011 was about 238 GW (the end of 2011 it increased by about 25 %) [2]. The development of wind energy on the planet in the 21st century is the exponential growth rate. And so that every three years, the total installed capacity of wind power plants of the world doubled [9]. On the «face» of scientific, technical and commercial interests of society in the development and implementation in practice of wind power.

1.1. Types and design of wind turbines. Wind power and wind turbines used in it are, in fact, the techni-

cal embodiment of a relatively new power generation technology. The main directions of development of modern wind power is autonomous, or «small» wind energy, based on the use of single wind turbine, and a centralized or «big» wind power, which is based on the use of wind power plants (WPP) [9]. The position of the rotor axis wind turbines are divided into horizontal-axis and vertical-axis [9]. Fig. 1 shows the appearance of the «farm» of modern horizontal-axis wind turbine installed capacity of up to 250 kW, erected under field conditions in the coastal zone of the Russian Federation west [10]. Note that in the Russian Federation is the largest windfarm station «Zelenograd» installed capacity of 5.1 MW (Kaliningrad region), Consisting of 21 wind turbines of the Danish company «SEAS Energi Service A.S.» [2]. Fig. 2 schematically shows the arrangement of modern wind turbines horizontal axis performance, as shown in Fig. 3 – a general view of a modern wind turbine vertical axis performance [11].

Fig. 1. General view of modern horizontal-axis three-bladed wind turbines installed, located on the flat coastal area up to 250 kW [10]

From the data (Fig. 2) it is shown that the main components of the wind turbine of this type is the actual wind turbine (*turbine*) and *tower* on which this wind turbine is located. Wind turbine contains a complex of structures and mechanisms.

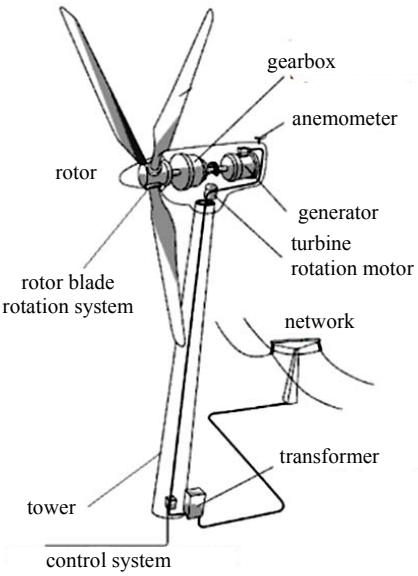

Fig. 2. A schematic design of the modern WPP [9, 10]

Shown in Fig. 2 components and machinery of wind turbines required for its effective work in industrial production of electricity from wind energy and its subsequent transfer to the grid. *Turbine* of the WPP consists of the *rotor* and *housing* in which there are (see Fig. 2): *anemometer*; *gearbox*; *generator*; *frequency converter*; *pitch system* and *yaw motor and yaw system*; *cooling system*; *control system* and *safety system* [9, 10]. *Transformer* can be placed directly near the foot of the *tower* of the WPP.

Fig. 3. General view of the Scottish vertical-axis wind turbines a twin sea-based with a helipad in the area of wind turbine capacity of up to 6000 kW [11]

Fig. 4-6 in an enlarged view show a giant turbine blades and modern three-blade horizontal axis wind turbine installed capacity of up to 1500 kW at holding them costly repair work [9, 11].

Fig. 4. The enlarged view of the turbine of modern horizontal-axis three-bladed wind turbines *NORDEX* marks the installed capacity of up to 1500 kW land-based during its maintenance at a height of about 70 m [11]

Fig. 5. A rare photo of the moment of service at altitude of about 70 meters and the turbine rotor blades of modern land-based horizontal-axis three-bladed wind turbine installed capacity of up to 1500 kW [11]

Fig. 6. Moment of involving maintenance of the helicopter crew at a height of 80 m land-based Norwegian horizontal axis three-bladed wind turbine with the largest installed capacity of up to 5000 kW [11]

All modern wind turbines on the nature of its placement of wind turbines are divided into land (see Fig. 1, 4-6) and the sea (Fig. 3, 7) based [9, 11].

Fig. 7. Moment of preparation for assembly work on the modern sea-based three-bladed horizontal axis wind turbine installed capacity of up to 600 kW [11]

1.2. Technical characteristics of the wind turbine and the economic aspects of wind energy. The amount of electricity generated by wind turbines depends significantly on wind speed. Wind turbine begins to produce electricity at a wind speed of 3 m/s and is automatically disabled when the wind speed exceeding 25 m/s [2]. It was found that the air flows from the earth's surface (sea) are substantially laminar – their underlying atmospheric layers situated above the brake [2]. This physical effect in the Earth's atmosphere is markedly reduced at altitudes of 100 m and more. So powerful modern wind turbines have a tower height of not less than 70 m.

Maximum power of wind turbines reached at a wind speed of 15 m/s [2]. From the available data suggest that the modern large wind turbines of 2 MW power is characterized by [2]: the height of the tower – 70 m; the blade length – 37 m; the weight of the turbine rotor – 52 m; the weight of the engine room – 82 m Today wind turbines with turbine brand *V90* of 3 MW power of the Danish company «Vestas» has the full height – 115 m, tower height – 70 m, and the blade diameter – 90 m [9].

Fig. 8 shows the appearance of the blades, designed for use in a wind turbine.

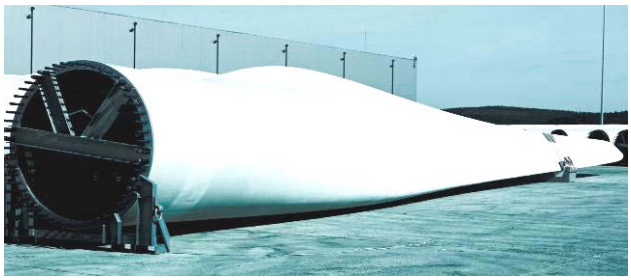

Fig. 8. Enlarged image of a single blade of the length of 40 m of modern horizontal-axis wind turbine, located on the plant site of the finished product [2, 11]

We point out that in 2009, the modern turbine wind turbine class (1.5-2.5) MW took up 82 % of the global «big» wind energy [2]. In addition, we note that the beginning of 2015 the total installed capacity of all wind turbines producing electricity around the world amounted to 369 GW [2]. The average increase in the amount of wind power world, since 2009, up to 40 GW per year. It is caused, first of all, the rapid development of the «big» wind power in the United States, India, China and Germany [2]. In wind power industry to 400 thousand people were employed in 2008 across the globe [2]. The cost price of electricity produced on a commercial scale wind turbines, to a large extent it depends on the wind speed. Thus, at a wind speed of 8 m/s, it is about 3.6 cents/(kW·h) [2]. As for the cost of construction of large wind turbines, it is, for example, for prototype, shown in Fig. 6 and erected recently in Norway, 67.5 mln US dollars [11]. This shows that the wind turbine is an expensive technique. The costs for its purchase pay off for the first 7 years of operation (with an estimated useful life of 25 years) [9, 11].

1.3. Disadvantages and problems of wind energy. The issue before us is a kind of alternative energy unregulated source of energy. Electricity generation by means of wind turbines depends significantly on this feature more

variability of natural factors as wind speed. It is believed that the construction of WPP advantageous in regions where the average annual wind speed is not less than (5-6) m/s [1]. Therefore, for a large windfarm characteristic uneven granting power to the grid. In this context, wind power requires a certain amount of power backup in appropriate energy systems. This feature greatly increases the cost of the wind turbines received from them electricity. Sometimes it came to the fact that the power system with great reluctance was connected wind turbines to the grid. In this connection, in some countries there are even special laws that require the power system controllers to perform data connection turbine [2]. Practice has shown that the problems in electric power systems and control due to the instability of wind turbines work begins after the proportion of them in the (20-25) % of the total installed capacity of the system [2]. As for the small wind turbine power unit (in the case of «small» wind energy), they may also have problems with the network infrastructure. This is due to fact that the cost of power lines and switchgear for their connection to the grid may be too large. Large wind turbines for power are experiencing significant problems with a repair, since the replacement of major parts (blades, rotor, etc.). At an altitude of about 100 m is a complex and expensive undertaking.

Certain disadvantages of this type of alternative energy are also generated by the rotating blades buzz around working windmills (because of his exclusion zone around large wind turbines is at a radius of at least 300 m), low-frequency vibration of the ground in the area of accommodation powerful wind turbine and technical difficulties resulting at the lightning protection of bulky turbines and wind turbine blades [2, 9]. Recently, experts have begun to pay attention to the deterioration of the television communication in the areas where wind farms [2, 9].

1.4. Wind power in Ukraine. Modern engineering of Ukraine, although slow, but progressive way, moving towards the development of clean energy based on alternative and renewable energy sources. Government programs we create favorable conditions for the development of new energy technologies, including wind power and. Fig. 9 shows a map of Ukraine coated with a zone average annual wind speeds. From the data in Fig. 9 and set forth in subsection 1.3 the information that the most rational areas of the construction of wind power plants are the Carpathians and all the Black Sea coast in Ukraine, where the average wind speed reaches values of 5 m/s or more [2, 9]. The largest wind farm in Ukraine is the station «Novoazovsk» with an installed capacity up to 23 MW (Donetsk region) [2, 9].

Fig. 9. Map of Ukraine with areas of average wind speeds [2]

Wind power in recent years has become one of the most popular sources of alternative energy. For all its faults, wind energy is an environmentally friendly way to generate energy. Therefore, in modern society it has received increased attention from both government institutions and civil society organizations. In conclusion, it should be noted that the share of wind power in Ukraine's energy system can be significantly increased due to the practical realization of large-scale national events in the field of energy efficiency.

2. Solar energy. This type of energy is one of the promising areas of renewable energy, based on the direct use of solar radiation for energy with its help in the form of electricity or thermal energy [3]. It is believed that this ***solar energy*** can be a real «successor» in the traditional energy, capable to pick up her baton in providing mankind with energy [12]. Modern course of development of our civilization requires people to take control of the flow of solar energy, while maintaining the unique climate of the Earth. It is known that at the inlet of the Earth's atmosphere solar radiation power density numerically averages 1367 W/m^2 [3]. It is necessary to remind the reader that this value is the solar constant [13]. After reaching the surface of the earth, this value is due to the absorption and scattering of atoms (molecules) of atmospheric gases, aerosols, water droplets and ice crystals is reduced and at the equator is already about 1020 W/m^2 [3]. At present, there are two basic physical and technical ways to use the energy of solar radiation [12]: the first – the *photoelectric* providing direct generating electricity using photovoltaic cells (PVC), irradiated by this radiation; second – *photothermal* providing receiving thermal energy by heating of liquid coolant under consideration radiation. As part of this review will focus in more detail on the first method, the practical application of solar radiation. As for the second method of converting solar radiation energy, it coolant (usually water) is heated in the reservoir (light absorbing pipe system) is installed on the roof of the building (Fig. 10) to a sufficiently high temperature (90 °C) and used further for space heating.

Fig. 10. General view of the solar collector at the photometric method of using the light flux of energy [3]

2.1. Brief fundamentals of physics of photovoltaic cells. As a basis of PVC monocrystalline silicon can be used with other additives in it chemical elements forming the structure of this material with *p-n*-junction [3]. The principle of operation of the semiconductor silicon PVC (Fig. 11) taking into account the physical positions adopted at today, set forth in [13], is as follows. It creates a «hole» in the *p*-layer of the semiconductor (positive) conductivity and *n*-layer – electron (negative). On the border of these layers there is a potential barrier to the movement of charge carriers (electrons and «holes») of a semiconductor layer to another. Therefore, prior to exposure to solar PVC (photon flux) in said semiconductor electric current will be omitted. If you fall on the same PVC flow of photons (quanta of electromagnetic energy) due to the absorption of these quasiparticles are created pairs electron-«hole». These couples will approach the boundary of these layers and reduce the potential (energy) barrier between the p and the n-semiconductor layers. Thus, in a semiconductor for its charge carriers (electrons and «holes») will be created conditions for their unimpeded passage from layer to layer. As a result, the semiconductor will occur in the induced electromotive force (EMF) and the semiconductor will become a source of electric current. You can say that the ability to produce electricity occurs in the semiconductor due to its special chemical structure on the subatomic level, and create in it an internal electric field under the influence of external energy to the structure of the electromagnetic quanta of light. The value of the photo-EMF in a semiconductor will be greater than would be the light intensity or the photon flux [13].

2.2. Types of photovoltaic cells. At present, the technology of photovoltaic cells to distinguish between the following three generations of PVC [3]: *the first generation* – crystalline, including monocrystalline silicon, polycrystalline (multicrystalline) silicon and thin-film polysilicon elements; *the second generation* – thin film, microcrystalline, nanocrystalline, based on cadmium telluride and copper-based diselenide-indium-gallium elements; *the third generation* – photosensibilised by dye organic (polymeric), inorganic and based on cascade structures elements. It should be pointed out that all these PVC inherently contain a *p-n*-junction [3].

It is interesting for the curious reader the information that is related to the physical and technical features obtaining *p-n*-junction to a single-crystal silicon PVC, shown in Fig. 11. According to the scheme of construction of the PVC monocrystalline silicon, has historically dominated the initial phase of production in the world of PVC (up to 90 % of market volume), in the form of a thin plate is placed on top of the metal base (lower base contact). Both end faces of the semiconductor plate of silicon filler is to change its conductivity. On one side of this plate is doped (enriched) to create electrons in the *n*-semiconductor transition layer to the silicon by adding a chemical element with a higher number of valence electrons (typically phosphorus), and on the other opposite side of the chemical element is doped with a small amount of stretching electrons (typically boron) for the creation in the semiconductor junction layer *p* [14, 15]. As a result of the single-crystal silicon doping in it and you want us to create a *p-n*-junction. Then a modified semiconductor with a *p-n*-junction fits very thin metal mesh (upper contact) and applied to the top antireflection coating (see Fig. 11). After joining the lower and upper metallic contacts on the external electric circuit PVC is ready to receive the light flux and development by manifesting it in the *photovoltaic effect* [13, 16] at its *p-n*-junction photo-EMF.

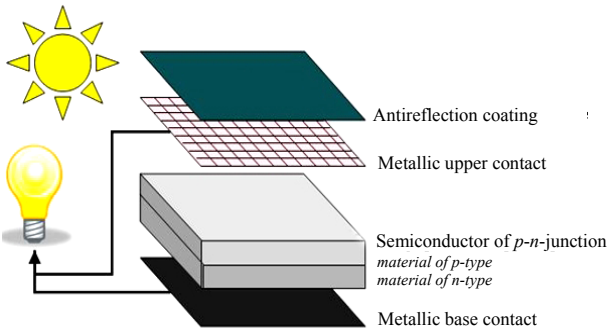

Fig. 11. Schematic representation of the first generation PVC with *p-n*-junction formed by the silicon single crystal doped with other chemical elements [3]

We should also note that in recent years there has been some progress in the creation of PVC on the basis of optical nanoantenna directly transform the electromagnetic energy of light radiation into electric current [3, 17]. The prospect nanoantenna due to their high theoretical efficiency, reaching up to 85 %, and potentially lower cost. Thus, under the PVC efficiency to be understood a parameter that indicates what portion of the electromagnetic energy of the luminous flux at the level of its working atomic structure of semiconductor material is converted into electrical energy. In the first half of the 20th century, the efficiency for sulfur-thallium PVC is less than 1 % [3]. For today's silicon PVC and manufactured based on gallium arsenide, and their efficiency reaches (10-20) % [15]. Great scientific and technical achievement was the development of the semiconductor industry and the creation of PVC silicon with an efficiency of up to 40 %. An important area in the global solar energy is to provide cheap and convenient photoelectric converters formed on the tape-based polycrystalline silicon struc-

tures, thin films of amorphous silicon and other semiconductor materials. Of the new semiconductor structures of the most high for use in the PVC structure was «aluminum-gallium-arsenic», industrial and commercial development of which has just begun in the solar technology market [15]. Great promise in the field of solar energy is open heterostructure (heterogeneous structure) semiconductors composed of a number of different chemical composition of semiconductors [15]. In practice, it turned out that when they are used as part of PVC they are twice as efficient as today's silicon semiconductors. Note that for scientific discovery, research and implementation in the area of solar energy, as well as in laser technology similar semiconductor heterostructures our countryman, Academician of the Russian Academy of Sciences, Director of the Leningrad Physico-Technical Institute of the Russian Academy of Sciences, Professor J.I. Alferov was awarded the Nobel Prize in Physics for 2000 [3, 15].

2.3. Methods for the technical implementation of photovoltaic cells. Single PVC, made on the basis of traditional crystalline silicon semiconductor, capable of producing a constant voltage is relatively small values (up to 0.5 V). [15] In practice, therefore collected in individual PVC modules, and a number of modules – a panel (battery), the output voltage from the nominal constant which may be 12, 24 and 48 V [3]. Solar cells can be performed as a rigidly fixed on the fixed base (Fig. 12) and mobile location tracking of the sun horizon (Fig. 13). Due to the fact that, as used in domestic and industrial consumers of electricity are adapted to supply a single-phase AC voltage a nominal level of 220 V or three-phase alternating voltage network a nominal level of 380 V, then the actual use of solar cells between them and the power consumer should be placed *inverter* – electrical device that converts DC voltage from our solar source to the corresponding alternating voltage. It is obvious that during daylight hours the solar panel will operate and generate electricity, and in the dark – «rest» [12].

Fig. 12. External view of a rigidly fixed small solar panel mounted on the roof of the house [15]

Since electric power supply to the consumer requires room, the solar electric system is necessary to introduce a powerful storage device of electric power – the battery [12].

Fig. 13. External view of a small mobile solar panel with a tracking system (rotation) «following the Sun» [15]

Charge of the batteries of solar panels requires compliance with a certain algorithm. Therefore a special electronic device – a *controller* (Fig. 14). [3, 12] is used for process control battery charging from PVC.

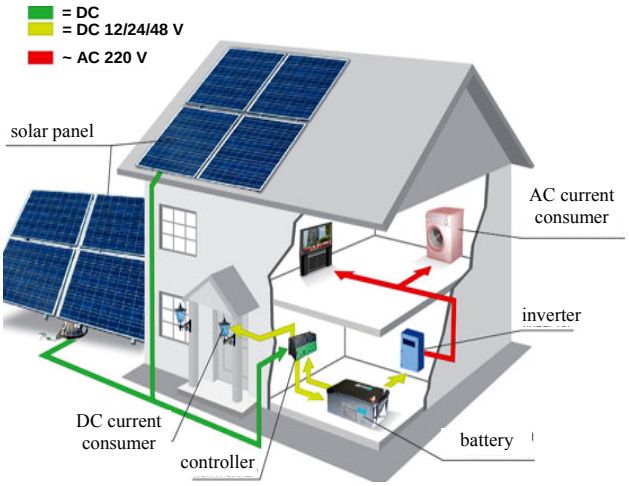

Fig. 14. Typical wiring diagram of solar panels connection to the networks of direct and alternating currents of an apartment house [3]

Currently, service life of solar cells increased to 25 years [12]. Changing the power output of the solar cell is achieved by the addition or removal of its individual modules solar cell cost is now around US $ 1.5 per 1 watt of its installed capacity. [12] This value falls from year to year. Installation in Ukraine on the subject of «turnkey» solar panels is estimated at about 4.5 $/W [12].

2.4. Industrial applications of photovoltaic elements and the economic aspects of solar energy. For such use it is necessary to create a PVS solar power plant (SPP) for direct conversion of solar radiation into electrical energy [18]. Note that the first experimental SPP, applied truth photothermal method for converting solar radiation, was built in 1985 in the USSR (Schelkino, Crimea). Its peak installed capacity of about 5 MW [18]. By the way, I have the same power and the nuclear reactor at the world's first nuclear power plant (NPP), built in 1954 in the USSR (Obninsk, scientific leader – Academician of the Academy of Sciences of the USSR I.V. Kurchatov) and marked the beginning of the nuclear power industry [19]. Since the Crimean power system was deficient, in

this region, solar energy has received intensive development. With this alternative source of energy in 2014 is using SPP produces up to 30 % of the required volume of electricity [18]. It should be noted that at the end of 2010 this figure actually generated electricity for Crimea was only 7 %. Currently, in the Crimea, solar power «parks» is already about 227.3 MW [18]. The basis of solar power make up SPP Crimea «Okhotnikovo» installed capacity of 80 MW (Fig. 15) and SPP «Perovo» installed capacity of 100 MW (Fig. 16). Both of these SPP were built by the «Activ Solar» company [18]: Station «Okhotnikovo» in 2011 about 160 hectares and the station «Perovo» in 2012 to 200 hectares.

Fig. 15. General view of a fragment of the territory of SPP «Okhotnikovo» with installed power of 80 MW (Crimea) [18]

Solar batteries of the SPP «Okhotnikovo» consist of about 365 thousand units based on polycrystalline PVC and can produce up to 100 GW·h of electricity per year. This SPP meets the electricity needs of about 20000 households. Solar panels of the SPP «Perovo» consist of 455 thousand polycrystalline PVC modules connected by about 1500 km of cable [18].

Fig. 16. General view of a fragment of the territory of the SPP «Perovo» with installed power of 100 MW (Crimea) [18]

SPP «Perovo», which was as of June 2012, the most powerful solar power plant in the world, produces up to 132.5 GW·h of clean electricity per year. We mention the fact that on 1 August 2015, the Crimea was launched SPP «Nikolaevka» with an installed capacity of 70 MW, which is now running in test mode of operation [18].

Solar energy is actively developing in the world. The rate of growth simply amazing. So, if in 2005, PVC production in the world was approximately 1.65 GW, then in 2012, the total installed capacity of the world's solar power plants exceeded 100 GW [3, 18]. At the beginning of 2014, this photovoltaic power plant in the world was estimated to have 139 GW [18]. The leader in terms of installed capacity there are EU countries, which Germany has the highest rate of «per capita» of the population to produce electricity through the use of solar power capacity. In mid-2011, more than 100 thousand people were employed only in the photovoltaic industry in Germany. In addition, in 2011, about 3 % of electricity produced in Italy, was obtained by means of photovoltaic installations [18]. According to projections obtained through solar energy is theoretically able to provide up to 2050 (20-25) % of the needs of mankind in electricity. This will dramatically reduce emissions of carbon dioxide in Earth's atmosphere. Energy market experts believe that the percentage of the world needs to ensure by 2050 electricity produced in the SPP will rest on the question of the cost of 1 kW·h at solar installation solar power plants «turnkey». In 2013, the price of 1 kW·h, generated in the SPP in regions with lots of sunlight (for example, to Southern California in the United States), was about 10 cents. The cost of 1 kW·h of electricity generated by nuclear power plants currently cost about 15 cents [18]. The annual output of the world's electricity in the SES in 2014 amounted to 185.9 TW·h (about 0.79 % of its total volume produced per year), with an annual growth rate of 38 % [3]. As for the payback of funds invested in solar energy, then, for example, for the United States when the average solar radiation energy intensity 1,700 kW·h/m² per year energy payback of solar power plants with a polycrystalline silicon modules in their batteries with an efficiency of 12 % is about 4 years [3, 18].

2.5. Largest SPP in the world. We point out the largest of the existing solar power plants on the world:

- Solar plant «Million Solar Roofs» 1000 MW (1st turn – 2015, California, USA);
- Solar plant with installed capacity of 550 MW (Mojave, CA, USA);
- Solar plant with an installed capacity of 290 MW (2012, Caliente, Arizona, United States);
- Solar plant with installed capacity of 200 MW (Golmud, China);
- Solar plant with an installed capacity of 166 MW (Schipkau, Germany);
- Solar plant with an installed capacity of 145 MW (Neuhardenberg, Germany);
- Solar plant with an installed capacity of 100 MW (2012, Perovo Crimea);
- Solar plant with installed capacity of 80 MW (2011, Okhotnikovo, Crimea);
- Solar plant with installed capacity of 70 MW (2015, Nikolaevka, Crimea).

Note that the world's largest SPP above the Arctic Circle is a station with an installed capacity of 1 MW (Batagai, Yakutia, RF) [18]. Nevertheless, the RF falls far behind the level of electricity generation with the help of the SPP leading countries of the world. Just exotic looks SES entered into service in September 2010, 100 kW, in the Belgorod region (RF) [18]. In September 2014, it was put into trial operation of Kosh-Agach SPP 5 MW (Altai, Russia). In the nearest plans of the Russian Federation

appears to increase by 2020 the total volume of installed capacities of SPP to 1500 MW [18].

2.6. The use of photovoltaic cells in transport. PVC can be installed on various vehicles: boats, electric cars, trains, airplanes, etc. [3]. One of the possible use of solar options embodied in Fig. 17. In these cases, the PVC produce electricity, which is used for either the on-board power supply of the vehicle, or for electric motors [3, 12].

Fig. 17. Unmanned aircraft of the NASA «Pathfinder Helios» with PVC, mounted on its original wings [3]

In Japan and Italy already have railway trains defined on the roofs of their cars with solar panels, which generate electricity used to power the air conditioning, lighting and alarm systems [3]. Currently, the company «Solatec LLC» sells thin-film PVC of 0.6 mm thickness to install them on the roof of a hybrid car brand Toyota Prius. The aerodynamics of the car from the use of PVC is not broken. Obtained from the PVC electricity in this case goes to recharge car batteries, which increases its mileage by about 10 % [3]. In 2010, a manned aircraft «Solar Impulse» with the PVC stayed in the air for about a day, which gives us hope for the use of such devices as a technical supplement to the satellites [3].

2.7. The invention of heteroelectrics and new prospects for solar power. Recent scientific discoveries and inventions in the field of PV can make dramatic changes in the area of solar energy. Russian scientists have reported the discovery of a new class of solar cells – heteroelectrics and creation on their basis of a new generation of PVC, as well as their manufacture using high performance solar cell – «star battery» (Fig.18) [3, 15].

The main components of the «star battery» are heteroelectrical cell and the capacitor [15]. Heteroelectrical solar cell converts solar energy into electrical energy and stores it heteroelectrical capacitor. «Stellar battery» can function in the absence of sunlight, capturing only the infrared radiation at the same time their work. When converting visible light, its efficiency is about 54 %, and for converting the infrared radiation – approximately 31 % [15].

Fig. 18. External view of a revolutionary invention by scientists of the RF in the field of solar cells – «star battery» [15]

In the «star battery» photocurrent is four times higher than in the solar panel, and its mass per one watt of power generated almost 1000 times smaller. Note that set in «star battery» heteroelectrical capacitor has a small size and large capacitance. Thus, for a volume of only 180 cm^3 capacity heteroelectrical capacitor «star battery» is about 0.11 F [15]. Due to what has been achieved in a «star battery» such extraordinary results? In the authors' opinion that the invention of the Scientific Center of semiconductor products (RF) – by supercoherence phenomenon occurring in a semiconductor with a pre-entered it with nanoparticles of other chemical elements when exposed to external electromagnetic fields [15]. Due to the phenomenon supercoherence of heteroelectrics appears in a new physical property – the ability to unite on a single frequency electromagnetic waves of sunlight, which is known to be characterized by different frequencies and wavelengths, respectively [13]. Application of heteroelectrics («star batteries») in the solar power offers great prospects for the development of this type of alternative energy [3, 15].

3. Geothermal energy. This type of renewable energy is based on the temperature difference between the boiling liquid metal core of a diameter of up to 7,000 km with a temperature of about 5000 °C of the planet cooled and its solid surface [20, 21]. Ground water as a result of this difference caused by temperature thermal processes occurring in the solid Earth's crust to 100 km thick, heated to high temperatures. Sometimes these temperatures are substantially above its boiling temperature. It is believed that the temperature of the rocks and the water in the earth's crust, heated by magma Earth rarely exceed 370 °C [20]. Only in some areas of the globe temperature of groundwater is sufficient to generate electricity with it. These areas are typically in areas of tectonic plates fault solid crust. Therefore, the practical use and the active development of geothermal energy should be expected in areas with low-lying geothermal resources of our planet are concentrated primarily in Iceland,

the RF (Kamchatka) and the US (California) [4]. Of deep geothermal resources of the earth because of the high cost in this exploratory geological and scouting and drilling operations are not suitable [4] for the purposes under consideration.

3.1. The main uses of heat of the Earth's core. By way of the use of geothermal energy are following two main technologies [20]: *the first* – its direct use in which emerging from the depths of the Earth's surface hot water and steam are used in building heating systems, horticultural and industrial processes; *the second* – production with the help of electricity, in which is used to drive geothermal steam turbine rotor movement of heat from the Earth's core. Fig. 19 shows a diagram of a first method of using geothermal heat [4].

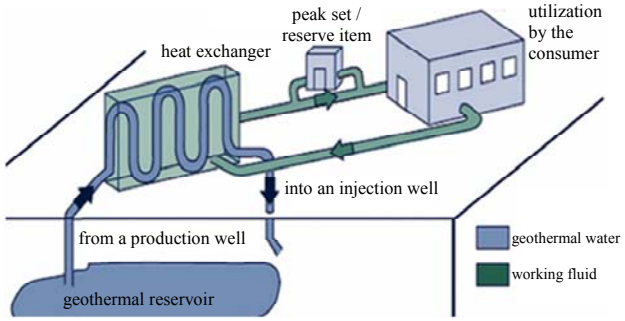

Fig. 19. Schematic representation of a first method of using geothermal heat for heating buildings [4]

In modern systems, the direct use of heat in the reporting discovered and surveyed experts geothermal reservoir well is drilled to provide a constant stream of ground-based devices with his hot water (see Fig. 18). In the case where the geothermal well is not a closed vessel for artesian groundwater under high positive pressure, the downhole pump is used. In geothermal wells depths than 250 m submersible pumps are used for applying hot water in a geothermal heat exchanger and further into the injection well. Heated in the heat exchanger working fluid is supplied for space heating.

Fig. 20 shows a possible diagram of a second method of using geothermal heat. In this case, raised from the depths of the special heat-resistant pipes is two-phase mixture (water and steam) is fed into a separator (see Fig. 19), from which selected the superheated steam is sent to a steam turbine blades, turbine generator rotor is rotating.

After hot geothermal water separator, and condensed in the condenser steam turbine by injection wells are sent back to the earth. Currently, there are two basic types of geothermal energy technologies [20]: *the first type* – «instant steam»; *the second type* – «dry steam». Fig. 20 illustrates a first type of technology that uses a pressurized flowing from a geothermal well with hot water temperatures above 180 °C. In this case, due to the pressure drop in the geothermal water raised partial boiling occurs and its formation in the separator «instantaneous steam», directed to the turbine. Geothermal power plants (GTPP), using the second type of technology, work on underground resources «dry steam» [20]. Since deposits of subterranean reservoirs «dry steam» hard to find, the GTPP operate typically in the «instantaneous steam» technology [4, 20].

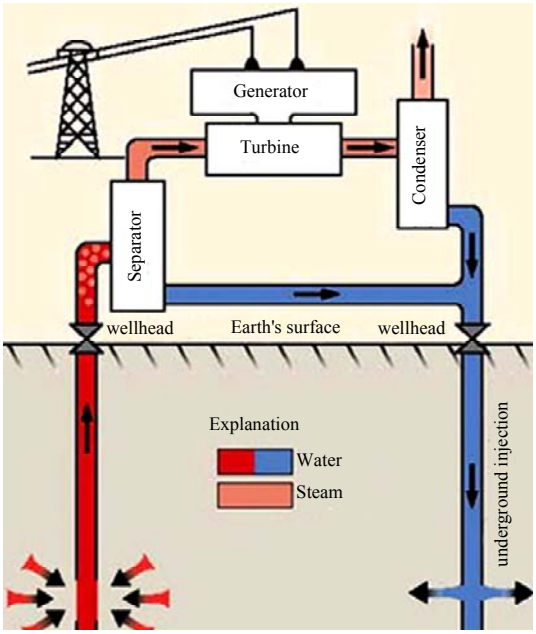

Fig. 20. Schematic representation of the second method of geothermal heat utilization, intended for electrical energy generation [4]

3.2. Industrial use of geothermal energy. Implemented by such use of geothermal heat using GTPP. The world's first GTPP with installed power of 7.5 MW was built in Italy in 1911 [22]. Today, the world leader in the number of GTPP (77 plants) and the volume of electricity produced by them takes the United States. Installed US GTPPs' power in 2010 was about 3,100 MW [22]. Produced in the United States at its GTPP electricity was in 2010, more than 40 % of all such powers of the then world [22]. The share of electricity generated by GTPP for the period amounted to the total electricity production is only 0.3 % in the US [22]. Most geothermal energy «per capita» of the population is now produced in Iceland, where about 95 % of homes are heated by geothermal energy [4]. According to [20] in Iceland currently up to 60 % of the total consumed energy is taken from the earth. The world practice of industrial use of geothermal heat shows that the most effective ones are characterized by GTPP in which the depth of water intake temperature of geothermal wells is not less than 250 °C [23]. Fig. 21 is a perspective view of a modern GTPP, built in Iceland [22].

Fig. 22 is a general view of the largest to date in the Russian object of geothermal energy – Mutnovskaya GTPP of power of 50 MW (Kamchatka), launched into operation in 2002 [22]. Annual electricity production of the gas turbine power plant as of 2010 amounted to 360.5 million KW·h [4]. Currently, it is working on the modernization of GTPP and increasing its capacity to 80 MW.

Fig. 21. External view of modern GTPP with installed power of 100 MW (2001, Nesyavellir, Iceland) [22]

Fig. 22. External view of Mutnovskaya GTPP with installed power of 50 MW (2002, Kamchatka, RF) [22]

Note that at the beginning of 2009, the total capacity of GTPP in the world has increased to 10.5 GW [22]. For comparison, at the beginning of 2000, a similar figure was around 6 GW. There is a clear trend in the annual growth of installed GTPPs' power worldwide to 500 MW. The main advantage of geothermal energy is a practical inexhaustibility of its underground resources and total independence from environmental conditions, time of day and year. According to estimates of geoscientists cooling rate of the Earth's core is about (300-350) °C per billion years [22]. Promising sources of superheated geothermal waters have many volcanic zones of the Earth, including Kamchatka, Kuril, Japanese and Philippine Islands, as well as the Caucasus, the New Zealand territory of the Cordillera of the Andes and in North and South America [4]. One of the disadvantages we have considered the type of alternative energy is still relatively high cost generated by a gas turbine power plant of 1 kW·h of electricity. It is now comparable to that of thermal power plants (TPP), which in Russian conditions on the production cost of TPP electricity is up to 1 RUB/(kW·h), but is 10 times higher than the cost of electricity production at hydropower plants. For the record, we note that the cost of this hydroelectric power station in Russia up to 10 kopecks/(kW·h) [20].

4. Biogas energy. The global renewable energy market is growing rapidly, according to expert estimates [1, 5]. ***Biogas energy***, as a small sector of the energy market, and biogas plants (BGP) are currently the typical elements of modern waste-free production in many areas of agriculture and food industry. The end product in the BGP output (Fig. 23) is a biogas, containing in its composition of approximately 60 % methane [5].

Fig. 23. General view of modern biogas plant [5]

The raw material for producing biogas in the BGP is liquid and solid manure from cattle, pigs and poultry. In addition, BGP can run on waste food production enterprises and specially grown energy crops (e.g. grass, corn and sunflower), increasing their output of biogas. On modern BGU from one ton of cattle manure get to (30-50) m^3 of biogas [5]. By the way, one cow can provide to obtain 2.5 m^3 of biogas per day. Resulting in the BGU biogas can then be used for the production of electricity using gas turbines and biofuels to fuel cars. In Sweden and Switzerland, biomethane has long been used in urban buses and trucks [5]. From one m^3 of biogas can produce about 2 kW·h of electricity [5]. Note that currently in Germany have been built around 4200 BGU, using biogas to produce about 13,000 GW·h of electricity per year [5]. The future plans of Germany shows an increase by 2020 the number of highly BSU new generation of up to 12 thousand, capable of an annual output of green electricity to 39,000 GW·h [5].

5. Tidal hydropower. Today we are well aware that the grand phenomenon in our nature, connected with the rhythmic for terrestrial days the movement of sea and ocean waters as the tides, contribute to the gravity of the Sun and Moon [13, 19]. Twice a day the sun and moon gravity force of his force to attack the seawater to the shore, then move away from him backwards. This phenomenon is known to people since ancient times, but use it to produce electricity mankind learned only recently. That ***tidal hydropower*** for the implementation of the physical and technical goals and aims. In practice, this aim is embodied by tidal power plants (TPP), the principle of which is illustrated in Fig. 24 [6].

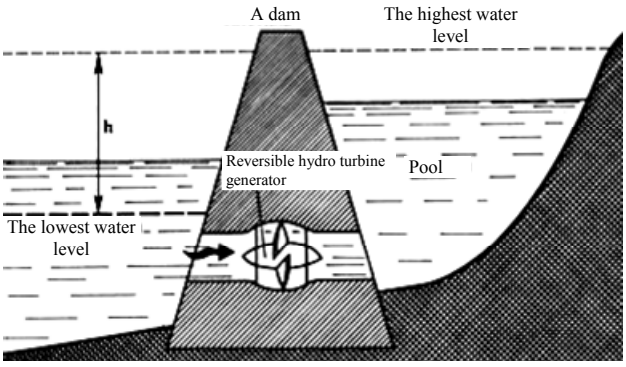

Fig. 24. Scheme for explaining the operation of a modern TPP [6]

TPP's mode usually consists of several process cycles. *The first cycle* – a period of high tide, when the sea water coming from the pool fills the TPP (see Fig. 24). During this period, the movement «coming» to the bank

and, accordingly, the dam water TPP rotates installed at the base of the concrete dam wheel capsule units and power plant generates an alternating electric current. *The second cycle* – during low tide, when the sea water «retreat» from the shore, and, respectively, from the TPP dam. The difference in water levels in the basin filled with TPP at high tide and in the «retreat» at low tide the sea can be up to h $h \approx 19$ m [6]. During low tide, the water leaving the TPP pool in the sea (ocean), again rotating impeller hydro turbine generators, but now only in the opposite direction. And the power plant continues to produce an alternating electric current. Operating units of modern TPP provide equally good and reliable operation of its generating hydro turbine generators during rotation of the wheel in either of the two parties. *The third cycle* – a period of idle wheels hydro turbine generators caused «lull» of seawater («dead zone»). During this period, the TPP stops power generation. For an exception during this cycle outages from TPP electricity to consumers using backup power grid from operating in its composition thermal, nuclear, hydroelectric, geothermal power plants and wind farms connected to the TPP. Interestingly, the TPP world's first built in 1913 near the city of Liverpool (Scotland) [24]. The installed power of the TPP was 635 kW. Scientists-hydrologists and power engineers estimated that for the efficient operation of the TPP need to drop sea water levels between the tide was more than four meters. The most suitable place for the PES placement is considered to be where the tides have their greatest amplitude and where the coastal rocky terrain allows you to create a large pool closed for this kind of power fills during high tide sea water [24]. In recent years, tidal, hydropower has been further developed. It replenishes fundamentally new technical solutions while creating the world of TPP. However, their main difference is the lack of expensive concrete dams. Instead of compact hydro turbines generators of new generation of TPP are driven by large diameter wheels blades from 10 to 20 m [24].

Fig. 25 shows the appearance of a modern TPP installed power of 240 MW, located on the French coast [6]. The length of the concrete dam of the TPP, which serves at the same time and on high-speed highway bridge is 800 m.

Fig. 25. General view of the TPP «La Rance» of power of 240 MW (1967, Rance River, Northern Brittany, France) [6]

By the way, the maximum amplitude of the tide in the north of France can be up to 14.7 m [24]. As for the record in the world of the sea tide amplitude values (of the ocean), they account for about 19.5 m. Such absolute levels of the tide have been reported in Canada on its Atlantic coast (in the Bay of Fundy). [24] An important factor in the creation of TPP is favorable geological conditions for the establishment of its partitions off the dam. Therefore, in the construction of TPP experts use data not only for the tide amplitude, but also the strength characteristics of soils, seismicity and their reliability in the operation of TPP.

Fig. 26 for comparison with the great French TPP is given a small Russian TPP with installed power as of 2009, 1.7 MW [6]. Back in the Soviet era construction project Penzhina PES was developed (Penzhina Bay in the Sea of Okhotsk, Far East, RF) [6]. The design capacity of this power plant was 87 GW. Such power indicator displays it on the level of the largest TPP in the world [6]. Currently, the status of the tempting project to create giant TPP is unknown to us. It should be noted that in the area of proposed construction in Russia Penzhina PES amplitude of sea tide reaches its highest level in the former USSR in the 11 m [24]. Of the other major force in the world of PES should indicate power plant with installed power of 254 MW, was built in 2011 in South Korea [6]. This TPP is able to provide power for a city with a population of 500 thousand people. The plans of the South Korean government appear launch in the near future TPP with an installed power of 812 MW [6].

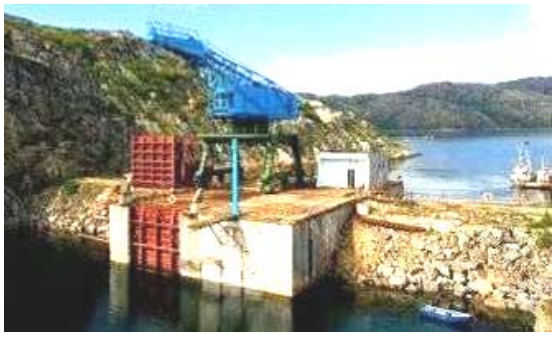

Fig. 26. General view of the TPP «Kislogubskaya» of power of 1.7 MW (1968, Sour lip, Kola Peninsula, Russia) [6]

The total potential of tidal energy in the world is now tentatively estimated installed capacity of 1,000 GW [24, 25]. The annual output of all TPP electrical energy the world by the beginning of 2015, approximately 2,000 billion kW·h, including in Russia – to 250 billion kW·h [24, 25].

6. Hydrogen energy. This type of alternative energy refers to the rapidly growing energy sector today [7]. Before humanity are becoming increasingly global issue arises concerning the change of power, «the foundation» of social development [26]. The main energy raw materials in the world today are oil and natural gas reserves which could create insurmountable problems in front of people about 50 years [26]. Oil and gas energy is already creating a lot of environmental problems on our planet. That's why experts drew their attention to the hydrogen reserves in the world is almost inexhaustible. ***Hydrogen energy*** is based on the use of hydrogen as a means for the generation, storage, transportation and energy consumption by humans, the transport infrastructure and various production technologies. Hydrogen is selected here as a working tool (energy source) is not by chance, but as the most common chemical element on the surface of our planet and in space [13]. In addition, this substance has

a high calorific value (approximately 143 MJ/kg, whereas the coal is 29.3 MJ/kg [7, 13]), and its combustion product oxygen is water. Moreover, the water formed by a chemical reaction can be re-introduced into the circulation of this species of alternative energy. Today is an insurmountable problem in the field of hydrogen energy is uneconomical for industrial production of hydrogen H_2.

6.1. Key technologies for hydrogen production. For these technologies produce hydrogen H_2 should be referred to today as follows [7, 27]: *a*) conventional steam reforming of natural gas; *b*) coal gasification; *c*) electrolysis of water; *d*) thermochemical processing of biomass; *e*) thermal water treatment (thermolysis) in solar concentrators; *f*) alternative catalytic conversion of natural gas from the heat of high-temperature gas-cooled nuclear reactor; *g*) aqueous alkaline electrolysis under pressure using nuclear electric power. Currently, hydrogen H_2 produced mostly (up to 95 % of the total volume) by the traditional conversion of natural gas (methane CH_4 under pressure in the presence of a catalyst and temperature (700-1000) °C is mixed with water vapor) [7]. Cost of this technology for producing hydrogen H_2 – 5 $/kg [27]. Gasification of coal is the oldest and relatively expensive method of producing hydrogen H_2, in which coal is heated by steam at a temperature (800-1300) °C without access of air [27]. Electrolysis of water, based on the chemical reaction $2H_2O$+energy → $2H_2 + O_2$, H_2 is characterized by cost hydrogen production to 7 $/kg [27]. The heating of the biomass (waste wood) without access of oxygen at the temperature. (500-800) °C results in obtaining a hydrogen H_2, carbon monoxide CO and methane CH_4. Thus the production cost of hydrogen H_2 is about 7 $/kg [27]. Direct thermolysis of water in the solar energy concentrators (at a temperature above 2500 °C decomposes water into hydrogen H_2 and O_2 oxygen) produces hydrogen at its cost at least 10 $/kg [27]. Application for the purpose of industrial production of hydrogen H_2 high-temperature nuclear gas cooled reactors, providing the high temperatures of its helium coolant (about 1000 °C) is used in the catalytic conversion of methane CH4, and cheap electricity NPP generated by it at night, is currently still at the stage of technological development [27, 28]. Note that at the present time in Russia the latest industrial hydrogen production technology is actively engaged in RRC «Kurchatov Institute» [26, 27].

6.2. The use of hydrogen in fuel cells to produce electricity and thermal energy. Production of electrical and thermal energy using hydrogen H_2 is realized in the fuel cell (FC) [27, 28]. The fuel cell chemical reaction type: $2H_2 + O_2 \rightarrow 2H_2O$ + Energy. It can be seen that this reaction is the reverse of that which takes place during electrolysis of water [7]. In late 2006, around the world it operated for about 5,000 small stationary hydrogen power plants based on fuel cells [27]. By mid 2008 in Japan was established about 3000 household stationary power plants (SPP) to 10 kW on hydrogen fuel cells, and their cost has dropped to 19,000 $ for 1 kW of power [27]. Note that in 2006 the world was established in the SPP 800 hydrogen fuel cell power more than 10 kW. Their total power was of 100 MW [7.] Now the world's booming market for mobile power units (MPU) that use hydrogen fuel cells to charge mobile phones, laptops and other electronic equipment [7, 27]. In 2008, world production of MPU with hydrogen fuel cell was about 9000 pieces. (The main consumer of these light sources and intensive is US Army.) [27]

Hydrogen fuel cells now have found a definite practical use in transport (Fig. 27). Moreover, the cost of hydrogen fuel cell car on the market decreased from 275 $ for 1 kW in 2002 to 110 $/ kW in 2005 [7, 27].

Fig. 27. Passenger bus brand Mercedes Benz Citaro, working on hydrogen fuel cells (2006, London) [7]

US Department of Energy plans to increase by 2020 the cost of hydrogen fuel cell car to 30 $ for 1 kW of power [7, 27]. In June 2008, the company «Matsushita Electric Industrial Co Ltd (Panasonic)» the beginning of the industrial production of hydrogen fuel cells in Japan. The company plans in 2016 to sell about 200 thousand household SPP and the MPU on hydrogen fuel cells [27]. It should be mentioned the fact that the hydrogen fuel cells produce power on board the shuttles USA, starting since 1981 [27]. In March 2008, during an expedition STS-123 of the space shuttle «Endeavour» Hydrogen fuel cells manufactured by USA «UTC Power» overcame the barrier of 100 thousand operating hours of the open space. The plans of the Ministries of Industry, Commerce and Economy of South Korea designated the strategic goal – the creation of a society by 2040 hydrogen economy producing at SPP with hydrogen fuel cells to 22 % of all electricity [27]. This gives us reason to believe such chemical sources of electric current as the fuel cell, which is the direct conversion of chemical energy into electrical energy with high efficiency value (up to 85 % [26]), «mover» of hydrogen energy [27, 28].

7. Small hydropower. Small hydropower has received in recent decades some progress in the world mainly because of the desire of people to avoid environmental damage caused by large hydro reservoirs. Most often, small hydropower plants (SHPP) include energy facilities with an installed capacity of less than 5 MW [8]. At the same time according to the requirements of the European Small Hydropower Association SHPP be considered as the installed capacity of which does not exceed 10 MW [8]. Note also that in the Soviet Union according to SNIP 2.06.01-86 requirements to those treated SHPP installed power of 30 MW, and the diameter of the impeller of the turbine was up to 3 m [8]. These data show that the uniform requirements of the world to the concept of small SHPPs on missing today.

However, in many countries of the world have their own specific SHPP energy «niche» in the annual balance of electricity generation [29].

7.1. The development of small hydropower in the world. In the Republic of Belarus as of 2010 operated 36 small SHPPs with a total installed power of 13.5 MW with an annual output of over 33 million KW·h of electricity [8]. In Sweden in 1350 operates SHPP, which generate up to 10 % of the country's electricity need. In the Russian Federation, which, in accordance with the requirements of GOST P51238-98 to carry SHPP station with a capacity of 30 MW, has about 100 such power stations with a total installed power of about 90 MW [8]. Their electricity production is about 200 million. KW·h per year [29]. We point out that the technical potential of the Russian Federation of small hydropower experts estimate about 360 billion. KW·h per year (this figure is close to 30 % of consumption in the Russian Federation's annual electricity volume) [8]. Note that in 2006 the total installed power of SHPP worldwide was about 73 GW. The leader here was China (47 GW), and followed by Japan (4 GW) and the US (3.4 GW). [29] It is interesting that the total global investment in small hydropower in 2006 amounted to about 6 billion $.

7.2. Small hydropower in Ukraine. The economic hydropower potential of small rivers of Ukraine experts is currently estimated at up to 1.5 bln KW·h annual electricity generation [30]. Lifting the page of history in our country, small hydropower, we note that in 1934 was commissioned in Korsun-Shevchenko SHPP installed power of 2.65 MW [30]. This SHPP on the technical performance was one of the best stations of its time. At the beginning of the 1950s the number of small hydro power plants operating in Ukraine amounted to 956 units with a total power of about 30 MW. It is interesting to note that at the end of 1929 the number of such hydroelectric power station on the territory of Ukraine was equal to 150 units with a total capacity of 8.4 MW [30]. Later, due to the concentration of production of electricity on high-power hydraulic and thermal power plants, SHPP construction was stopped, and the hundreds of small SHPPs were stopped. One of them was suspended, the other part is removed, and the remaining part is simply destroyed. As a result, today only 48 units SHPP remained in Ukraine (Fig. 28), most of which require the reconstruction [30]. These include a relatively powerful station as Tereble-Rikskaya, Gaivoronskaya, Korsun-Shevchenko, Steblevskaya, Ladizhinskaya and others.

Fig. 28. General view of the dam and engine room of the domestic SHPP (2009, Ukraine) [30]

Of course, small hydropower of Ukraine because of its small specific weight (up to 0.2 % [30]) in the total energy balance of the country may not significantly affect the conditions of its energy supply. However, exploitation of SHPP now makes it possible to produce about 250 million. KW·h of electricity per year. This is equivalent to annual savings of up to 75 thousand tons of scarce fossil fuels [8].

Conclusion. Alternative energy, despite its small share (up to 10 %) in the current total world annual balance of electricity generation due to the forced change in the next 50 years, oil and gas, «the foundation» of world energy on a large raw, potential and environmental capacity is large prospects for the development and use by the society.

REFERENCES

1. Available at: http://alt-energetic.ucoz.ru/index/0-10 (accessed 11 July 2015). (Rus).

2. Available at: https://en.wikipedia.org/wiki/Wind_power (accessed 25 October 2013).

3. Available at: https://en.wikipedia.org/wiki/Solar_energy (accessed 03 May 2014).

4. Available at: https://en.wikipedia.org/wiki/Geothermal_energy (accessed 08 June 2014).

5. Available at: http://www.agro-t.de/Bio/biogas.html (accessed 05 January 2014).

6. Available at: https://en.wikipedia.org/wiki/Tidal_power (accessed 17 May 2015).

7. Available at: https://en.wikipedia.org/wiki/ Hydrogen_economy (accessed 20 February 2015).

8. Available at: https://en.wikipedia.org/wiki/Small_hydro (accessed 20 March 2015).

9. Available at: http://altenergy.in.ua/category/vetryanaya-energiya (accessed 02 April 2015).

10. Available at: http://www.molomo.ru/myth/wind_energy.html (accessed 10 June 2015). (Rus).

11. Available at: http://masterok.livejournal.com/220814.html (accessed 10 May 2015). (Rus).

12. Available at: http://www.avante.com.ua/rus/library/lib_perspektiv_soln_energetiki.htm (accessed 28 September 2014). (Rus).

13. Kuz'michev V.E. *Zakony i formuly fiziki* [Laws and formulas of physics]. Kiev, Naukova Dumka Publ., 1989. 864 p. (Rus).

14. Alferov Z.I., Andreev V.M., Rumyantsev V.D. Solar photovoltaics: Trends and prospects. *Semiconductors*, 2004, vol.38, no.8, pp. 899-908. **doi: 10.1134/1.1787110**.

15. Available at: http://alteco.in.ua/technology/solar-energy (accessed 20 October 2014).

16. *Bol'shoj illjustrirovannyj slovar' inostrannyh slov* [Large illustrated dictionary of foreign words]. Moscow, Russkie slovari Publ., 2004. 957 p. (Rus).

17. Krasnok A.E., Maksymov I.S., Denisyuk A.I. Belov P.A., Miroshnichenko A.E., Simovskii C.R., Kivshar Yu.S. Optical Nanoantennas. *Uspehi fizicheskih nauk − Successes of physical sciences*, 2013, vol.183, no.6, pp. 561-589. **doi: 10.3367/ufnr.0183.201306a.0561**.

18. Available at: https://en.wikipedia.org/wiki/Photovoltaic_power_station (accessed 22 November 2014).

19. Khramov Yu.A. *Istoriia fiziki* [History of Physics]. Kiev, Feniks Publ., 2006. 1176 p. (Rus).

20. Available at: http://re.energybel.by/en/geothermal/ (accessed 09 April 2014).

21. Baranov M.I. *Izbrannye voprosy elektrofiziki. Tom 3: Teorija i praktika elektrofizicheskih zadach* [Selected topics of Electrophysics. Vol. 3: Theory and practice of electrophysics tasks]. Kharkiv, Tochka Publ., 2014. 400 p. (Rus).
22. Available at: http://www.energyofnature.org/2387 (accessed 12 March 2013).
23. Berman E., Mavritskiy B.F. *Geotermal'naja energija* [Geothermal energy]. Moscow, Mir Publ., 1978. 416 p. (Rus).
24. Available at: http://alternativenergy.ru/energiya/553-prilivnaya-elektro-stanciya-princip-foto.html (accessed 18 May 2014). (Rus).
25. Available at: http://energetika.in.ua/ru/books/book-5/part-1/section-2/2-5 (accessed 27 November 2014). (Rus).
26. Available at: http://federalbook.ru/files/TEK/Soderzhanie/Tom%2010/V/Kovalchuk.pdf (accessed 27 November 2014). (Rus).
27. Available at: http://www.o8ode.ru/article/energy/energy.htm (accessed 04 March 2012). (Rus).
28. Legasov V.A. *Atomno-vodorodnaja energetika i tehnologija* [Atomic hydrogen energy and technology]. Moscow, Atomizdat Publ., 1978. 475 p. (Rus).
29. Available at: http://www.cleandex.ru/articles/2008/03/18/hydropower2 (accessed 18 March 2008). (Rus).
30. Available at: http://alterpower.com.ua/energy-water/41-malaya-gidro-energetika-ukraini (accessed 07 May 2015). (Rus).

Received 26.10.2015

M.I. Baranov, Doctor of Technical Science, Chief Researcher,
Scientific-&-Research Planning-&-Design Institute «Molniya»
National Technical University «Kharkiv Polytechnic Institute»,
47, Shevchenko Str., Kharkiv, 61013, Ukraine,
phone +38 057 7076841, e-mail: eft@kpi.kharkov.ua

How to cite this article:
Baranov M.I. An anthology of the distinguished achievements in science and technique. Part 32: Alternative energy: state and prospects of development. *Electrical engineering & electromechanics*, 2016, no.3, pp. 3-16. doi: 10.20998/2074-272X.2016.3.01.

UDC 648.3.048.1 **doi: 10.20998/2074-272X.2016.3.02**

V.V. Vasilevskij

DYNAMICS MODEL OF MOISTURE IN PAPER INSULATION-TRANSFORMER OIL SYSTEM IN NON-STATIONARY THERMAL MODES OF THE POWER TRANSFORMER

Introduction. An important problem in power transformers resource prognosis is the formation of moisture dynamics trends of transformer insulation. Purpose. Increasing the accuracy of power transformer insulation resource assessment based on accounting of moisture dynamics in interrelation with temperature dynamics. Working out of moisture dynamics model in paper insulation-transformer oil system in conjunction with thermodynamic model, load model and technical maintenance model. Methodology. The mathematical models used for describe the moisture dynamics are grounded on nonlinear differential equations. Interrelation moisture dynamics model with thermodynamic, load and technical maintenance models described by UML model. For confirming the adequacy of model used computer simulation. Results. We have implemented the model of moisture dynamics in power transformers insulation in interrelation with other models, which describe the state of power transformer in operation. The proposed model allows us to form detailed trends of moisture dynamics in power transformers insulation basing on monitoring data or power transformers operational factors simulation results. We have performed computer simulation of moisture exchange processes and calculation of transformer insulation resource for different moisture trends. Originality. The offered model takes into account moisture dynamics in power transformers insulation under the influence of changes of the power transformers thermal mode and operational factors. Practical value. The offered model can be used in power transformers monitoring systems for automation of resource assessment of oil-immersed power transformers paper insulation at different phase of lifecycle. Model also can be used for assessment of projected economic efficiency of power transformers exploitation in projected operating conditions. References 7, figures 4.

Key words: **oil-paper insulation, power transformer, computer model, moisture dynamics.**

С целью повышения точности расчета ресурсных характеристик силового трансформатора предложена модель прогнозирования динамики влажности бумажно-масляной изоляции. Предложенная модель отличается от существующих учетом процессов миграции влаги в бумажно-масляной изоляции под влиянием изменения теплового режима силового трансформатора. Проведено компьютерное моделирование износа бумажно-масляной изоляции и произведена оценка влияния возможного изменения степени увлажненности на ресурс. Библ. 7, рис. 4.

Ключевые слова: **бумажно-масляная изоляция, силовой трансформатор, компьютерное моделирование, динамика влажности.**

Introduction. Establish of monitoring systems for transformer equipment is actual scientific and technical task. A number of systems, such as domestic manufacturers (LLC «Energoavtomatizatsiya», JSC «ZTR» [1]), and foreign (ABB, Siemens) [2], one of the functions of which is the possibility of residual life assessment unit of the power transformer (PT) based on monitoring data are known.

Life of oil-filled power transformer is mainly determined by resource of its paper insulation (PI). Effect on consumption of resource of the PI PT the following factors: the change in temperature, the degree of hydration of cellulose and transformer oils (TO), and the degree of oxidation of the oil. Water may be produced during operation in the PT as a product PI aging, and exposed from the environment due to the partial depressurization tank. The migration of moisture in the insulation system is influenced by changes in the thermal regime PT.

An important problem in the calculation of the projected resource characteristics in operation is the construction PT possible humidity trends paper-oil insulation (POI), TO and acidity changes in operating factors such as ambient temperature and load current.

Analysis of investigations. The existing models of moisture exchange are defined by their purpose – determining moisture of PI based on TO moisture measurement in monitoring the use of PT with equilibrium moisture content curves [3] or computational methods [4]. In such models do not take into account (or not sufficiently taken into account), possible change of operation factors in the forecast horizon.

It is also possible to form the trend humidity PI based on the assumption that the moisture content of the growth of POI of PT due to aging would be approximately 2-3 % [5] and that this growth will occur linearly during operation.

In this case the reduced rate forecast accuracy PT resource, there is no opportunity to get a complete picture of the dynamics of moisture and to evaluate its impact on resource consumption.

At this stage there are no models by which to predict the dynamics of moisture in the insulation system based on PT dynamics operating factors, maintenance (M) parameters.

Problem definition. The purpose of research is to improve the accuracy of calculation of lifetime characteristics of POI of PT by taking into account the dynamics of moisture in conjunction with the temperature dynamics of the PI and maintenance in resource consumption model. To achieve this goal it is necessary to solve the following tasks:

- to propose ways to assess the impact of moisture migration in POI PT to the resource PI PT;
- to build a model of the dynamics of the POI of humidity in the moisture content in the non-equilibrium state, in cooperation with the POI model load, ambient temperature, and maintenance of PT;

• to conduct computer simulations of POI resource consumption in order to assess the impact of migration of moisture on the resource consumption POI.

Results of investigations. Block diagram of the relationship model of moisture exchange in POI PT with other elements of the model predictive resource consumption is shown in Fig. 1. It includes a model of the external operating factors (OF, it forms loads I_d and coolant temperature θ_a current trends), a model of technical condition and maintenance of the POI (POI TC and M, forming the heat capacity and thermal resistance of the trends for different types of cooling R_{ON}; R_{OF}; C_{ON}; C_{OFF}), a thermodynamic model (TDM, generates temperature trend most heated point (TMHP), θ_h), moisture exchange model in POI PT and wear evaluation unit (WE, the calculation of the resources expended L) [6].

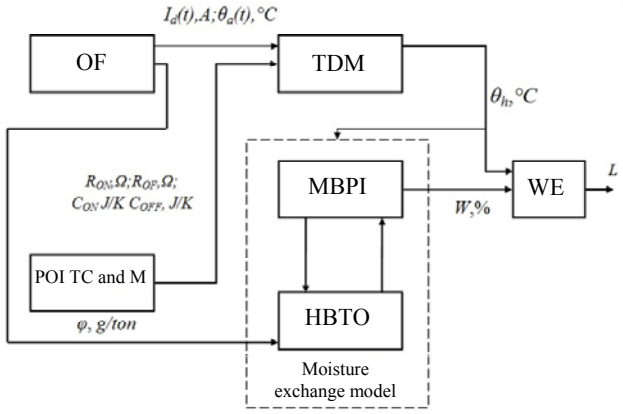

Fig. 1. Block diagram of the relationship of moisture exchange model with other models

A moisture exchange model, in turn, consists of a moisture block of PI (MBPI) and humidity of TO block (HBTO) which are interconnected.

Calculated PI humidity at certain time t is given by [5]:

$$W_c = A \cdot e^{-B \cdot \Theta_h} \cdot p^{k + a \cdot \Theta_h}, \qquad (1)$$

where W_c is the calculated PI humidity, %; A, B, k, a are the table data for certain type of insulation; θ_h is the TMHP, °C; p is the partial water vapor pressure, mmHg.

Dynamics humidity of PI TO system is described using UML model shown in Fig. 2.

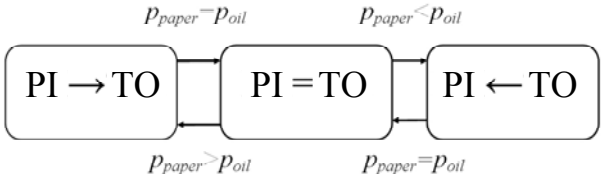

Рис. 2. Moisture exchange model in the system PI TO

Model is a diagram of states, transitions between which are carried out taking into account the relationship between the partial pressure of water vapor in the PI (p_{paper}) and TO (p_{oil}). In each state, the appropriate action is carried out:

1) PI→TO – humidity transfer from PI to TO. The amount of moisture that migrates from PI to TO during time dt at change of the TMHP value is determined by the differential equation:

$$\frac{dW_{paper}}{dt} = \frac{W_{c.paper(\Theta_{h1})} - W_{paper(\Theta_{h2})}}{\tau}, \qquad (2)$$

where τ is the moisture transfer time constant; $W_{c.paper(\Theta_{h1})}$ is the PI humidity W_c at TMHP θ_{h1}, %; $W_{c.paper(\Theta_{h2})}$ is the PI humidity W_c at TMHP θ_{h2}, %.

Change of TO degree of moisture as a result of the migration of moisture from PI:

$$\frac{dW_{oil}}{dt} = \frac{W_{c.oil(\Theta_{h1})} + \frac{W_{paper} \cdot m_{oil}}{m_{paper}}}{\tau}, \qquad (3)$$

where $W_{c.oil(\Theta_{h1})}$ is the TO humidity at TMHP θ_1, %; m_{oil} is the total mass of TO in the PT, t; m_{paper} is the total mass of the PI in the PT, t.

Value of TO humidity at TMHP θ_{h1} is determined either on the monitoring results, or the results of peer review.

2) PI←TO – humidity transfer from TO to PI. The amount of moisture that migrates from TO to PI during time dt is characterized by TMHP change:

$$\frac{dW_{paper}}{dt} = \frac{W_{c.paper(\Theta_{h2})} - W_{paper(\Theta_{h1})}}{\tau}. \qquad (4)$$

Changing the degree of hydration of TO as a result of the humidity migration to PI in this case:

$$\frac{dW_{oil}}{dt} = \frac{W_{c.oil(\Theta_{h1})} - \frac{W_{paper} \cdot m_{oil}}{m_{paper}}}{\tau}. \qquad (5)$$

3) PI = TO – equilibrium state, to which the system tends at equality temperatures PI, TO and the cooling medium.

In all states in the operation phase occurs moisture increase in the PI and TO, the dynamics of the increase described by the following differential equations:

$$\frac{dm_{oil}}{dt} = k_{oil}, \quad \frac{dm_{paper}}{dt} = k_{paper}, \qquad (6)$$

where k_{oil}, k_{paper} are the coefficients which characterize the increase in mass of the moisture in TO and PI, respectively, g/kg·h; m_{oil}, m_{paper} is the moisture mass in TO TM and PI, respectively, kg.

The initial state is the state PI = TO, in which the system is for a period of time dt until the equality of the partial pressure of water vapor in the POI PT. The initial data for the model are moisture exchange values TMHP measured relative humidity of transformer oil, the oil temperature near the humidity sensor, the content of aromatic hydrocarbons in the oil and table data for certain types of insulation. The equilibrium value of PI humidity is determined by (1) θ_{h1} and relative humidity TO φ (%), the value of φ is determined according to TO or monitoring by experts. Moisture gain in POI PT due to the aging of cellulose or depressurization tank PT is calculated using the formula (6).

When you change the temperature PT is a violation of the balance of the partial pressures and the system goes into a state of PI→TO ($p_{paper}>p_{oil}$) or in the state of PI←TO ($p_{paper}>p_{oil}$). Dynamics of humidity changes in PI and TO due partial pressure and humidity gradients within the time period *dt* is calculated by the formulas (2-5).

Sources of raw data to calculate the moisture exchange is the data model of external operational factors (moisture value growth as a result of decomposition of cellulose and water revenues from the environment), the technical condition of the POI model (changes in baseline), a thermodynamic model (TMHP). The resulting paper insulation moisture value is used in calculating the resource in the resource evaluation unit.

Then the model of M provides for both routine M and M by technical condition. Result of M of PT is to reduce the humidity and PI TO acidity to certain minimum values. When working on the model variant planned M lowering humidity indicators and acidity POI PT occurs at predetermined periods of time (by drying and regeneration POI PT). In the case of condition based M decrease in humidity and acidity indicators POI PT occurs upon reaching these parameters critical values.

In the proposed model allowed the following simplifications:

- the process of M is accepted as the CT process with zero duration;
- simulation does not include changes in resource characteristics PI PT in the time period from the moment of installation of PT on site prior to its inclusion under the load;
- increase the degree of oil oxidation occurs linearly over the period of operation between the two M.

As the base used for the trend test the adequacy of the model obtained from the results may be accepted PT trend resource flow with the same parameters, the monitoring system equipped and located in similar environments.

To set up a model of moisture exchange used or curves of Oommen or Fabr and Piccioni [7] for the equilibrium moisture content in a system PI – TO. It is expected that before turning on the PT under the load as a result of the thermodynamic processes in the system temperature POI PT – environment called and will be equal to θ_a. In accordance with the law of equilibrium [5], the partial pressure of water vapor in the system is also equalized. To set the initial conditions of simulation θh assumed constant and equal θ_a, TO is equal to the absolute humidity of 10-15 g/m (which corresponds to the TO PT humidity class I [5]). Next is W_c calculation for given initial conditions and the resulting humidity value of PI is compared with a reference point on the curves of Oommen or Fabr and Piccioni and to validate the calculation. The resulting value will be the value of W_c PI humidity at the beginning of operation of PT.

Proposed models are implemented in the program Matlab Simulink. As an example of simulation model to assess POI performance deterioration held for two variants of the system dynamics humidity PI – TO.

In the first variant, moisture value during the simulation and decreases linearly increases up to a certain initial value after M of PT (Fig. 3, curve *a*). In the second embodiment applied humidity trend obtained by using the proposed model (Fig. 3, curve *b*).

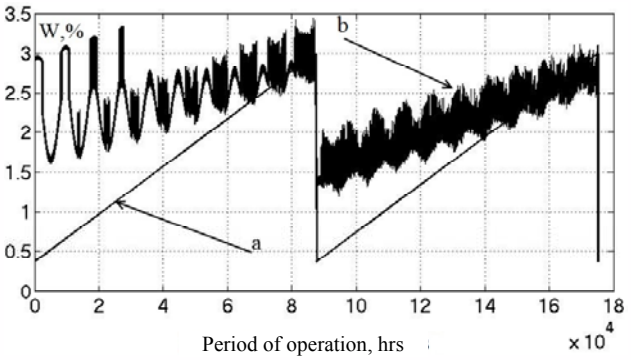

Fig. 3. POI humidity trends

Initial data for OF models, the TC POI and M and TDM and rated current of the transformer is equal to 406 A, output no-load losses is equal to 29.3 kW, the maximum acidity TO equals 0.29 mg KOH/g, the base value of acidity TO 0.2 mg KOH/g, the average annual ambient temperature is 9.4 ^{0}C, the amplitude of the annual change in the average daily temperature θ_a equal to 12.6 ^{0}C, the amplitude of the diurnal changes θ_a equal to 4 ^{0}C, the average annual rate of change θ_a is 2 ^{0}C, the rate of change Id average 2 A, the average daily change I_d 20 A, the average annual change I_d 20 A, I_d = 244.2 A maximum value TMHP taken equal to 150 ^{0}C, the maximum value of the moisture content of the paper insulation – 5%.

Initial data for trending humidity Fig. 3, curve *a*: base value is equal to the moisture content of PI 0.37%, the maximum moisture content of 3% PI.

Initial data for trending humidity Fig. 3, curve *b*: the content of aromatic hydrocarbons in oil C_A = 17% (oil T-750 GOST 982-80), A = 5.55, B = 0.034, k = 0.49, a = –0.0007 (cardboard electrotechnical ЭМЦ).

Simulation period – 20 years. The simulation results under the above defined raw data shown in Fig. 4. The *x*-axis represents the life of PT in hours, and the vertical axis – the value of the consumed resources of *L*, as in hours.

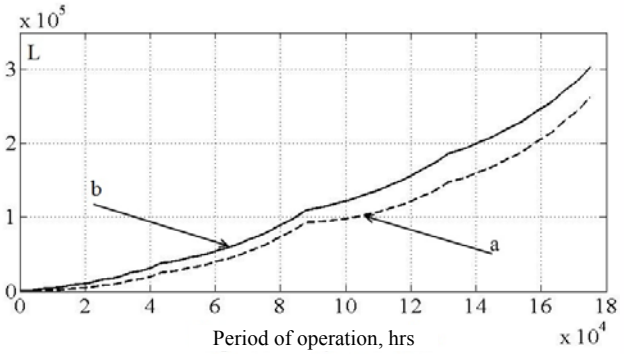

Fig. 4. Results of simulation

From obtained results it is seen that the use of different versions of humidity PI trend has a significant effect on the final value of the consumed resource. So, wear of the PT when the trend Fig. 3, it was 30.03 years and 20 years of operation in the case of Fig. 3, *b* – 34.6 years.

Conclusions.

A model of moisture exchange in the system of «paper insulation – transformer oil» in conjunction with the other models, which describe the state of the power transformer in operation is proposed: a model of operation factors, the thermodynamic model of a power transformer model and the technical condition of paper-oil insulation.

The proposed model allows you to build a detailed trend dynamics humidity paper-oil insulation according to the monitoring unit power transformer or on the results of the simulation changes operational parameters of the power transformer.

Given the dynamics of moisture content of paper-oil insulation of a power transformer can improve the accuracy of estimation of the resource of paper insulation.

REFERENCES

1. *E'kspertnaya sistema monitoringa, diagnostiki i upravleniya transformatornym oborudovaniem «E'SMDU TRANS» proizvodstva PAO «ZTR»* (Expert system for monitoring, diagnostic and control of transformer equipment «E'SMDU TRANS» produced by PAO «ZTR») Available at: http://www.ztr.com.ua/ru/monitoring-system. (accessed 13 May 2014). (Rus).

2. Rusov, V.A., Ovsyannikov, A.G., Zhivodernikov S.V. Foreign experience of oil-filled equipments monitoring. *Materialy IV nauchno-prakticheskogo seminara Obshchestvennogo soveta spetsialistov Sibiri i Vostoka po problemam monitoringa transformatornogo oborudovaniya i diagnostiki elektricheskikh ustanovok* [Proceedings of the IV scientific workshop of the Public Council of experts of Siberia and the East on the monitoring of transformer equipment and diagnostics of electrical installations]. Novosibirsk, Russia, 20-24 April 2009, pp. 7-22. (Rus).

3. Cheng J., Robalino D., Werelius P., Ohlen M. Advanced technique for moisture condition assessment in power transformers. *Journal of International Council on Electrical Engineering*, 2014, vol.4, no.3, pp. 185-191. **doi: 10.5370/JICEE.2014.4.3.185**.

4. Mordkovich A.G. The system of management, monitoring and diagnostics of transformers SUMTO. *ELEKTRO. Elektrotekhnika, elektroenergetika, elektrotekhnicheskaia promyshlennost' – ELEKTRO. Electrical engineering, power industry, electrical industry*, 2007, no.6, pp. 23-28. (Rus).

5. Lizunov S.D., Lokhanin A.K. *Silovye transformatory. Spravochnaia kniga* [Power transformers. Handbook]. Moscow, Energoizdat Publ., 2004. 616 p. (Rus).

6. Polyakov M.A., Vasilevskij V.V. Prediction of wearing out of power transformer winding insulation. *Tekhnichna elektrodynamika – Technical electrodynamics*, 2014, no.5, pp. 65-67.

7. Du Y., Zahn M., Lesieutre B.C., Mamishev A.V., Lindgren S.R. Moisture equilibrium in transformer paper-oil systems. *IEEE Electrical Insulation Magazine*, 1999, vol.15, no.1, pp. 11-20. **doi: 10.1109/57.744585**.

Received 04.02.2016

V.V. Vasilevskij, Postgraduate Student,
Zaporozhye National Technical University,
64, Zhukovsky Str., Zaporozhye, 69063, Ukraine,
phone +380 50 8893073, e-mail: Lisses@ukr.net

How to cite this article:
Vasilevskij V.V. Dynamics model of moisture in paper insulation-transformer oil system in non-stationary thermal modes of the power transformer. *Electrical engineering & electromechanics*, 2016, no.3, pp. 17-20. doi: 10.20998/2074-272X.2016.3.02.

UDC 621.313.33 **doi: 10.20998/2074-272X.2016.3.03**

V.S. Malyar, A.V. Malyar

MECHANICAL CHARACTERISTICS OF THREE-PHASE INDUCTION MOTORS WITH SINGLE-PHASE POWER SUPPLY

Aim. Development of a method for calculating mechanical characteristics of three-phase induction motors with single-phase power supply. Methods. The developed algorithm is based on the high-adequacy mathematical model of motor and projection method for solving the boundary problem for equations of electrical circuits balance presented in the three-phase coordinate system. As a result of asymmetry of power supply to the stator windings, in steady state, flux-linkage and current change according to the periodic law. They are determined by solving the boundary problem. Results. The developed mathematical model allows determining periodic dependence of coordinates as a function of slip and, based on them, mechanical characteristics of motors. Academic novelty. The developed method relies on a completely new mathematical approach to calculation of stationary modes of nonlinear electromagnetic circuits, which allows obtaining periodic solution in a timeless domain. Practical value. Using the developed calculation algorithm, one can select capacitance required to start an induction motor with single-phase power supply and calculate static mechanical characteristics at a given capacitance. References 5, figures 3.

Key words: **mechanical characteristic, induction motor, single-phase power supply, boundary problem, projection method, capacitor.**

Предложен метод расчета механических характеристик трехфазных асинхронных двигателей, которые питаются от однофазной сети. Вращающееся магнитное поле создается за счет включения последовательно в одну фазу конденсаторов. Задача решается как краевая в трехфазной системе координат. В математической модели двигателя учитывается насыщение магнитопровода и вытеснение тока. Библ. 5, рис. 3.

Ключевые слова: **механическая характеристика, асинхронный двигатель, однофазное питание, краевая задача, проекционный метод, конденсатор.**

Introduction. Induction motors (IM) are mainly produced with three-phase windings that are powered symmetrical three-phase system voltages. However, in practice may need to switch to a single-phase network [1], which use capacitors that create shifting the phase current in a coil and a magnetic field motor becomes pulsating and rotating, causing electromagnetic torque. Also developed and are widely used capacitor electric motors, which are designed to operate on single-phase network [5]. And in the first and second cases, there is a problem of calculation of their starting characteristics and capacitors' capacitance choice.

In technical literature since the calculation method for different values of capacitors are known [1, 2], but these methods are not sufficient accuracy, since not adequately take into account factors such as asymmetry of power magnetic saturation and displacement current. Problems of analysis of operation modes of IM by mathematical modeling needs to solve two problems: the choice of a mathematical model of the motor and the method of calculation. These problems are interrelated, since using a simplified mathematical model of IM can not adequately take into account the factors that determine the accuracy of the calculations, and the use of more complex models requires utilization of appropriate mathematical apparatus.

The goal of the work is developing methods and algorithm of calculation of mechanical characteristics of asynchronous motors that are powered by a single-phase network.

The system of equations. A three-phase IM with capacitors in one phase by definition is skewed on the part of the stator, and therefore for the analysis of electromagnetic processes in their most adequate and optimal coordinate system is a three-phase, but not physical, so-called inhibited [4]. In this system the outlines of the stator are not converted, allowing adequately describe processes in them, and three-phase winding rotor is replaced by an equivalent stationary phase, the axis of which coincides with the axis of the stator winding.

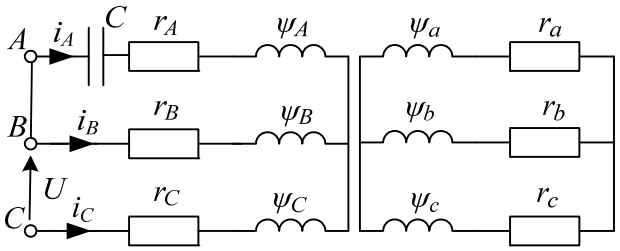

Fig. 1

The system of equations describing the electromagnetic processes in IM, three-phase stator winding is powered from a single-phase network shown in Fig. 1 has the form [4]

$$\begin{aligned}
&\frac{d\psi_A}{dt}-\frac{d\psi_B}{dt}=-r_A i_A+r_B i_B-u_k;\\
&\frac{d\psi_B}{dt}-\frac{d\psi_C}{dt}=-r_B i_B+r_C i_C+u_{BC};\\
&i_A+i_B+i_C=0;\\
&\frac{d\psi_a}{dt}-\frac{d\psi_b}{dt}=-r_a i_a+r_b i_b-\alpha(\psi_b-2\psi_c+\psi_a);\\
&\frac{d\psi_b}{dt}-\frac{d\psi_c}{dt}=-r_b i_b+r_c i_c-\alpha(\psi_c-2\psi_a+\psi_b);\\
&i_a+i_b+i_c=0;\\
&\frac{du_k}{dt}=\frac{i_A}{C},
\end{aligned} \quad (1)$$

where $u_{BC} = \sqrt{3}U_m \sin(\omega_0 t - \pi/2)$ is the linear supply voltage; U_m, ω_0 are the phase voltage amplitude and angular frequency; $\alpha = \omega_0(1-s)/\sqrt{3}$; s is the slip; ψ_ξ, i_ξ, r_ξ ($\xi = A, B, C, a, b, c$) are the flux linkages, currents and active supports of circuits; u_k is the voltage on the capacitor with capacitance C.

A technique and algorithm of calculation. We write (1) by one vector equation m = 7th order in the form

$$A\frac{d\vec{y}}{dt} = B\vec{y} + D\vec{x} + \vec{u}\,, \qquad (2)$$

where

$$\vec{A} = \begin{pmatrix} 1 & -1 & & & & & \\ & 1 & -1 & & & & \\ & & & & & & \\ & & & 1 & -1 & & \\ & & & & 1 & -1 & \\ & & & & & & \\ & & & & & & 1 \end{pmatrix};$$

$$\vec{y} = \begin{pmatrix} \psi_A \\ \psi_B \\ \psi_C \\ \psi_a \\ \psi_b \\ \psi_c \\ u_k \end{pmatrix}; \quad \vec{x} = \begin{pmatrix} i_A \\ i_B \\ i_C \\ i_a \\ i_b \\ i_c \\ u_k \end{pmatrix}; \quad \vec{u} = \begin{pmatrix} 0 \\ u_{BC} \\ 0 \\ 0 \\ 0 \\ 0 \\ 0 \end{pmatrix};$$

$$\vec{B} = \begin{pmatrix} & & & & & & \\ & & & & & & \\ & & & & & & \\ & & & \alpha & \alpha & -2\alpha & \\ & & & -2\alpha & \alpha & \alpha & \\ & & & & & & \\ & & & & & & \end{pmatrix};$$

$$\vec{D} = \begin{pmatrix} -r_A & r_B & & & & & -1 \\ & -r_B & r_C & & & & \\ 1 & 1 & 1 & & & & \\ & & & -r_a & r_b & & \\ & & & & -r_b & r_c & \\ & & & 1 & 1 & 1 & \\ & & & & & & \end{pmatrix}.$$

The system of differential equations (2) in the form of Cauchy looks

$$\frac{d\vec{y}(\vec{x},t)}{dt} = z(\vec{y},\vec{x},\vec{u},t). \qquad (3)$$

Since the vector $\vec{u}(t) = \vec{u}(t+T)$ is a periodic function of time, in the steady state (at s = const) the solution of the system of equation (3) is T-periodic dependences of the vector $\vec{x}(t) = \vec{x}(t+T)$ components. Determining the periodic functional relationships of the vector $\vec{x}$ components by calculating the transition to institutionalization unacceptable for many reasons. Such a problem can most effectively be solved in a timeless region by solving the boundary problem developed on the basis of the general theory of nonlinear oscillations projection method based on a theoretical approximation coordinates state splines of third order [3]. Formation of the boundary problem is carried out on a grid of n nodal points of the period T. The result of approximating one differential equation of the system (3) is a system of algebraic equations of the n-th order

$$H\vec{Y} - \vec{Z} = \vec{U}\,, \qquad (4)$$

where H is the transition matrix from continuous coordinates to their nodal values, elements of which are determined by only mesh nodes [3]; $\vec{Y} = \left(\overline{y_1, y_n}\right)^*$; $\vec{Z} = \left(\overline{z_1, z_n}\right)^*$; $\vec{U} = \left(\overline{u_1, u_n}\right)^*$, and for the system of differential equations (2) – m vector equations in the form (4)

$$H_c\vec{Y}_c - \vec{Z}_c = \vec{U}_c\,, \qquad (5)$$

where $H_c = diag\left(\overline{H_1, H_m}\right)$; $\vec{Y}_c = \left(\overline{\vec{Y}_1, \vec{Y}_m}\right)^*$;

$\vec{Z}_c = \left(\overline{\vec{Z}_1, \vec{Z}_m}\right)^*$; $\vec{U}_c = \left(\overline{\vec{U}_1, \vec{U}_m}\right)^*$.

Nonlinear system (5) of algebraic equations of mn-th order is a discrete reflection of nonlinear system of differential equations (2) order m and it approximates to the period T. Its solution is a vector $\vec{X}$ whose components are the values of currents legs and voltage on the capacitor in the grid. With its help you can calculate not only steady but also investigate the impact of the operation of the motor change any position, which is part of the system. To calculate the steady mode for a given slide the method of continuation on parameter. For this system (5) we enter the parameter ε by multiplying the voltage vector applied to ε and differentiate her on it. As a result, we obtain the differential equation (DE)

$$W\frac{d\vec{X}_c}{d\varepsilon} = \vec{U}_c\,, \qquad (6)$$

where $W = \left(H_c - \frac{\partial\vec{Z}_c}{\partial\vec{Y}_c}\right)\frac{\partial\vec{Y}_c}{\partial\vec{X}_c} - \frac{\partial\vec{Z}_c}{\partial\vec{X}_c}$ is the Jacobi matrix block elements of which $\left.\frac{\partial\vec{y}}{\partial\vec{x}}\right|_j$, $\left.\frac{\partial\vec{z}}{\partial\vec{y}}\right|_j$, $\left.\frac{\partial\vec{z}}{\partial\vec{x}}\right|_j$ are determined by values of IM parameters in the j-th node.

$$\left.\frac{\partial\vec{y}}{\partial\vec{x}}\right|_j = \begin{pmatrix} L_j & 0 \\ 0 & 1 \end{pmatrix}; \quad \left.\frac{\partial\vec{z}}{\partial\vec{y}}\right|_j = B; \quad \left.\frac{\partial\vec{z}}{\partial\vec{x}}\right|_j = D;$$

$$L_j = \begin{array}{|c|c|c|c|c|c|}\hline L_{AAj} & L_{AB_j} & L_{ACj} & L_{Aaj} & L_{Abj} & L_{Acj} \\ \hline L_{BAj} & L_{BBj} & L_{BCj} & L_{Baj} & L_{Bbj} & L_{Bcj} \\ \hline L_{CAj} & L_{CBj} & L_{CCj} & L_{Caj} & L_{Cbj} & L_{Ccj} \\ \hline L_{aAj} & L_{aBj} & L_{aCj} & L_{aaj} & L_{abj} & L_{acj} \\ \hline L_{bAj} & L_{bBj} & L_{bCj} & L_{baj} & L_{bbj} & L_{bcj} \\ \hline L_{cAj} & L_{cBj} & L_{cCj} & L_{caj} & L_{cbj} & L_{ccj} \\ \hline \end{array}.$$

Integrating system of DR (6) by ε from $\varepsilon = 0$ to $\varepsilon = 1$ we find the values of the vector $\vec{X}$ at a given voltage, which can be refined by Newton method.

To investigate the effect on IM operation mode of the change any coordinates needed considering the vector applied voltage unchanged we differentiate the system (5) by this coordinate as a parameter. In particular when calculating the mechanical characteristics we obtain the system of DE

$$W\frac{d\vec{X}_c}{ds} = \frac{\partial \vec{Z}_c}{\partial s}, \qquad (7)$$

integrating which we obtain a multi-dimensional characteristic. Thus Jacobi matrix such as in (6) and a right parts vector consists of n vectors in the form

$$\left.\frac{\partial \vec{z}}{\partial s}\right|_j = \frac{\partial B}{\partial s}\vec{y}_j,$$

where $\partial B/\partial s$ equals to the matrix B in which $\alpha = -\omega_0/\sqrt{3}$.

The problem of calculating the mechanical characteristics is solved in two stages: at the first we calculate the steady mode at slip s = 1.0, and at the second - dependences of coordinates as a function of the slip from s = 1.0 to the specified value, and based on it - mechanical characteristic $M_e = M_e(s)$. The electromagnetic moment of IM is calculated by the formula [4]

$$M_e = \frac{p}{\sqrt{3}} I_\mu \left(\left(i_{\mu B} - i_{\mu C}\right) i_A + \left(i_{\mu C} - i_{\mu A}\right) i_B + \left(i_{\mu A} - i_{\mu B}\right) i_C \right).$$

To determine the matrix elements L_j of differentiated inductances characteristic magnetization of the main magnetic path and scattering depending flux leakages of the stator (s) and rotor (r) of the respective current are used [4]

$$\psi_\mu = \psi_\mu(i_\mu),\ \psi_{\sigma s} = \psi_{\sigma s}(i_s),\ \psi_{\sigma r} = \psi_{\sigma r}(i_r),$$

where i_s, i_r are the modules of vectors representing these currents.

To take into account of the displacement current in rotor bars each of them together with short-circuited rings divided by height into k layers. That is believed that the rotor there are k short-circuited windings with the appropriate dimensions and each are substituted by three-phase one. Under these conditions, the system of equations (1) instead of three equations for the rotor we must write $3k$ equations like

$$\frac{d\psi_{ak}}{dt} - \frac{d\psi_{bk}}{dt} = \\ = -r_{ak}i_{ak} + r_{bk}i_{bk} - \alpha\left(\psi_{bk} - 2\psi_{ck} + \psi_{ak}\right);$$

$$\frac{d\psi_{bk}}{dt} - \frac{d\psi_{ck}}{dt} = \\ = -r_{bk}i_{bk} + r_{ck}i_{ck} - \alpha\left(\psi_{ck} - 2\psi_{ak} + \psi_{bk}\right);$$

$$i_{ak} + i_{bk} + i_{ck} = 0.$$

Increasing the number of equations does not change the calculation algorithm and has little effect on the amount of computation as poorly filled Jacobi matrix, allowing for solving the system of equations using an algorithm that takes into account its structure.

Examples of results of mathematical modeling are shown in Fig. 2, 3.

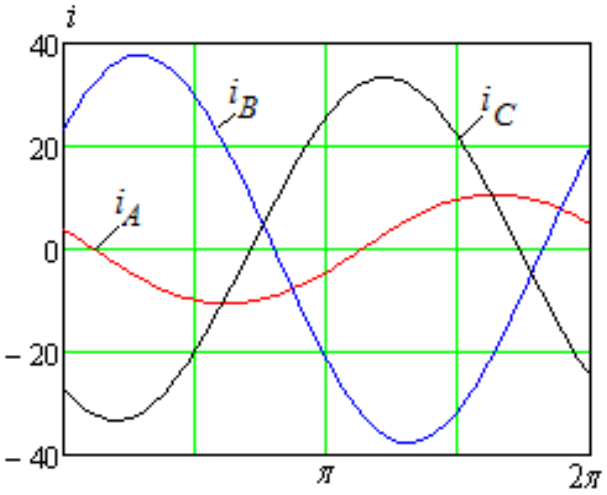

Fig. 2. Periodical dependences of phase currents of the motor 4A80B2Y3 at slip s = 1.0 and capacitors' capacitance C = 100 μF

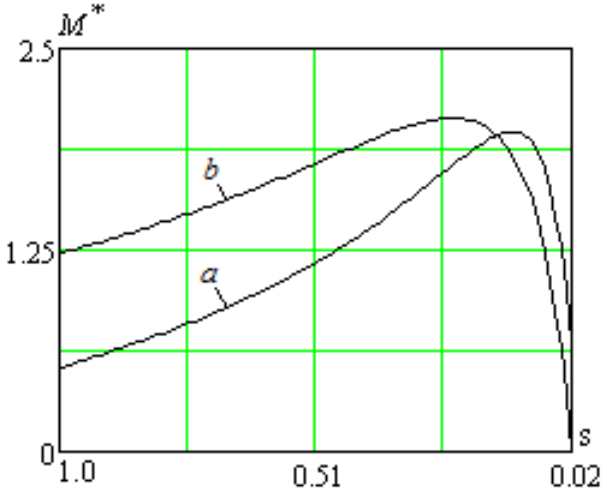

Fig. 3. Static mechanical characteristics of the motor 4A80B2Y3 at various capacitors' capacitances: C = 100 μF (a) and C = 200 μF (b)

Conclusion.

The developed method of calculation of static mechanical properties of three-phase squirrel cage IM that are powered by a single-phase network allows you to explore the influence of capacitors' capacitance on the process to select a start and its value, which provides the necessary starting torque. The basis of the algorithm is a mathematical model of IM, which considers magnetic saturation and displacement of current in the bars of the rotor, and the differential method for calculating the static characteristics based on solving the boundary problem for a system of differential equations of electrical balance.

REFERENCES

1. Bespalov V.Ya., Moshchynskyy Yu.A., Petrov A.P. Dynamic indicators of three-phase induction motors connected to single-phase supply. *Elektrotekhnika – Electrical engineering*, 2000, no.1, pp. 13-19. (Rus).

2. Beshta A.S., Semin A.A. Evaluation of parameters of the equivalent circuit of the induction motor for asymmetrical power supply to the stator. *Elektromekhanichni i enerhozberihaiuchi systemy – Electromechanical and energy saving systems*, 2014, vol. 2, pp. 10-16. (Rus).

3. Malyar V.S., Malyar A.V. Mathematical modeling of periodic modes of electrotechnical devices. *Electronnoe modelirovanie – Electronic Modeling*, 2005, vol.27, no.3, pp. 39-53. (Rus).

4. Fyl'ts R.V. *Matematicheskie osnovy teorii elektromekhanicheskikh preobrazovatelei* [Mathematical foundations of the theory of electromechanical transducers]. Kyiv, Naukova Dumka Publ., 1979. 208 p. (Rus).

5. Shurub Yu.V. A mathematical model of an asynchronous capasitor engine with a thyristor control. *Tekhnichna elektrodynamika – Technical electrodynamics*, 1999, no.4, pp. 52-56. (Rus).

Received 09.03.2016

V.S. Malyar[1]*, Doctor of Technical Science, Professor,*
A.V. Malyar[1]*, Doctor of Technical Science, Professor,*
[1] Lviv Polytechnic National University,
12, S. Bandera Str., Lviv, 79013, Ukraine,
phone +380 32 2582119,
e-mail: svmalyar@polynet.lviv.ua

How to cite this article:

Malyar V.S., Malyar A.V. Mechanical characteristics of three-phase induction motors with single-phase power supply. *Electrical engineering & electromechanics*, 2016, no.3, pp. 21-24. doi: 10.20998/2074-272X.2016.3.03.

UDC 621.3 13.175.32 **doi: 10.20998/2074-272X.2016.3.04**

V.B. Finkelshtein, A.B. Yegorov

CHARACTERISTICS OF A 4-PHASE VALVE RELUCTANCE MOTOR WHEN POWERED BY UNCAPACITOR SWITCHBOARD

Purpose. ***Nowadays more and more in a variety of machines and mechanisms applied switched reluctance motor. When designing these engines solve the problem selection switch. While the switch scheme comprises symmetrical bridge and eight transistors, eight diodes; Miller switch comprises six transistors and six diodes; in company Graseby Controls Ltd switch circuit but four transistors and four diodes includes two capacitors. The aim is to develop a mathematical model, calculation program, a numerical analysis of the characteristics and parameters of the WFD and the characteristics of their work.*** ***Methodology.*** ***It is assumed that the resistance in the open state transistors and diodes for direct current is zero and the resistance of the transistors in the closed state, and diode reverse voltage is infinity. When feeding a single-phase motor and power at the same time two adjacent phases determined by the flow through the tooth.*** ***Results.*** ***The motor powered by a switch on the circuit symmetrical bridge power, which provides a maximum permissible winding temperature is 1.665 kW. But at the same time the surge up to 38.8%, resulting in high levels of noise and vibration. Through the installation of switching angles, ensuring reduction of torque ripple and reduce engine power to a level below which there is a decrease in the value of torque ripple, received power of 1,066 kW and a torque ripple value of 21.18 %. For engines with improved vibration acoustic characteristics necessary to use a switch of four transistors and four diodes.*** ***Practical value.*** ***For motors with improved vibration acoustic characteristics appropriate to apply uncapacitor switch on four transistors and four diodes, which allows you to receive half the value of torque ripple than the lowest value of the motor torque ripple, eating from a switch on the circuit asymmetric bridge. The cost of reluctance motor with uncapacitor switch on the circuit with four transistors and four diodes is more than two times less than the motor with the switch on the circuit asymmetric bridge.*** References 9, tables 1, figures 10.

Key words: **valve reluctance motor, switchboard, flux linkage of phases, rotor angle of rotation, motor power.**

Рассмотрены электромеханические процессы в вентильном реактивном двигателе и его характеристики при питании от коммутатора фирмы Graseby Controls Ltd с изъятыми из его схемы конденсаторами. Разработана математическая модель, проведен численный и экспериментальный анализ характеристик и параметров вентильного реактивного двигателя. Результаты, которые представлены в статье, разрешают проводить выбор числа витков и мощности двигателя в сравнении с двигателем, который питается от коммутатора по схеме асимметрического моста в зависимости от технических требований. Библ. 9, табл. 1, рис. 10.

Ключевые слова: **вентильный реактивный двигатель, коммутатор, потокосцепление фаз, угол поворота ротора, мощность двигателя.**

Introduction. Problem definition. Nowadays more and more in a variety of machines and mechanisms applied switched reluctance motor (SRM), known in the western countries and the United States as the Switched Reluctance Motor (SRM) [7-9], in Russia – as the valve-inductor motors [6] (VIM) and valve inductor-reluctance motors [2] (VIRM), in Ukraine – VRM. When designing these engines a problem of switch selection is solved.

Analysis of recent achievements and publications on the subject. While the switch scheme asymmetric bridge [9] (Fig. 1) comprises eight transistors, eight diodes; Miller switch [9] (Fig. 2) contains six transistors and six diodes; a switch circuit by Graseby Controls Ltd [9] (Fig. 3), but four transistors and four diodes includes two capacitors. Furthermore, in the switch (Fig. 3), a voltage imbalance that increases the torque ripple and a significant reduction in motor power.

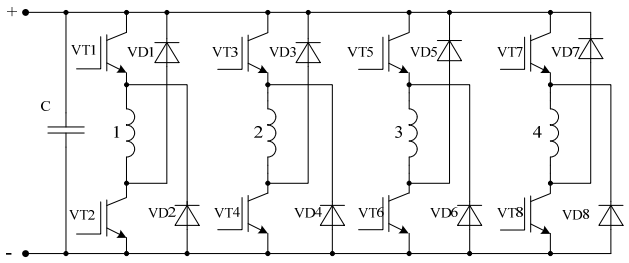

Fig. 1. Switch on the circuit of asymmetrical bridge

When the motor is powered by the scheme Miller its capacity is reduced by 20 % compared to the power of the engine when it is powered by a switch on the circuit asymmetric bridge [4]. Maximum engine power is obtained when it is powered by an asymmetrical bridge circuit compared to the power of the engine when powered by any of switches on other schemes. To a large extent determined by the properties of the switch performance.

In [5, 6], the switch (Fig. 5) used to supply four-phase VRM. This switch consists of four transistors and four diodes, but particularly of the circuit, and a mathematical model of the engine characteristics, as with a normal and a beak rotor during feeding from that switch are not considered.

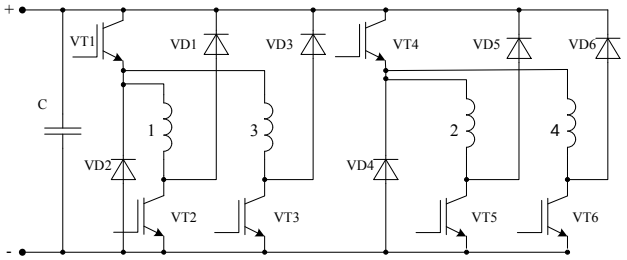

Fig. 2. Miller switch

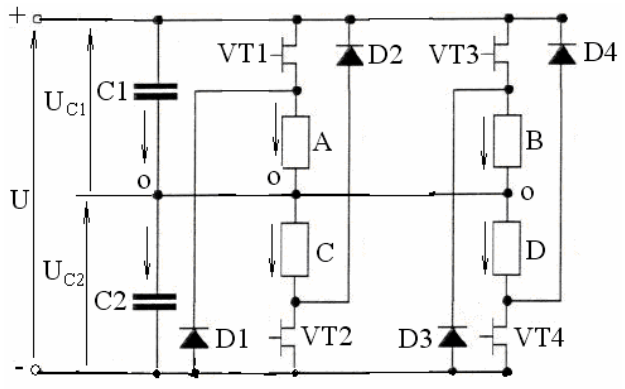

Fig. 3. Switch by Graseby Controls Ltd

The goal of the work is to develop a mathematical model to calculate the electromechanical characteristics of the VRM when powered by a switch with four transistors and four diodes to determine the parameters of the motor windings allowing to improve vibroacoustic characteristics and have strong economic performance.

Development of mathematical model. The magnetic circuit of the motor with windings with the combined phases is shown in Fig. 4.

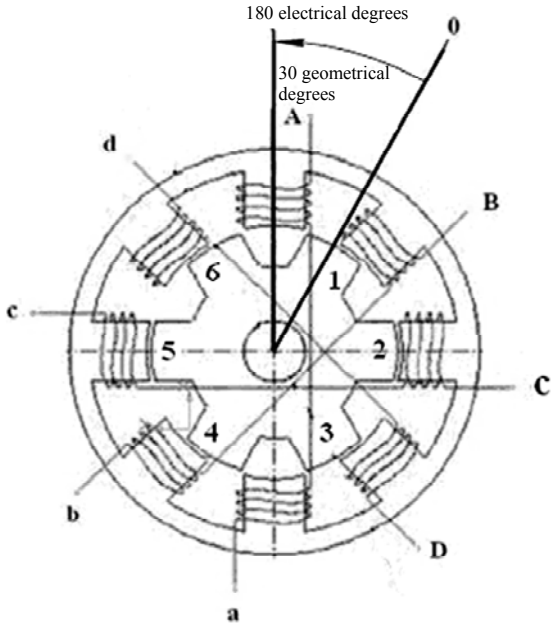

Fig. 4. Magnetic circuit of the motor

The switch circuit is shown in Fig. 5, the individual circuit units consist of the phases *A* and *D*; *C* and *B*.

It is assumed that the resistance of the transistors in the open state, and diode forward current to zero and the resistance of the transistors in the closed condition and co-diode reverse voltage is infinity. When feeding of one motor phase and simultaneously feeding the two adjacent phases (Fig. 4) is defined by tooth stream [2]. When you connect the second phase of the flow of the first phase has changed by 2.5 %. This allows you to accept the assumption of the absence of mutual phase inductance.

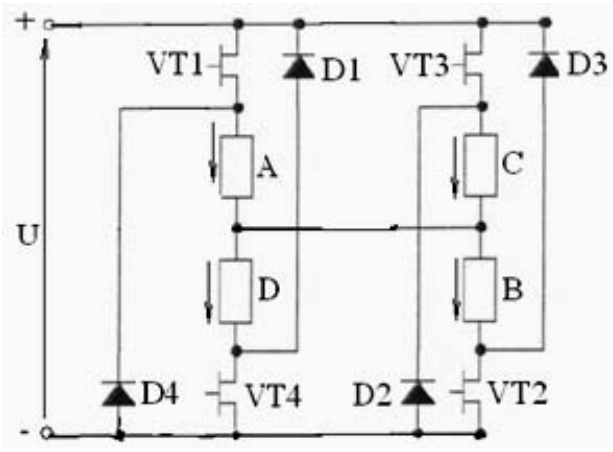

Fig. 5. Applied switch circuit

When the angle of rotation of the rotor ζ in electrical radians in the range $0 \le \zeta \le \pi / 2$, the transistors VT1 and VT2 are open and, if this current in *D* phases and *C* are not equal to zero, then phase *D* through the D1 diode and VT1 transistor being connected parallel to the phase *A* and phase *C* through VT2 transistor and a diode D2 is connected in parallel to phase *B*. The transistors VT3 and VT4 locked.

In this interval of the rotor rotation angle phase current, flux and torque of the VRM describes by the system of differential equations (1)

$$\begin{aligned} & i_A \cdot r + \frac{d\Psi_A(i_A,\zeta)}{dt} + i_B \cdot r + \frac{d\Psi_B(i_B,\zeta)}{dt} = U; \\ & i_C \cdot r + \frac{d\Psi_C(i_C,\zeta)}{dt} = -i_B \cdot r - \frac{d\Psi_B(i_B,\zeta)}{dt}; \\ & i_D \cdot r + \frac{d\Psi_D(i_D,\zeta)}{dt} = -i_A \cdot r - \frac{d\Psi_A(i_A,\zeta)}{dt}; \\ & i_D = i_A + i_C - i_B, \end{aligned} \tag{1}$$

where i_A, i_B, i_C and i_D are the phase currents, $\Psi_A(i_A, \zeta)$, $\Psi_B(i_B, \zeta)$; $\Psi_C(i_C, \zeta)$, $\Psi_D(i_D, \zeta)$ are the phase flux linkages as a function of the currents and the rotor rotation angle; *r* is the active phase winding resistance (all values – in SI units).

The fourth equation (1) holds in all bands of the rotor rotation angles.

In the rotor rotation angle range in electric radians $\pi/2 \le \zeta \le \pi$ transistors VT1 and VT4 are opened, and the transistors VT2 and VT3 – locked. In this case, the phase *B* is connected in parallel with phase *A* and phase *C* – in parallel with phase *D*. The initial phase of the parallel system of equations for the angles of rotation of indicated rotor interval may be represented as

$$\begin{aligned} & i_D \cdot r + \frac{d\Psi_D(i_D,\zeta)}{dt} + i_A \cdot r + \frac{d\Psi_A(i_A,\zeta)}{dt} = U; \\ & i_B \cdot r + \frac{d\Psi_B(i_C,\zeta)}{dt} = -i_A \cdot r - \frac{d\Psi_A(i_A,\zeta);}{dt} \\ & i_C \cdot r + \frac{d\Psi_C(i_C,\zeta)}{dt} = -i_D \cdot r - \frac{d\Psi_D(i_D,\zeta)}{dt}. \end{aligned} \tag{2}$$

In the rotor rotation angle range in electric radians $\pi \le \zeta \le 3 \cdot \pi/2$ transistors VT3 and VT4 open phase *A*

through VT4 transistor and a diode D4 connected in parallel *D* phase and phase *B* through the diode D3 and transistor VT3 is connected parallel to the phase *C*. Transistors VT1 and VT2 are locked. Electromagnetic processes in the VRM in the rotor rotation angle range described by the system

$$\begin{aligned} i_C \cdot r + \frac{\partial \Psi_C(i_C,\zeta)}{\partial i_C} + i_D \cdot r + \frac{\partial \Psi_D(i_D,\zeta)}{\partial i_D} = U; \\ i_A \cdot r + \frac{d\Psi_A(i_A,\zeta)}{dt} = -i_D \cdot r - \frac{d\Psi_D(i_D,\zeta)}{dt}; \\ i_B \cdot r + \frac{d\Psi_B(i_B,\zeta)}{dt} = -i_C \cdot r - \frac{d\Psi_C(i_C,\zeta)}{dt}. \end{aligned} \quad (3)$$

In the range of angles of rotation of the rotor in electrical radians $3\cdot\pi/2 \le \zeta \le 2\cdot\pi$ transistors VT3 and VT2 open, and transistors VT1 and VT4 – locked. The phase *A* is connected in parallel to the phase *B*, and the phase *D* – in parallel to the phase *C*. The VRM equations can be written as

$$\begin{aligned} i_B \cdot r + \frac{d\Psi_B(i_B,\zeta)}{dt} + i_C \cdot r + \frac{d\Psi_C(i_C,\zeta)}{dt} = U \\ i_D \cdot r + \frac{\partial \Psi_D(i_D,\zeta)}{\partial i_D} = -i_C \cdot r - \frac{\partial \Psi_C(i_C,\zeta)}{\partial i_C}; \\ i_A \cdot r + \frac{d\Psi_A(i_A,\zeta)}{dt} = i_B \cdot r + \frac{d\Psi_B(i_B,\zeta)}{dt}. \end{aligned} \quad (4)$$

Analytical flux dependences on the current phase and angle of rotation of the rotor are presented in [3].

To solve systems (1-4) by the Runge-Kutta method should be presented as a system of linear algebraic equations for the production of time-phase currents. Given that

$$\begin{aligned} \frac{d\Psi(i,\zeta)}{dt} = \frac{\partial \Psi}{\partial i} \cdot \frac{di}{dt} + \omega \cdot \frac{\partial \Psi}{\partial \zeta}; \\ \omega = \frac{d\zeta}{dt}. \end{aligned} \quad (5)$$

Systems of differential equations (1-4), authorized with respect to the first derivatives of currents, in conjunction with the fourth equation of (1), the second equation of (5) and equation (6) allow using Runge-Kutta method, to get depending on the currents, torques and the phase flux linkage on the time and angle of the rotor in the gate, and the speed on time

$$\begin{aligned} \frac{d\omega}{dt} = \left(\int_0^{i_A} \frac{\partial \Psi_A(i_A,\zeta)}{\partial \zeta} \cdot di_A + \int_0^{i_B} \frac{\partial \Psi_B(i_B,\zeta)}{\partial \zeta} \cdot di_B + \right. \\ \left. + \int_0^{i_C} \frac{\partial \Psi_C(i_C,\zeta)}{\partial \zeta} \cdot di_C + \int_0^{i_D} \frac{\partial \Psi_D(i_D,\zeta)}{\partial \zeta} \cdot di_D - M_c \right) / J, \end{aligned} \quad (6)$$

where M_c is the drag torque on the motor shaft; J is the moment of inertia of the rotating masses.

In the correspondence with the presented mathematical model the calculation program in the environment MathCAD 2001 is developed.

Fig. 6 shows the torque phase of the angle of rotation of the rotor when powered from a switch on the VRM of Fig. 5 at the maximum power (solid curve), at equal specific losses (dot dashed line) with specific losses when powered by the VRM switch scheme asymmetrical bridge, at least torque ripple (dashed curve).

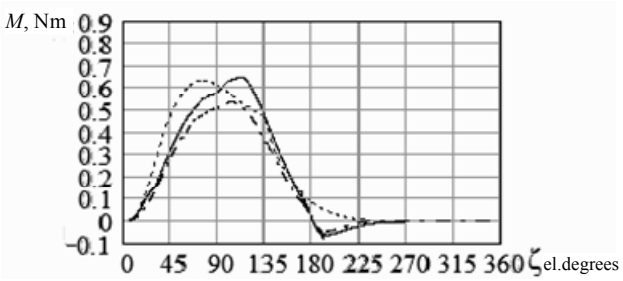

Fig. 6. Dependence of the phase torque on the angle of rotation of the rotor when VRM powered from the switch according to Fig. 5

Fig. 7 shows the resulting torque on the angle of rotation of the rotor when powered from a switch on the VRM of Fig. 5 at the maximum power (solid line), with equation of specific losses (dash dotted line) with specific losses when powered by the VRM switch by the scheme asymmetrical bridge, at least torque ripple (dashed curve).

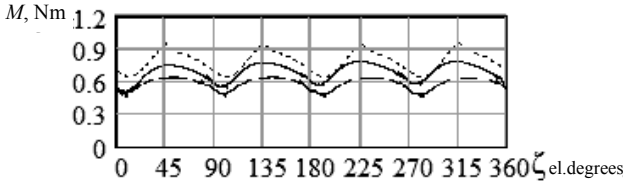

Fig. 7. Dependence of the resultant moment on the angle of rotation of the rotor when VRM powered from the switch according to Fig. 5

Figures 8, 9 show curves of current change and the phase flux linkages, respectively.

Fig. 8 shows the phase current dependence on the angle of rotation of the rotor when powered from a switch on the VRM of Fig. 5 at the maximum power (solid curve), at equal specific losses (dot dashed line) with specific losses when powered by the VRM switch scheme asymmetrical bridge, at least torque ripple (dashed curve).

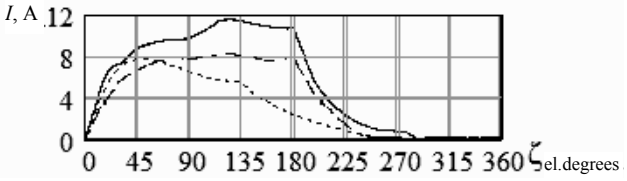

Fig. 8. Dependence of the current phase on the angle of rotation of the rotor when VRM powered from the switch according to Fig. 5

Fig. 9 shows the dependence of the phase flux linkage on angle of rotation of the rotor when powered from a switch on the VRM of Fig. 5 at the maximum power (solid curve), at equal specific losses (dot dashed line) with specific losses when powered by the VRM switch scheme asymmetrical bridge, at least torque ripple (dashed curve).

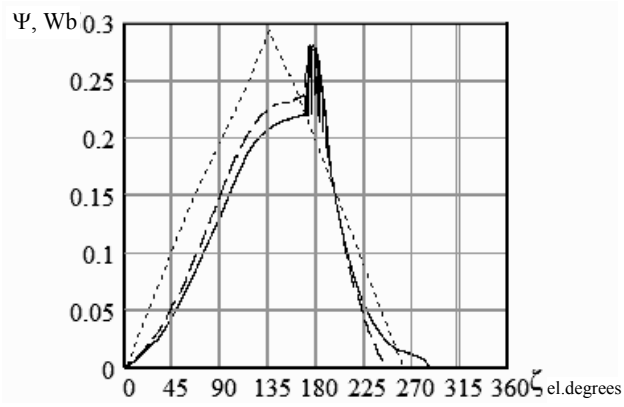

Fig. 9. Dependence of the phase flux linkage on the angle of rotation of the rotor when VRM powered from the switch according to Fig. 5

Fig. 10 shows the dependence of the phase voltage of the rotor rotation angle. The results of calculation of the time of one phase of the VRM are shown in Fig. 6, the resulting torque – in Fig. 7.

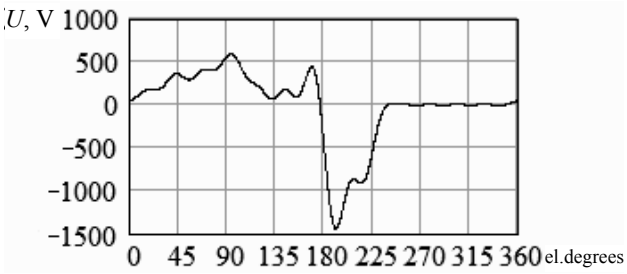

Fig. 10. Phase voltage dependence on the rotor rotation angle

The calculated data of motors are given in Table 1 where P_2 is the net power; n is the rotational speed; I_{ph} is the phase current; P_o are the winding losses; P_{Fe} are the iron losses; P_{sch} are the losses in the switch circuit; P_{mech} are the mechanical losses; ΔM is the value of torque ripple; p_t are the losses per unit of outer lateral surface of the stator core (specific losses – the ratio of total losses in the motor area to the outer lateral surface of the stator core); W_p is the number of turns in the phase winding.

Table 1

P_2, W	n, RPM	I_{ph}, A	η, %	P_o, W	P_{Fe}, W	P_{sch}, W	P_{mech}, W	ΔM, %	p_t, W/cm^2	B, T	W_p	Switch circuit
1665	6006	3.863	61.6	59.8	540	114	325	38.8	1.621	1.121	130	Asym. bridge (Fig. 1)
1066	5997	2.67	60.7	34.56	256	79	322	21.18	1.07	0.772	143	Asym. bridge (Fig. 1)
1066	5937	3.464	53.2	29.61	524	30.4	325	12.18	1.59	1.128	102	4 diodes, 4 transistors (Fig. 5)

* Note. Calculation of losses in the steel is carried out by [1].

The motor powered by a switch on the circuit asymmetric bridge (Fig. 1), the power, which provides a maximum permissible winding temperature is 1.665 kW. But at the same time the surge up to 38.8 %, resulting in high levels of noise and vibration. Through the installation of switching angles, to ensuring reduction in torque ripple and reduce engine power to a level below which there is a decrease in the value of torque ripple, received power of 1.066 kW and a torque ripple value of 21.18 %. The same performance is achieved when the engine power switch to it from four transistors and four diodes. At the same time the cost of the switch according to the scheme of the asymmetric bridge to date is 1200 UAH. The switch according to Fig. 5 cheaper, the cost of it is 540 UAH. The pulsations of the engine torque with the switch, as shown in Table 1, almost half that of the smallest torque ripple motor powered by a switch on the circuit asymmetric bridge.

Consequently, for motors with improved vibroacoustic characteristics it is necessary to apply switch according to Fig. 5.

Conclusions.

1. For improved vibroacoustic characteristics of the VRM is advisable to apply uncapacitor switch on four transistors and four diodes, which allows you to receive half the amount of torque ripple than the lowest value of the motor torque ripple, eating from a switch on the circuit asymmetric bridge.

2. The cost of the VRM with uncapacitor switch on the circuit with four transistors and four diodes is more than two times less than the engine with the switch on the circuit asymmetric bridge.

REFERENCES

1. Galaiko L.P. The account of magnetic losses for want of designing switched reluctance motors. *Elektrotekhnika i elektromekhanika – Electrical engineering & electromechanics*, 2003, no.2, pp. 17-18. (Rus). **doi: 10.20998/2074-272X.2003.2.04**.

2. Gollandtsev Y.A. *Ventil'nye induktorno-reaktivnye dvigateli* [Valve inductor and jet engines]. St. Petersburg, GNC RF CNII Elektropribor Publ., 2003. 148 p. (Rus).

3. Zinchenko E.E., Finkelshtein V.B. T A technique of magnetization curve approximation for switched reluctance motors. *Elektrotekhnika i elektromekhanika – Electrical engineering & electromechanics*, 2009, no.1, pp. 13-16. (Rus). **doi: 10.20998/2074-272X.2009.1.03**.

4. Zinchenko E.E., Finkelshtein V.B. Performance analysis of a switched reluctance motor fed through an asymmetric half-bridge converter and a Millers bridge converter. *Elektrotekhnika i elektromekhanika – Electrical engineering & electromechanics*, 2012, no.1, pp. 33-35. (Rus). **doi: 10.20998/2074-272X.2012.1.07**.

5. Luchko A.R. *Povyshenie effektivnosti electroprivoda bytovyh pogruzhnych nasosov putem ispolzovaniya ventilnych dvigatelei. Diss. cand. techn. nauk* [Increase of efficiency of the electric drive of household submersible pumps by use of valve inductor engines. Cand. tech. sci. diss.]. Zaporozhye, 2005. 160 p. (Rus).

6. Shabayev V.A., Kruglikov O.V., Tubis Ya.B. *Ventil'no-induktornyi chetyrekhfaznyi nereversivnyi dvigatel'* [Valve inductor 4-phase irreversible motor]. Patent Russian Federation, no. 2390085, 2010. (Rus).

7. Krishnan R. *Switched Reluctance Motor Drives. Modeling, Simulation, Analysis, Design and Applications*. CRC Press, 2001. 398 p. **doi: 10.1201/9781420041644**.

8. Lawrenson P.J., Stephenson J.M., Fulton N.N., Blenkinsop P.T., Corda J. Variable-speed switched reluctance motors. *IEE Proceedings B Electric Power Applications*, 1980, vol.127, no.4, p. 253. **doi: 10.1049/ip-b.1980.0034**.

9. Miller T.J.E. *Switched reluctance motors and their control*. Magna Physics Publishing and Clarendon Press. Oxford, 1993.

Received 22.03.2016

V.B. Finkelshtein[1]*, Doctor of Technical Science, Professor,*
A.B. Yegorov[2]*, Candidate of Technical Science, Associate Professor,*
[1] O.M. Beketov National University of Urban Economy in Kharkiv,
12, Revolution Str., Kharkiv, 61002, Ukraine,
phone +380 57 7319528, e-mail: finalvb@gmail.com
[2] Ukrainian Engineering Pedagogics Academy,
16, Universitetskaya Str., Kharkiv, 61003, Ukraine,
phone +380 66 7228206, e-mail: diaskk@yandex.ru

How to cite this article:
Finkelshtein V.B., Yegorov A.B. Characteristics of a 4-phase valve reluctance motor when powered by uncapacitor switchboard. *Electrical engineering & electromechanics*, 2016, no.3, pp. 25-29. doi: 10.20998/2074-272X.2016.3.04.

UDC 621.9:681.54 **doi: 10.20998/2074-272X.2016.3.05**

A.V. Chaban, V.R. Levoniuk, I.M. Drobot, A.F. Herman

MATHEMATICAL MODEL OF ELECTROMAGNETIC PROCESSES IN LEHERA LINE AT OPEN-CIRCUIT OPERATION

Purpose. The work proposed for the modeling of transients in Lehera line uses a modified Hamilton-Ostrogradskiy principle. The above approach makes it possible to avoid the decomposition of a single dynamic system that allows you to take into account some subtle hidden movements. This is true for systems with distributed parameters, which in the current work we are considering. Methodology. Based on our developed new interdisciplinary method of mathematical modeling of dynamic systems, based on the principle of modified Hamilton-Ostrogradskiy and expansion of the latter on the non-conservative dissipative systems, build mathematical model Lehera line. The model allows to analyze transient electromagnetic processes in power lines. Results. In this work the model used for the study of transients in the non-working condition Lehera line. Analyzing the results shows that our proposed approach and developed based on a mathematical model is appropriate, certifying physical principles regarding electrodynamics of wave processes in long power lines. Presented in 3D format, time-space distribution function of current and voltage that gives the most information about wave processes in Lehera line at non-working condition go. Originality. The originality of the paper is that the method of finding the boundary conditions of the third kind (Poincare conditions) taking into account all differential equations of electric power system, i.e. to find the boundary conditions at the end of the line involves all object equation. This approach enables the analysis of any electric systems. Practical value. Practical application is that the wave processes in lines affect the various kinds of electrical devices, proper investigation of wave processes is the theme of the present work. References 12, figures 12.

Key words: **mathematical modeling, Hamilton-Ostrogradskiy principle, Euler-Lagrange equation, electric power system, power line with distributed parameters.**

В работе, на основе обобщенного междисциплинарного (интердисциплинарного) метода математического моделирования, основанного на модификации интегрального вариационного принципа Гамильтона-Остроградского, предложена математическая модель двухпроводной длинной линии электропередач, которая работает на холостом ходу. Представлены результаты компьютерной симуляции переходных процессов в виде рисунков, которые анализируются. Библ. 12. рис. 12.

Ключевые слова: **математическое моделирование, принцип Гамильтона-Остроградского, уравнение Эйлера-Лагранжа, электроэнергетическая система, линия электропередач с распределенными параметрами.**

Introduction. Mathematical modeling of complex electrical systems today is an important technical problem. With mathematical simulation device can analyze electromagnetic and electromechanical transient processes in electrical facilities and systems, not using for the latest expensive full-scale experiments. No exception here and electricity.

In the current work as an example Lehera system analysis [1] uses a long line with distributed parameters that runs on direct current. We know that these lines have found their proper place in power systems around the world. Transmission of electricity in this way: it reduces losses in the lines (due absence of skin effect phenomenon) makes possible association between local power systems that operate with varying frequency and reduces the cost of construction for large distances due to fewer wires and auxiliary fittings, etc.

Unfortunately, in our country for some reason, however, and economic, in 2014 were brought down the only DC line Volgograd-Donbass, which has been designed for a voltage of 800 kV. But in highly developed foreign countries mentioned lines are not only effective, but commissioned new due to certain advantages mentioned above. Here we can mention the following lines: Line Pacific DC power 1400 MW, ± 400 kV voltage, length of 1362 km for the transmission of electricity from hydropower plants in Oregon grid in Los Angeles; power transmission line HPP «Xiangjiaba» – China's Shanghai ± 800 kV voltage guarantees transmitting 6400 MW over a distance of 2000 km; Canada three transmission line length of about 900 km, built by HPP Nelson River, located in the Arctic Circle, to the city Winnipeg in the South of country. Epps was the third power of 2000 MW at a voltage of ± 500 kV; Brazil put into operation two chains of the line of HPP Itaipu of throughput of 3,150 MW at a voltage of ± 600 kV. The length of each circuit of about 800 km, and others [2].

Analysis of last investigations. Among a number of scientific papers devoted to the analysis of transient processes in power systems look at some of them, next to the theme of this work.

In [3] developed a mathematical model of two- and three wire power line AC to study transient processes and phenomena of overvoltage in a 500 kV line. Based on the software code ATP-EMTP transients were calculated and investigated the phenomenon over during the emergency state line.

A practical approach in the study of transient electromagnetic processes in [4] is represented. After describing the many cases of simulation modeling for selected items grid requirements are presented. Also, a comparative analysis of studies of transient electromagnetic processes in the correct and incorrect model grid is made.

In [5] the mathematical model of electromagnetic transients in electrical systems that is based on discrete nodal equations in phase coordinates and implicit numerical integration methods, which enables modeling transients with symmetric and asymmetric switching and injuries in electrical networks of any configuration.

The work [6] covers a wide range of analysis and derivatives re-established processes in electricity under the original angle. Materials book is based on the classical approach to the modeling of electric-energy-systems. Unfortunately, apparently because of the limitation of the volume of the book, the latter did not present the results of computer simulation of wave processes in lines.

The goal improvement on the base of utilization of variation approaches, methods of mathematical modeling of transients in Lehera line which operates on a non-working pace, and due to this more correctly simulation of wave processes.

Variation model of the Lehera line. To build mathematical models of objects under consideration with a high level of adequacy to properly use basic fundamental laws applied physics, applied in the relevant fields of science [9]. In our case this is electrodynamics [1, 6, 7].

Mathematical modeling is usually using two approaches. The first – a classic approach based on the law of conservation of energy and the second – variation based on minimizing functional of the system [9]. Each of these approaches has its advantages and drawbacks, but when used properly leads to reliable results [8]. In other words, the roads leading to the final model is differ but obtained the result – the same. Usually, choosing the right approach to modeling is a proper of researcher.

We offer analysis of transients in line Lehera use modified Hamilton-Ostrogradskiy principle (variation technique) [9]. The above approach allows you to avoid decomposition of single dynamic system, and to obtain initial state equation energetic exclusively on a single approach, enhanced by constructing Lagrange function [9]. In other words, the proposed way allows you to build dynamic systems models based on interdisciplinary approaches. This is especially true for systems with distributed parameters, and in that long transmission lines, as in the equations of the facility it is necessary to consider: electrostatic effects (arc phenomenon), thermodynamic effects (conductors heating, especially during melting ice) mechanical impacts on wires, in particular, various oscillations (especially resonant and close to resonance (beat fluctuations) processes) and others. In the current work we do not consider the above mentioned effects, but these effects, we plan to further consider our investigations actually for that we offer this approach.

A key element of the principle of modified Hamilton-Ostrogradskiy is extended non-conservative Lagrangian. We present its analytical form [8, 10]:

$$L^* = \widetilde{T}^* - P^* + \Phi^* - D^*, \quad (1)$$

where L^* is the modified Lagrange function, $\widetilde{T}^*$ is the kinetic co-energy, P^* is the potential energy, Φ^* is the dissipation energy, D^* is the energy of external on-potential forces.

We have already mentioned that the line Lehera generally seen as a system with distributed parameters [10, 11]. Then the elements of the modified Lagrange function will not feature power, and their respective densities [1]. So, functional of action by Hamilton-Ostrogradskiy will have a form [9]:

$$S = \int_{t_1}^{t_2} \left(L^* + \int_l L_l dl \right) dt, \; I = \int_l L_l dl \text{, here } L^* = 0, \quad (2)$$

where S is the action by Hamilton-Ostrogradskiy, L_l is the linear density of the modified Lagrange function, I is the energetic functional.

We write components of the expanded Lagrange function (mean linear density) [9]:

$$\frac{\partial T^*}{\partial x} \equiv T_l = \frac{L_0 Q_t^2}{2}, \frac{\partial P^*}{\partial x} \equiv P_l = \frac{1}{2C_0} Q_x^2, Q_t \equiv \frac{\partial Q}{\partial t} = i; \quad (3)$$

$$\frac{\partial \Phi^*}{\partial x} \equiv \Phi_l = \Phi_{l3} - \Phi_{lB} = \int_0^t \left(\frac{R_0}{2} Q_t^2 - \frac{g_0}{2C_0^2} Q_x^2 \right)_{|t=\tau} d\tau, \quad (4)$$

where $i(x, t)$ is the current in the line, R_0, g_0, C_0, L_0 are the line parameters, Φ_{l3} is the external energy dissipation, Φ_{lB} is the internal energy dissipation, $Q(x,t)$ is the charge of the line.

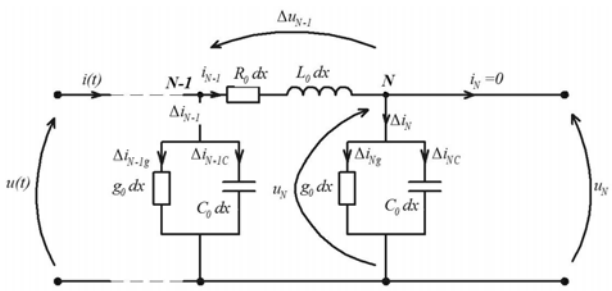

Fig. 1. Electric circuit of the Lehera line at open-circuit operation

It is important to note that in equation (4) minus sign appears! This is due to the fact that the function external dissipation depends on the leakage current that flow between the line wires. Obviously, the electric transmission line during the transfer of energy from the source to the consumer consumes the energy dissipated in in space. In other words, energy is transferred exclusively via the electromagnetic field lines and wires only indicate the direction of electromagnetic wave propagation [1].

Taking into account the equations (3), (4) the energy functional will look like [9]:

$$I = \int_l \left\{ \frac{L_0}{2} Q_t^2 - \frac{1}{2C_0} Q_x^2 + \int_0^t \left(\frac{R_0}{2} Q_t^2 - \frac{g_0}{2C_0^2} Q_x^2 \right)_{|t=\tau} d\tau \right\} dl. \quad (5)$$

We write the variation of the energy functional (5) and equate it to zero

$$\int_l \left\{ \left(L_0 Q_t + R_0 \int_0^t Q_{t|t=\tau} d\tau \right) \delta Q_t - \left(\frac{1}{C_0} Q_x + \frac{g_0}{C_0^2} \int_0^t Q_{x|t=\tau} d\tau \right) \delta Q_x \right\} dl = 0. \quad (6)$$

Next, for each element of integrand expressions we use the rule of integration by parts, also known as Gauss-Ostrogradskiy theorem. Then, for the first bracket will be [9]:

$$-\int_l \frac{\partial}{\partial t}\left(L_0 Q_t + R_0 \int_0^t Q_{t|t=\tau} d\tau \right) \delta Q dl + \Omega_t \qquad (7)$$

and for the second one:

$$-\int_l \frac{\partial}{\partial x}\left(\frac{1}{C_0} Q_x + \frac{g_0}{C_0^2} \int_0^t Q_{x|t=\tau} d\tau \right) \delta Q dl + \Omega_x , \quad (8)$$

where Ω_t, Ω_x are the boundary conditions for the functional (5).

From here we can write

$$\delta I = \int_l \left\{ \frac{1}{C_0} \frac{\partial^2 Q}{\partial x^2} + \frac{g_0}{C_0^2} \int_0^t \frac{\partial^2 Q}{\partial x^2}_{|t=\tau} d\tau - L_0 \frac{\partial^2 Q}{\partial t^2} - \right. \\ \left. - R_0 \frac{\partial}{\partial t} \int_0^t \frac{\partial Q}{\partial t}_{|t=\tau} d\tau \right\} \delta Q dl + \Omega = 0, \ \Omega = \Omega_t + \Omega_x. \qquad (9)$$

It is easy to see that variation of energy functional can be zero only when equality to zero of integrand or variations function of the charge of the line. As δQ never can be equal to zero [9, 12] the energy functional (9) obtains a stationary value only in the case when integrand equals zero, i.e. at presence of the Euler-Poisson equation [9, 12]

$$\frac{1}{C_0} \frac{\partial^2 Q}{\partial x^2} + \frac{g_0}{C_0^2} \int_0^t \frac{\partial^2 Q}{\partial x^2} d\tau - L_0 \frac{\partial^2 Q}{\partial t^2} - R_0 \frac{\partial Q}{\partial t} = 0 . \quad (10)$$

We write for the equation (10) an expression of steady-state connections [1, 10]

$$-\frac{1}{C_0} \frac{\partial^2 Q}{\partial x^2} = L_0 \frac{\partial^2 Q}{\partial t^2} + R_0 \frac{\partial Q}{\partial t} . \qquad (11)$$

Taking into account the expression [1]

$$\int_0^t \frac{\partial^2 Q}{\partial t^2}_{|t=\tau} d\tau = \frac{\partial Q}{\partial t}, \ \int_0^t \frac{\partial Q}{\partial t}_{|t=\tau} d\tau = Q \qquad (12)$$

we obtain finally the commonly known telegraph equation [1, 10]

$$\frac{\partial^2 Q}{\partial x^2} = L_0 C_0 \frac{\partial^2 Q}{\partial t^2} + \left(R_0 C_0 + g_0 L_0 \right) \frac{\partial Q}{\partial t} + g_0 R_0 Q . \quad (13)$$

The equation of the Lehera line (telegraph equation) is written for the function of the charge of the line. However, it is easily transformed to the common telegraph equation

$$\frac{\partial^2 \lambda}{\partial x^2} = L_0 C_0 \frac{\partial^2 \lambda}{\partial t^2} + \left(R_0 C_0 + g_0 L_0 \right) \frac{\partial \lambda}{\partial t} + g_0 R_0 \lambda, \ \lambda = (Q, u, i) . \quad (14)$$

Experience shows that for more optimal description of physical processes in the line it is useful to use as a general function a function of voltage, i.e. $\lambda = u(x,t)$ [1, 10].

We rewrite (14) in such a way:

$$\frac{\partial v}{\partial t} = \left(C_0 L_0 \right)^{-1} \left(\frac{\partial^2 u}{\partial x^2} - \left(g_0 L_0 + C_0 R_0 \right) v - g_0 R_0 u \right), \ \frac{\partial u}{\partial t} = v . \quad (15)$$

The most important problem solving equations (15) is to determine the initial ($v(x,t)|_{t=to}$) and boundary ($u(x,t)|_{x=0}$ and $u(x,t)|_{x=l}$) conditions. As to the first, then the problem is solved in the accustomed way (they calculate their from previous research or take zero). The main problem is to find the boundary conditions. In general, the voltage at the beginning $u(x,t)|_{x=0}$ and at the end $u(x,t)|_{x=l}$. Of the line are unknown. In the particular case (on the current work) voltage is known at the beginning of the line, while at the end of the line – no. Actually finding this voltage we loan.

We write equations (11) in such a way (taking into account $Q_x(x,t) = C_0 u(x,t)$):

$$-\frac{\partial u(x,t)}{\partial x} = R_0 i(x,t) + L_0 \frac{\partial i(x,t)}{\partial t} . \qquad (16)$$

Further, for the power transmission line we write equations (15), (16) in the discrete space (we discretize them by the line method)

$$\frac{dv_j}{dt} = \left(C_0 L_0 \right)^{-1} \left(\frac{u_{j-1} - 2u_j + u_{j+1}}{(\Delta x)^2} - \left(g_0 L_0 + \right. \right. \\ \left. \left. + C_0 R_0 \right) v_j - g_0 R_0 u_j \right), \ u_1 = u(x,t)\big|_{x=0}, \ u_N = u(x,t)\big|_{x=l} \qquad (17)$$

$$-\frac{u_{j+1} - u_{j-1}}{2\Delta x} = R_0 i_j + L_0 \frac{di_j}{dt} ; \qquad (18)$$

$$\frac{du_j}{dt} = v_j , \quad j = 2, ..., N-1 . \qquad (19)$$

We rewrite equations (17), (18) for the N-th node of discretization in the correspondence with Fig. 1 in such a form:

$$\frac{dv_N}{dt} = \frac{1}{C_0 L_0} \left[\frac{1}{(\Delta x)^2} \left(u_{N-1} - 2u_N + u_{N+1} \right) - \right. \\ \left. - \left(g_0 L_0 + C_0 R_0 \right) v_N - g_0 R_0 u_N \right] ; \qquad (20)$$

$$-\frac{u_{N+1} - u_{N-1}}{2\Delta x} = 0 , \qquad (21)$$

where u_{N+1} is the discretization node voltage function at the fictitious layer [10] which will be found from the equation (21).

Then,

$$u_{N+1} = u_{N-1} . \qquad (22)$$

Taking into account (20) and (22) we write the final equation of the long line for the N-th node

$$\frac{dv_N}{dt} = \frac{2}{C_0 L_0 (\Delta x)^2} u_{N-1} - \left(\frac{2}{C_0 L_0 (\Delta x)^2} + \frac{g_0 R_0}{C_0 L_0} \right) u_N - \\ - \frac{g_0 L_0 + C_0 R_0}{C_0 L_0} v_N , \qquad (23)$$

$$\frac{du_N}{dt} = v_N . \qquad (24)$$

An important functional dependence that is interesting for the potential users is current value in elements of the Lehera line. Its calculation is possible in such a way. Discretizing equation (16) by the line method (right derivative) we have:

$$-\frac{u_{j+1} - u_j}{\Delta x} = R_0 i_j + L_0 \frac{di_i}{dt} . \qquad (25)$$

From here we obtain finally

$$\frac{di_j}{dt} = \frac{1}{L_0 \Delta x} \left(u_j - u_{j+1} \right) - \frac{R_0}{L_0} i_j , \ j = 1, ..., N-1 . \quad (26)$$

Compatible integration is subject to this system of differential equations: (17), (19), (23), (24), (26).

Computer simulation results. Computer simulation is carried out for the Lehera line at DC at open-circuit operation. The line has the following parameters: $R_0 = 0.86 \cdot 10^{-1}$ Ω/km, $L_0 = 0.134 \cdot 10^{-12}$ H/km, $C_0 = 0.85 \cdot 10^{-8}$ F/km, $g_0 = 0.375 \cdot 10^{-7}$ S/km, length of the line l = 600 km. The line is supplied by the DC voltage $u(x,t)|_{x=0}$ = 400 kV.

In Fig. 2-4 spatial distribution of the electromagnetic wave as functional dependences of currents (1) and voltages (2) is presented. From these Figures we can see physical basics of electromagnetic processes in the long Lehera line. Let us analyze these processes.

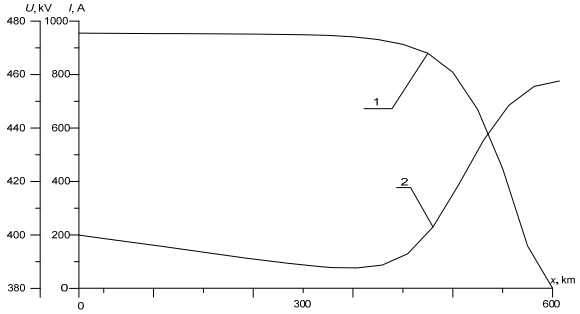

Fig. 2. Distributions of current (1) and voltage (2) in the line at t = 0.002 s

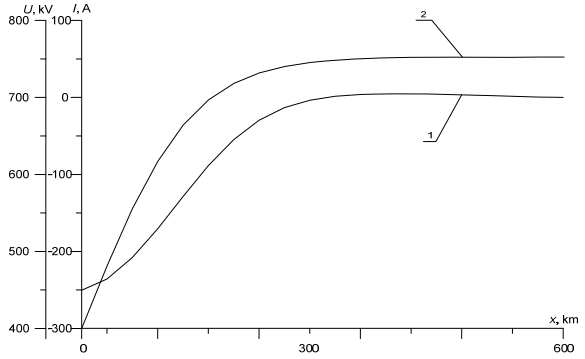

Fig. 3. Distributions of current (1) and voltage (2) in the line at t = 0.004 s

Fig. 2 shows the spatial distribution of functions of current and at time 0.002 s. Analyzing the mentioned Figure it is easy to see that the function of voltage begins to decrease, and the central line rises sharply upward. A stream function in the same place on the contrary – falls.

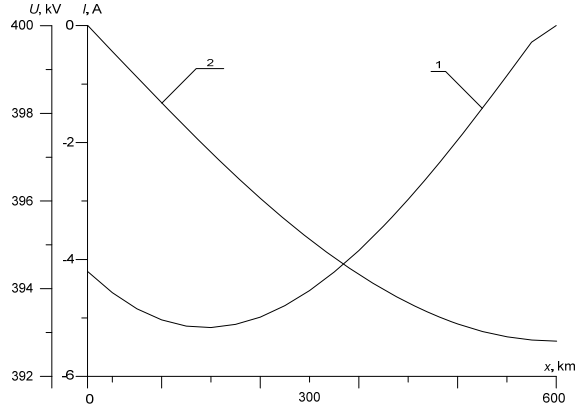

Fig. 4. Distributions of current (1) and voltage (2) in the line at t = 0.1 s

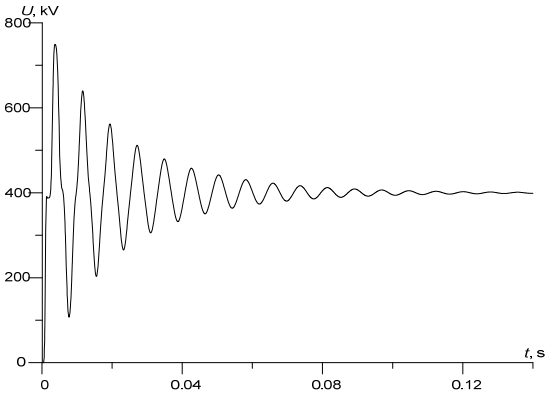

Fig. 5. Representation of the voltage transient function in the central point of the line

Recall that although the line is at open-circuit operation, leakage currents and currents in cell lines will be present. Actually the reason – is capacitive currents between the wires line. Obviously, at the end of the transmission line current will equal zero because the line is unloaded.

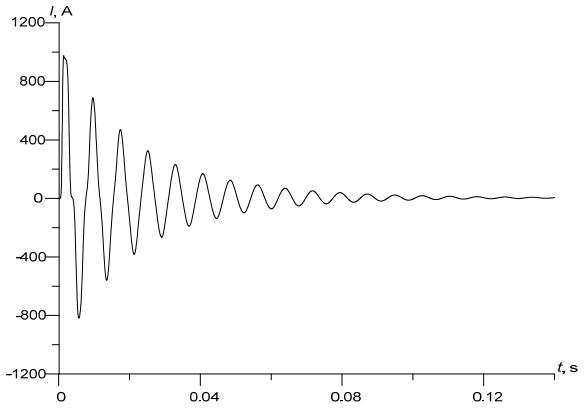

Fig. 6. Representation of the current transient function in the central point of the line

Fig. 3 shows the same, but in time 0.004 s. If at time 0.002 s (see Fig. 2) function of voltage increased to 460 kV but at time 0.004 s this growth was 750 kV. Voltage has almost doubled. As for the current, they fell by almost four times.

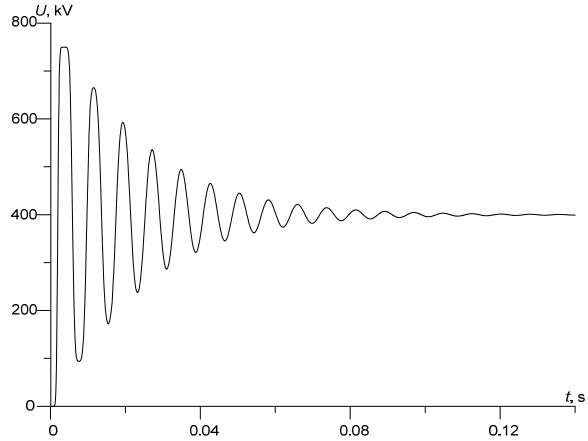

Fig. 7. Representation of the voltage transient function at the end of the line

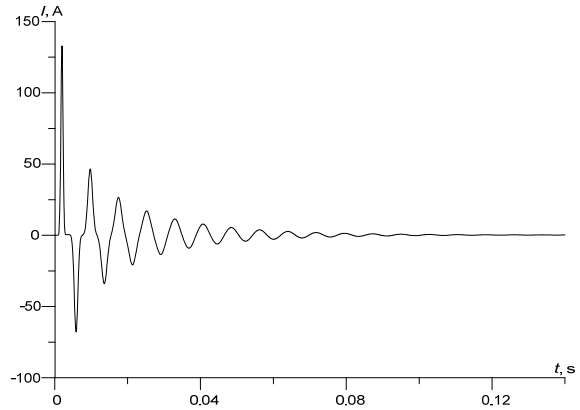

Fig. 8. Representation of the current transient function at the end of the line

Fig. 4 shows again the same as in Fig. 2 and 3 at the time when the transition process is almost completed. Of the Figure shows that deviation of functions of voltage and current almost took a minimum value. In other words, the amplitude of the electromagnetic wave due dissipative process significantly decreased. Oscillation process practically attenuates.

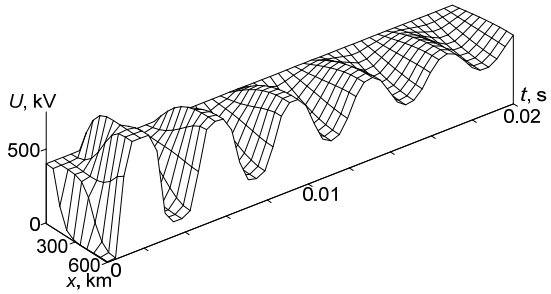

Fig. 9. Temporal-spatial distribution of the voltage function at $t \in [0; 0.02]$ s

Fig. 5-8 show transient functional dependences of voltage and current (temporal distribution). The first two Figures concern central node of the line for voltage and the central segment of the line for line. The second two Figures – the penultimate node of the line and penultimate discrete circuit of the line.

Through a comparative analysis of the above Figures it is easy to see that the function of voltage (see Fig. 5 and 7) changes little. See quite a different picture (see Fig. 6 and 8) regarding currents. The current changes almost 8 times. This is because the line power transmission line is (open-circuit operation).

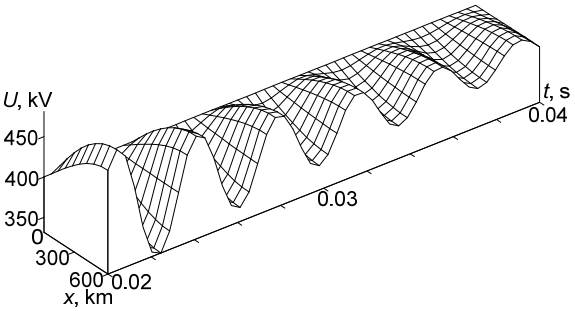

Fig. 10. Temporal-spatial distribution of the voltage function at $t \in [0.02; 0.04]$ s

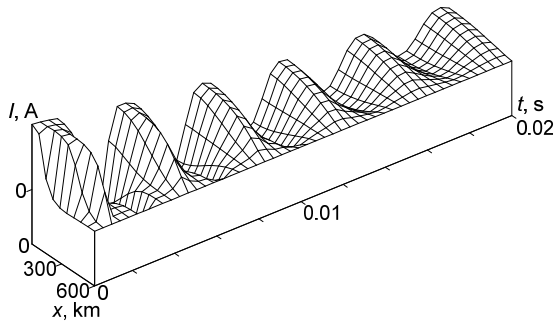

Fig. 11. Temporal-spatial distribution of the current function at $t \in [0; 0.02]$ s

Fig. 9 and 10 represent the line voltage as a function of time and spatial coordinates. These figures are presented in 3D format. Notably relatively high information content of these figures, which is that the spatial and temporal distribution of creating three-dimensional space. It is advisable to analyze the Figures mentioned in comparison with Fig. 2-5 and 7.

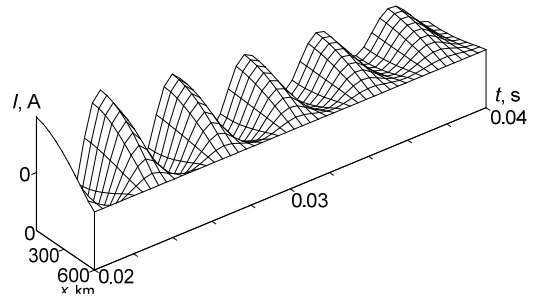

Fig. 12. Temporal-spatial distribution of the current function at $t \in [0.02; 0.04]$ s

Fig. 11 and 12 show the same as the previous two, but the function of current. As we see the function of voltage and current are in opposite phase. Because the nature of the stress associated with the electric field and the magnetic current we can make a conclusion of space perpendicular fields E and B which maintains the classic electrodynamics [1]. The presented figures it is advisable to analyze in comparison with Fig. 2-4, 6, 8.

Conclusions.

1. Variation approaches to modeling processes in long power lines make it possible to avoid the decomposition of a unified system, while the final form of the equation of state exclusively from single energy approach by building Lagrange expanded function.

2. An important point in the solution of differential equations of state of long line is a search of boundary conditions that often is veiled, incorrectly set, and the use of boundary conditions Neumann and Poincare boundary conditions. Finding these conditions entails full engagement of system of differential equations of studied object including transformers, reactors, compensation devices, etc., which greatly complicates the calculation of transients in a long line.

3. Experience shows that during the analysis of local power systems as the best option long line the telegraph equation it is advisable to write in a function of voltage. In the case of modeling of local energy systems where they use electromagnetic model elements of these systems

(Ψ – type and A – type) have difficulty with utilization of known method of nodal voltages which makes impossible to determine voltage at the beginning and end of the line and therefore it is impossible to correctly solve the equation. All this calls into question the degree of adequacy o eventual results that are obtained by known engineering program Mathematica, MatLab, etc., a especially the use of these programs becomes impossible when considering the circuit-field model elements. In this case, each actual task we must use appropriate apparatus of mathematical modeling.

4. Based on the results of computer simulation we can make a number of conclusions:

- voltage function has the greatest amplitude of oscillations at the end of the line when the current function – at the beginning of the line;
- spatial distribution of functional dependence of the line of sending (Fig. 2, 3 and 4) confirms the physical principles regarding electrodynamics of wave processes in long lines of power supply;
- presented in 3D format temporal-spatial distribution of functions of current and voltage provides most information on wave processes in Lehera line at open-circuit operation.

Materials of this work will be used in further studies that will cover long three-phase power lines with various kinds and types of loads.

REFERENCES

1. Shimoni K. *Teoreticheskaya elektrotekhnika* [Theoretical Electrical Engineering]. Moscow, Mir Publ., 1956. 773 p. (Rus).

2. Available at: https://www.energetika.in.ua (Accessed 25 July 2014).

3. Nayir A. Simulation of transient processes on overvoltage in electric transmission lines using ATP-EMTP. *Turkish Journal of Electrical Engineering & Computer Sciences*, 2013, no.21, pp. 1553-1556. **doi: 10.3906/elk-1108-8**.

4. Sowa P., Kumala R., Łuszcz K. Modeling of power system components during electromagnetic transients. *International Journal of Innovative Science, Engineering & Technology*, 2014, vol.1, iss.10, pp. 715-719.

5. Vepryk Yu.N., Minchenko A.A. Switching overvoltage in 750 kV power line. *Elektrotekhnika i elektromekhanika − Electrical engineering & electromechanics*, 2009, no.4, pp. 17-20. (Rus). **doi: 10.20998/2074-272X.2009.4.04**.

6. Kyrylenko O.V. *Matematychne modelyuvannya v elektroenerhetytsi* [Mathematical modeling in the power]. Lviv, Lviv Polytechnic National University Publ., 2010. 608 p. (Ukr).

7. Neyman L.R., Demirchyan K.S. *Teoreticheskie osnovy elektrotekhniki. V 2-kh t. T. 1* [Theoretical bases of electrical engineering. In 2 vols. Vol. 1]. Leningrad, Energoizdat Publ., 1981, p. 536. (Rus).

8. Uayd D., Vudson G. *Elektromekhanicheskoye preobrazovaniye energii* [Electromechanical energy conversion]. Leningrad, Energiia Publ., 1964. 539 p. (Rus).

9. Chaban A.V. *Pryntsyp Hamiltona-Ostrohradskoho v elektromekhanichnykh systemakh* [The principle of Hamilton-Ostrogradskii in electromechanical systems]. Lviv, Taras Soroka Publ., 2015. 488 p. (Ukr).

10. Chaban A.V *Matematychne modeliuvannia kolyvnykh protsesiv v elektromekhanichnykh systemakh* [Mathematical modeling of oscillating processes in electromechanical systems]. Lviv, Taras Soroka Publ., 2008. 328 p. (Ukr).

11. Zeveke G.V., Ionkin P.A., Netushil A.V., Strakhov S.V. *Osnovy teorii tsepey* [Fundamentals of circuit theory]. Moscow, Energiia Publ., 1975. 752 p. (Rus).

12. Vasydzu K. *Variatsionnyye metody v teorii uprugosti i plastichnosti* [Variational methods in the theory of elasticity and plasticity]. Moscow, Mir Publ., 1987. 542 p. (Rus).

Received 22.01.2016

A.V. Chaban[1]*, Doctor of Technical Science, Professor,*
V.R. Levoniuk[1]*, Assistant Lecturer,*
I.M. Drobot[1]*, Senior Instructor,*
A.F. Herman[1]*, Senior Instructor,*
[1] Lviv National Agrarian University,
1, V. Velykoho Str., Dubliany, Lviv Region, 30831, Ukraine,
e-mail: atchaban@gmail.com, bacha1991@ukr.net

How to cite this article:
Chaban A.V., Levoniuk V.R., Drobot I.M., Herman A.F. Mathematical model of electromagnetic processes in Lehera line at open-circuit operation. *Electrical engineering & electromechanics*, 2016, no.3, pp. 30-35. doi: 10.20998/2074-272X.2016.3.05.

UDC [62-83:621.313.333]-57-592 **doi: 10.20998/2074-272X.2016.3.06**

V.I. Lobov, K.V. Lobova

INTENSITY SETTER FOR A DEVICE OF SMOOTH START OF SUBMERSIBLE PUMP ELECTRIC MOTOR

Purpose. Development of an intensity setter, which in a rational law changes the opening thyristor the voltage regulator and effectively to changing power supply voltage stator windings of the electric pump deepening, ensuring a smooth start in a wide range. Methodology. Electric submersible pump belongs to the small inertia electric, since it is not significant total moment of inertia, not exceeding two moments of inertia of the motor and static moment on the shaft does not exceed forty percent of the nominal torque. For technical requirements that electric acceleration time should have no less than twenty seconds or more. Office starting modes of electric submersible pumps economically justified using thyristor voltage regulator by forming the dial changes the intensity of the necessary legislation in time voltage feeding the stator windings. This ensures a smooth start right rotor of the electric submersible pump. Results. A block diagram of the intensity setter that is: with control unit, two units that form the exponential voltage supply emitter follower and regulatory elements. The mathematical expressions for voltage at the stator windings of the motor, changing exponentially, opening the angle of thyristor power unit thyristor the voltage regulator, which is determined through the initial angle of opening. Provided formula for pick-up voltage and minimum voltage, time constants, which are determined from the basic equations of motion and mechanical characteristics of the electric motor. Analytical investigated by the voltage dependence violation by changing the time constant flowing and growing exhibitor supply voltage stator electric circuit deepening pump. Originality. Proposed in the initial time on the stator windings of the electric pick-up voltage is applied. Under the influence of this voltage, motor rotor begins to accelerate. At the same time, pick-up voltage decreases the minimum startup voltage varies exponentially in which the rotor of the electric motor continues to rotate more steadily. Now the voltage at the motor stator windings increases exponentially to the nominal voltage of the supply network. This start flowing smoothly for the right time to establish nominal rotor speed of the motor. Practical value. Developed dial allows you to increase the intensity of the electric motor acceleration time and reduce the dynamic loads of the electric submersible pump. References 9, tables 1, figures 2.

Key words: **submersible pump, induction motor, thyristor voltage regulator, opening angle of thyristor, intensity setter, start-up, acceleration time.**

Рассматривается задача построения задатчика интенсивности для формирования изменения угла открывания тиристоров регулятора напряжения. Это позволяет менять по сложной траектории напряжение питания на статоре электродвигателя погружного насоса, обеспечивая, тем самым, нужное время плавного ускорения вращения ротора. Для реализации задатчика интенсивности аппаратными средствами автоматизации представлена блок-схема, а программным путем – математические выражения. Библ. 9, табл. 1, рис. 2.

Ключевые слова: **погружной насос, асинхронный электродвигатель, тиристорный регулятор напряжения, угол открывания тиристоров, задатчик интенсивности, пуск, время ускорения.**

Introduction. The growth of both residential and industrial construction in recent years has made steady and quality supply one of the priorities. The most promising way is to use its underground water sources via wells of varying depth, which is a complex hydraulic structure that requires a skilled approach to construction and reliable equipment – borehole pumps. These units are specifically designed to work in rather difficult conditions. They are expensive and, because of the specific installation, repair them connected with considerable difficulties and costs. Therefore, when selecting such equipment should pay attention to detail and a number of practical points to help extend the smooth operation of the equipment and minimize operating costs.

One of these key parameters – a way to start an induction electric submersible pump (IESP), which is one of the most negative modes for the electric motor and water-lifting pipe and water supply part of the well. The electric pump in this period briefly exposed to peak, so it inrush current of 4.7 times the nominal value at a relatively low starting point. This leads to increased wear thermal insulation of stator windings, which greatly depends on the reliability and durability of the motor. Noxious a launch for the unit and the well as a whole, as is often accompanied by a hammer that breaks pipeline valves and pump itself. The most effective solution to all these problems is to ensure smooth start IESP.

Analysis of investigations and publications. Create and start the study of controlled AC motors are widely covered in domestic and foreign literature. Generally, for this purpose, the following ways: switching scheme of «star» in the scheme «triangle» or the inclusion of the electric motor via a starting transformer or by phase control voltage on the stator or the use of frequency converters [1-9]. In practice for IESP economically feasible is a relatively simple device parametric phase control. It uses thyristor voltage regulators (TVR), which is the most widespread, their operation will be used in the future for electric low and medium power [1-3, 6, 8].

Control starting modes of electric drives using TVR most simply perform by creating necessary laws intensity dial changes the time pressure that feeds the stator winding. Applied to the stator supply voltage regulating by means of open angle α_s thyristors TVR included in the stator electric circuits. Running start on a constant or continuous (linear or exponential in law) changing angles α_s, formed via hardware or software setters of intensity. When the static load on the shaft of the mechanism can not regulate a wide range of time starter motor, thereby reducing starting currents and electromagnetic shock value points [2, 3, 6, 7]. However, the known laws regulating angle α_s not allowed to perform controlled start IESP, the technical requirements that need to have time to disperse at least 20 s or more. IESP refers to small inertia drives, since it is not significant total moment of inertia $J_\Sigma \le 2J_e$, (J_e is the motor moment of inertia) and static torque on the shaft $M_s \le 0.4M_n$ (M_n is the rated moment). Therefore, at the start of the IESP methods known enough moving voltage U_s, to electric overclocked to speeds close to par. This launch is not controlled and executed by a time equal to 0.4-0.8 s and is not regulated in time. Further increase in the nominal voltage does not significantly impact on the smooth start-up, as the motor speed changes in a small range [8, 9].

The aim of the work is the theoretical study, development and implementation of controlled smooth start asynchronous electric submersible pump when used TVR with dials of intensity, which in a rational law will change the angle of opening thyristors that will effectively influence the supply voltage stator windings of the electric motor to provide a wide range of time smooth start and extend the smooth operation of hydraulic structures and minimize operating costs.

Results of investigations. Smooth start of IESP is performed in the following manner. At the initial time in the stator winding electric voltage is applied start U_s. Under the influence of this voltage motor rotor begins to accelerate. At the same time, the voltage decreases U_s moving during the start t1 exponentially to the minimum voltage $U_{\min}$. At this voltage motor rotor has steadily continued to rotate. Since at time t_1 and achieve a minimum voltage $U_{\min}$, the voltage at the motor stator windings increases exponentially to the nominal voltage of the supply network U_{sn}. This start flowing smoothly at the right time t_2 to establish nominal rotor speed of the motor.

To implement this method of launching hardware device used by intensity setter block diagram of which is given in Fig. 1.

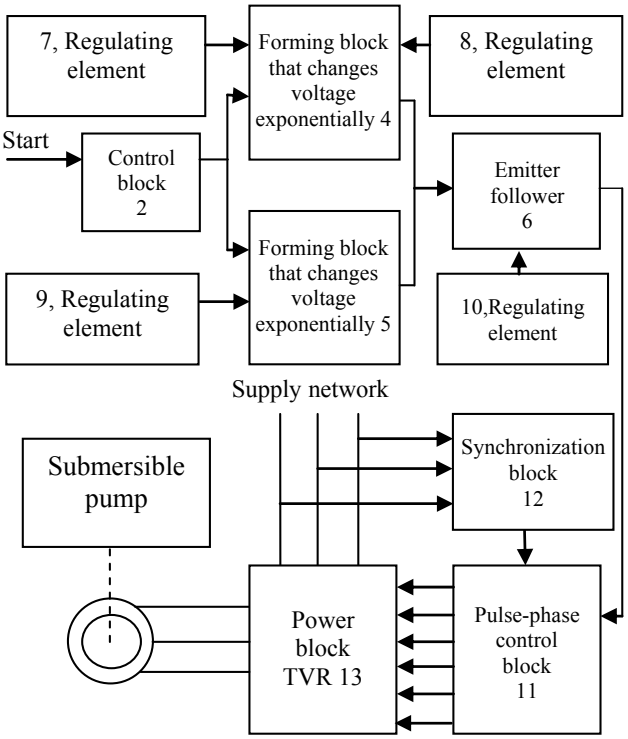

Fig. 1. The block diagram of the intensity setter for smooth start for motor type IESP

When implementing this method by software the following mathematical expression is used:

$$U_{sn} = \begin{cases} U_s e^{-t_1/t_n}, & \text{at} \quad 0 \le t \le t_1; \\ U_s + U_{\min}\left(1 - e^{-t_2/t_n}\right), & \text{at} \quad t_1 \le t \le t_2, \end{cases} \tag{1}$$

where t_1, t_2 are the time constants, t_n is the total time of the IESP start.

Opening angle of thyristors of the power block of the TVR is determined by the initial angle of opening $\alpha_{(0)}$:

$$\alpha_s = \begin{cases} \alpha_{(0)}\left(1 - e^{-t_1/t_n}\right), & \text{at} \quad 0 \le t \le t_1; \\ \alpha_{(0)} e^{-t_2/t_n}, & \text{at} \quad t_1 \le t \le t_2. \end{cases} \tag{2}$$

The voltage of moving and minimum voltage in expression (1), respectively, are determined by formulae:

$$U_s = U_{sn}\frac{\sqrt{M_s^0}}{M_n}, \tag{3}$$

$$U_{\min} = U_{sn}\frac{\sqrt{M_s^1}}{M^s}, \tag{4}$$

where M_s^0 is the static torque at a fixed electrical motor rotor motor; M_n is the electrical motor starting torque at the rated supply voltage; M_s^1 is the static loading torque at a minimum rotor speed of an electric motor; M^s is the torque of the electrical motor at the rated voltage and the minimum rotor speed of the electrical motor.

Time constant t_1 in expressions (1) and (2) is determined from the basic equation of motion of the electric motor and mechanical characteristics:

$$t_1 \approx J_{\Sigma}\omega_r^s \ln\left|\frac{(M_\alpha + M_s^0)\omega_{\min} - M_s^0\omega_r^s}{M_s^0\omega_r^s}\right|, \qquad (5)$$

where J_{Σ} is the superficial electric moment of inertia of electric drive; ω_r^s, $\omega_{\min}$ are the synchronous and minimum rotor speed of the electric motor; M_α is the electromagnetic torque, determined by the mechanical characteristics of the electric motor.

Substituting numerical data gives the value t_1 (5), not exceeding five periods of the mains voltage and calculated for a specific drive. Became time t_2 in the same expressions (1) and (2) is chosen within one or two values specified time launch. This is because the voltage is sufficient to disperse IESP in the area of operating speeds, defines smooth start-up, significantly below the nominal voltage is calculated from the parameters of a particular drive. Therefore, increasing the acceleration time IESP in the area of operating speeds, it is necessary to increase the daily time t_2.

The Table gives values and Fig. 2 – depending $U_s = f(t/t_n)$ by changing the time constants t_1, t_2 and voltage U_s, which was calculated by the expression (1). Charts voltage U_s are a fraction of nominal voltage U_{sn} and the current time – a fraction of time in direct starting asynchronous machine with a nominal voltage and T_{ss} – between the supply voltage change network U_{sn}.

From the results obtained it follows that increasing the time constant t2 from 5 to 25 T_{ss} the minimum voltage $U_{\min}$ on the stator of the electric motor reaches a value equal $0.3U_{sn}$ (Fig. 2,*a*). Increasing the time constant t_2 of values required time t_n of the start of the electric drive to a value equal $10t_n$ leads to the fact that this stress significantly reduced and reaches a value equal $0.05U_{sn}$.

Table

Dependences $U_s / U_{sn} = f(t/t_n)$

Characteristic No. (Fig. 2,*a*)	t_1	t_2	Characteristic No. (Fig. 2,*b*)	U_s
1	$5t_n$	$25T_{ss}$	1	0.85
2	$5t_n$	$5T_{ss}$	2	0.65
3	$5t_n$	$12{,}5T_{ss}$	3	0.5
4	t_n	$5T_{ss}$		
5	$3t_n$	$5T_{ss}$		
6	$10t_n$	$5T_{ss}$		

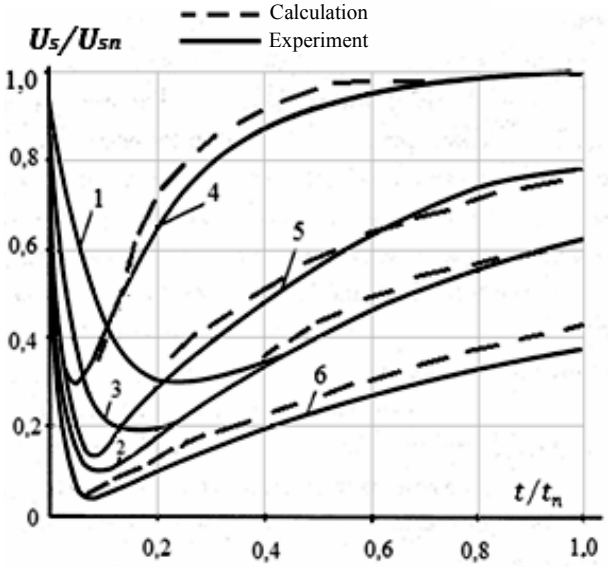

a

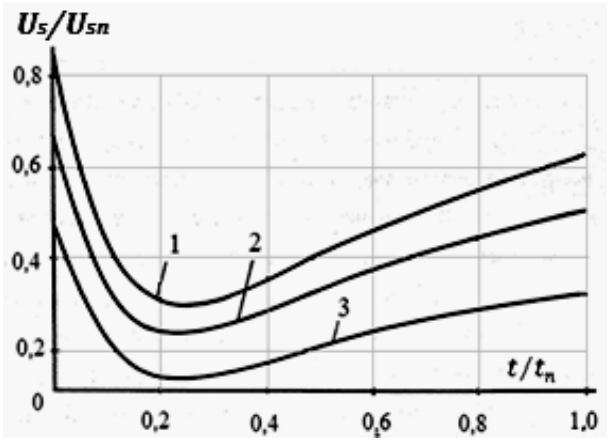

b

Fig. 2. Dependences $U_s / U_{sn} = f(t/t_n)$

As the U_s decrease to $0.5U_{sn}$ (Fig. 2,*b*, the third curve) this function for a time equal to $t/t_n = 1$ reaches a value equal $0.35U_s/U_{sn}$ at $U_s = 0.8U_{sn}$ (the second curve) – $0.43U_s/U_{sn} – 0.43$ (Fig. 2,*b*). At the same time at U_s/U_{sn} (the first curve) function has already reached the value of 0.62. Reducing voltage U_s leads to longer rise of the function $U_s/U_{sn} = f(t/t_n)$.

Conclusions.

1. The necessity of using a wide range of acceleration time of rotor induction motor TVR submersible pump with dial intensity, which has two time constants that vary exponentially and takes into account the magnitude of the voltage moving of the motor rotor is proved. If you change a designed dial intensity constant voltage value of time and moving of the rotor turns the family characteristics of feeding pressure from TVR which could be given to stator windings to form the starting modes asynchronous electric submersible pump and extend the smooth operation of hydraulic structures and minimize operating costs.

2. Developed intensity setter can be used to form the frequency converter starting modes used, for example, in electric drives of conveyor machines for burning pellets.

REFERENCES

1. Lobov V.I., Lobova K.V. Method of determining the start time of induction motors in the control of resistor-thyristor modules. *Elektrotekhnika i elektromekhanika – Electrical engineering & electromechanics*, 2015, no.4, pp. 40-44. (Rus). **doi: 10.20998/2074-272X.2015.4.07**.

2. Petrushin V.S., Yakimets A.M., Bangula V.B. Analysis of a thyristor voltage converter fed induction motor start. *Elektrotekhnika i elektromekhanika – Electrical engineering & electromechanics*, 2012, no.6, pp. 31-33. (Rus). **doi: 10.20998/2074-272X.2012.6.06**.

3. Braslavskiy I.Ya., Ishmatov Z.S., Polyakov V.N. *Energosberegayushchiy asinkhronnyy elektroprivod* [Energy-saving asynchronous electric]. Moscow, Academiya Publ., 2004. 256 p. (Rus).

4. Figaro B.I., Vasilyev D.S. Application of squirrel-cage induction motor soft starting and braking in the electric drives of crane travel mechanisms. *Elektrotekhnichni ta kompiuterni systemy – Electrotechnic and computer systems*, 2011, no.4, pp. 30-38. (Rus).

5. Lobov V., Lobova K. Choice of braking method of asynchronous electric motor for using in electric drives of conveyor equipment. *Metallurgical and Mining Industry*, 2015, no.8, pp. 6-12.

6. Lobov V. Method for research of parametric control schemes by asynchronous motor. *Metallurgical and Mining Industry*, 2015, no.6, pp. 102-108.

7. Chernyi A.P., Gladyr A.I., Osadchuk Y.G. *Puskovye sistemy nereguliruemykh elektroprivodov: Monografiia* [Starting unregulated electric system: Monograph]. Kremenchuk: PP Cherbatyh A.V. Publ., 2006. 280 p. (Rus).

8. Lobov V.I. *Issledovanie puskovykh i tormoznykh rezhimov asinkhronnykh elektroprivodov s tiristornym parametricheskim upravleniem.* Diss. kand. techn. nauk [Research of starting and braking modes of asynchronous electric drives with thyristor parametric-hydraulic control. Cand. tech. sci. diss.]. Moscow, 1983. 269 p. (Rus).

9. Brodsky Y.A., Egorova S.A., Lobov V.I., Shvets S.A. *Sposob puska maloinertsionnogo asinkhronnogo elektrodvigatelia* [Method of starting a fast-response induction motor]. USSR Certificate of Authorship, no.1108589, 1984. (Rus).

Received 10.02.2016

V.I. Lobov[1], *Candidate of Technical Science,*
K.V. Lobova[1], *student,*
SIHE «Kryvyi Rih National University»,
11, XXII Partz'izdu Str., Kryvyi Rih, 50027, Ukraine,
phone +380 564 4090635,
e-mail: lobov.vjcheslav@yandex.ru

How to cite this article:
Lobov V.I., Lobova K.V. Intensity setter for a device of smooth start of submersible pump electric motor. *Electrical engineering & electromechanics*, 2016, no.3, pp. 36-39. doi: 10.20998/2074-272X.2016.3.06.

UDC 621.3.022: 621.319.53 **doi: 10.20998/2074-272X.2016.3.07**

M.I. Baranov, V.V. Kniaziev, V.I. Kravchenko, S.V. Rudakov

RESULTS OF CALCULATION-EXPERIMENTAL INVESTIGATIONS OF ELECTRO-THERMAL RESISTIBILITY OF SHEET STEEL SAMPLES TO ACTION OF RATIONED COMPONENTS OF PULSED CURRENT OF ARTIFICIAL LIGHTING

Purpose. *Calculation and experimental researches of the electro-thermal resistibility of the steel sheet samples to action standard pulse current components of the artificial lightning with amplitude-time parameters (ATP), corresponded the requirements of normative documents of USA for SAE ARP 5412 & SAE ARP 5416.* ***Methodology.*** *Electrophysics bases of technique of high tensions and large impulsive currents (LIC), and also scientific and technical bases of planning of devices of high-voltage impulsive technique and measuring in them LIC. Current amplitude I_{mA}=±200 kA (with a tolerance of ±10 %); current action integral $J_A=2\cdot10^6$ $A^2\cdot s$ (with a tolerance of ±20 %); time, corresponding to the amplitude of the current I_{mA}, $t_{mA}\leq50$ microseconds; the duration of the current flow $\tau_{pA}\leq500$ microseconds.* ***Results.*** *The results of the evaluation of the calculated and experimental studies of electro-thermal resistance of the samples of plates measuring 0,5 m × 0,5 m stainless steel 1 mm thickness to the action on them artificial lightning impulse currents with rationed ATP on the requirements of normative documents of USA for SAE ARP 5412 & SAE ARP 5416. A pulse A- component have a first amplitude 192 kA, the corresponding time of 34 μs, and the duration aperiodic component amplitude 804 A, corresponding to the time 9 ms. It has been shown that the long C- component current of artificial lightning can lead to keyhole these samples. The diameter of the holes in this thin steel sheet, which is formed during the flow of current C- components can reach 15 mm. The results of calculation and experiment agree within 28 %.* ***Originality.*** *For the first time in world practice on the generator large pulsed currents experimental studies of resistibility of sheet steel samples to the action of artificial lightning currents with critical parameters.* ***Practical value.*** *Using the results obtained in the practice of lightning protection will significantly improve the functionality and fire safety of different objects in conditions of exposure to linear lightning.* References 15, figures 15, tables 5.

Key words: **main components of lightning current, impulse current generator of artificial lightning, flat steel sample, electro-thermal resistibility to lightning.**.

Приведены результаты оценочных расчетных и экспериментальных исследований электротермической стойкости опытных образцов пластин размером 0,5 м × 0,5 м из нержавеющей стали толщиной 1 мм к воздействию на них импульсных токов искусственной молнии с нормированными по требованиям нормативных документов США SAE ARP 5412 и SAE ARP 5416 амплитудно-временными параметрами (АВП). Использовались колебательная импульсная А- компонента с первой амплитудой 192 кА, соответствующей времени 34 мкс, и апериодическая длительная С- компонента амплитудой 804 А, соответствующей времени 9 мс. Показано, что длительная С- компонента тока искусственной молнии с нормированными АВП может приводить к сквозному проплавлению указанных образцов. Библ. 15, рис. 15, табл. 5.

Ключевые слова: **основные компоненты тока молнии, генератор импульсного тока искусственной молнии, плоский стальной образец, электротермическая молниестойкость.**

Introduction. For direct impacts of linear lightning, developing in an air atmosphere of the Earth with an average rate of 100 discharges per second [1, 2], in the high-altitude engineering structures placed on the earth's surface, the amplitude-time parameters (ATP) pulsed current in the plasma channel its discharge may taking dangerous both for external structural elements, as well as electrical power and low voltage electronic equipment contained within these structures. According to the requirements of the current normative US SAE ARP 5412 and SAE ARP 5416 documents [3, 4], relating mainly to be exposed to direct lightning strikes aerospace objects, the pulse current of the lightning discharge consists of two main components: the pulse *A*- and long-term *C*-components. This ATP of normalized pulse *A*-components of lightning current according to [3, 4] take the following numerical values: current amplitude I_{mA} =± 200 кА (with a tolerance of ± 10%); current action integral $J_A=2\cdot10^6$ $A^2\cdot s$ with (with a tolerance of ± 20 %); time corresponding to the amplitude of the current I_{mA}, $t_{mA}\leq50$ μs; the duration of the current flow $\tau_{pA}\leq500$ μs. In this case, the normalized ATP of the aperiodic long-term *C*-component of lightning current should be the following numerical values [3, 4]: the current amplitude I_{mC} = ±(200-800) A; transferred electric charge q_C = ±200 C (with a tolerance of ± 20%); the duration of the current flow τ_{pC} = (0,25−1) s. In 2007, at the Research and Design Institute «Lightning» of the NTU «KPI» a powerful high-voltage generator type УИТОМ-1 artificial lightning current was created [5], which forms on the test technical object ATP pulse current of the lightning discharge on the requirements of the normative documents [3, 4]. The authors are not known publication of the effects of lightning on the elements of technical installations, made of thin-walled stainless steel.

Therefore, estimates of theoretical and experimental studies of the stability of the level (resistance) of such elements to direct lightning strike them with the current parameters close to the limit, are of practical interest.

1. Problem definition. Consider a flat sample with size in plane of 500×500 mm from stainless steel 12X18H10T of 1 mm thickness, which is experiencing the outdoors a direct effect of the plasma channel of artificial lightning, which has a cylindrical shape. Let this channel flow pulsed *A*- and long-term *C*- current components of lightning, standardized ATPs that correspond to the requirements given in [3, 4]. It is required initially carry an estimate of the results of the electro-thermal effects on the reporting sample of said pulse current component of artificial lightning, and then using a generator-type УИТОМ-1 perform experimental testing electrothermal lighting resistibility prototype to the direct impact it plasma channel artificial lightning.

2. The calculated electrothermal resistance of steel samples to the current of the artificial lightning. We perform the first assessment of the stability of the test specimens of thin steel to act on them pulse current flowing in the channel of the lightning discharge, according to the procedure recommended in [6] by the International Electrotechnical Commission.

2.1. The results of calculations by standardized methodology of evaluate thermal lighting resistibility. The international standard IEC 62305-1 (see Appendix D, formula D.9) shows the analytical relationship, provide an estimate of V_0 metal object melted due to the effects of lightning current to it, depending on the elapsed with the amount of electricity in the next form [6]:

$$V_0 = \frac{U_{ac} \cdot q_{Ac}}{d_0} \times \frac{1}{C_w(\Theta_m - \Theta_e) + C_s}, \qquad (1)$$

where V_0 is the volume of melted metal of the object, m^3; U_{ac} is the anode or cathode DC voltage drop near the object, V; q_{Ac} is the the amount of charge carried by the *A*- or *C*- component of the lightning current, C; d_0 is the density of the object's material, kg/m^3; C_w is the heat capacity of the object's material, J/(kg·°C); Θ_m is the melting temperature of the object's material, °C; $\Theta_e = \theta_0$ is the ambient temperature of the surrounding media, °C; C_s is the heat of fusion of the object's material, J/kg.

To assess the size of holes or cavities, which may be formed in this sheet sample of stainless steel with a predetermined thickness h exposed to lightning current, known numerical indicators contact the main physical parameters for stainless steel have been used 12X18H10T shown in Table 1.

After substituting the values of the parameters of the Table 1 in (1) by varying the charge $q_{Ac} = q_c$ values were obtained cylindrical volume V_0 of the molten steel, which, when divided into a thickness h of the sheet, gives the corresponding values of the area round the heating zone and the radius r_c of penetration holes in a steel specimen shown in Fig. 1.

Table 1

Parameters for the steel 12X18H10T [6-8]

Parameter	Dimensionality	Value
U_{ac}	V	10
d_0	kg/m^3	7900
C_w	J/(kg·°C)	462
Θ_m	°C	1455
Θ_e	°C	20
C_s	J/kg	$84 \cdot 10^3$

For a lightning current *C*- component of duration τ_{pC} from 2 to 40 ms charge $q_c = q_{Ac} = 10$ C at a current strength is achieved in its channel, ranging from 5 kA to 250 A. When assessing the radius r_c formed holes should be borne in mind that the heat flux is supplied in a steel sample is not a dot, and for the area of a circle of radius r_{mc}. Therefore, the molten metal spot radius can not be less than r_{mc}. Radius r_{mc} channel of lightning depends on the strength of the current flowing in it and to normal atmospheric conditions is defined as [8]:

$$r_{mc} = 0.11 \cdot 10^{-3} (I_{mc})^{0.5}. \qquad (2)$$

where I_{mC} is the maximal value of current for the long-term *C*-component of lighting current in the plate, A.

The results of calculation by (2) of the value of radius r_{mc} of the channel with *C*- current component are presented in Table 2.

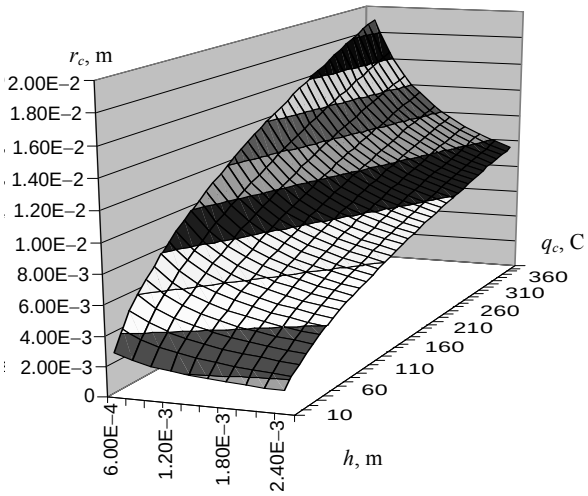

Fig. 1. The dependence of the radius r_c of the melting hole formed in the test steel sheet of thickness h via leaked through his material amount of electricity q_c

Table 2

Values of radius r_{mc} of the channel of lightning depending on the current of *C*-component

Current I_{mC}, A	100	200	400	800
Radius r_{mc}, mm	1.10	1.56	2.20	3.11

When the thickness of the steel sheet h=1 mm and the elapsed charge q_c=10 C at radius of melting holes therein in accordance with (1) will be approximately equal to r_c=1.64 mm. The same radius, starting from (2),

has a lightning channel at a current in it I_{mC} = 222 A. We can therefore assume that the action of the steel sheet (h=1 mm) C- components lasting approximately 40 ms and the current strength (the average for the time of the action), about 220 A burning of the sheet will occur. For particular values of C- component q_c charge current components which have been observed in experiments (see subsection 4 below), the estimated value of the hole diameter $2r_c$ of the selected sample is melted steel (h=1 mm) at q_c=187 C reaches 20.8 mm; and at q_c=165 C - 18.0 mm. The results of penetration of the steel plate (h=1 mm) calculated by the method of [6] did not consider the process of heat removal from the sample of the local heating zone of presence of skin effect and merely assume its cylindrical hole burning. Therefore, they are numerically overstated.

2.2. The results of calculations by the method of mathematical modeling based on the applied code. Method of solution of the problem used electrothermal further based on known fundamental analytical solution of the thermal problem for the massive flat metal conductor with instant surface point source disc-shaped heat radius r_0 [9]. This analytical solution [8] was the first approximation extended to the case of pulsed current at direct lightning strike into a sheet. Between time $0 \le t \le t_0$ in the area of the circular support band channel has a lightning shape heat source disk radius r_0 with average heat flux $q_0(t)$ applied to the flat outer surface of the metal plate uniform wall. In the cylindrical coordinate system for spatial and temporal changes in the temperature rise $\theta(r,z,t)$ in the material of the wall of a steel sample thickness h in a circular area of effect to it in time air t surface heat flow with the average density $q_0(t)$ of the plasma channel lightning current can write the following approximate solution of the unsteady electrothermal problem [8]:

$$\theta(r,z,t) = \frac{1}{(\pi\lambda_0 c_0)^{1/2}} \int_0^{t_0} r_0(\tau) q_0(\tau) F(r,z,t-\tau) d\tau, \quad (3)$$

where $\theta(r,z,t) = (\theta_t - \theta_0)$ is the temperature rise of the wall material of the metal sample; θ_t is the current and time-varying temperature of the flat wall of the sample material; θ_0 is the ambient temperature of the air around the wall; r is the radial coordinate directed from the axis of the current channel of lightning along the wall of a flat sample; z is the longitudinal coordinate directed from the lightning current hearth heat exposure inside the center of the flat walls of the sample; $q_0(\tau)$ is the average density acting on the wall surface steel sample heat flow caused by lightning plasma channel;

$$F(r,z,t-\tau) = \exp[-z^2 c_0 / 4\lambda_0 (t-\tau)] \times$$

$$\times (t-\tau)^{-1/2} \int_0^{\infty} \exp[-\lambda_0 (t-\tau) \nu^2 / c_0] J_0(\nu r) J_1(\nu r_0) d\nu;$$

τ, ν are the auxiliary variables; $r_0(\tau)$ is the current value of the lightning current channel radius; t is the current time; t_0 is the duration of the pulsed A- and long-term C- components of the lighting current; J_0, J_1 are the respectively the Bessel functions of zero and first order; λ_0, c_0 are the respectively the thermal conductivity and specific heat capacity of the wall of the volume of flat steel material sample taken for the solved problem constants.

Described briefly the mathematical model has been implemented as an application program [10], which allows the calculation of the consequences of thermal effects on the pulsed A- and long-term C- components of lightning current. Here joint consistent effect on steel samples of said lightning current component is not considered. The results of the approximate numerical calculations on the program [10] the thermal action of only one pulse A- component lightning current on a steel sample (h=1 mm) are presented in Table 3.

Table 3

Results of assessment of the thermal action of A- component on the steel sample [10]

I_{mA}, кА	t_{mA}, μs	τ_{pA}, μs	Melting depth h_{mA}, mm	Melting radius r_{mA}, mm
192	34	500	0.04	31.6

In addition to the above, we note that we are considering the case of the radius r0A channel lightning pulse A- component according to its current by the Braginsky formula as follows [8]:

$$r_{0A} = 0.093 (I_{mA})^{1/3} (t_{mA})^{0.5}. \quad (4)$$

When I_{mA}=192 kA and t_{mA}=34 μs radius r_{0A} of the lightning channel, calculated at (4) is equal to 31.3 mm. It is evident that this numerical value of radius r_{0A}=31.3 mm is consistent with the radius of r_{mA}=31.6 mm surface melting steel sample zone, caused by the action of pulse A- component to it. As a result of pulsed A- component with a current I_{mA}=192 kA, through penetration of the sheet is not observed. In accordance with Table A.3 of the Standard [6] with a current probability of lightning more 200 kA is not more than 0.01 (1 %). Therefore, thermal effect alone activities A- lightning impulse current component of the steel sheet with a thickness h=1 mm and more can be ignored in terms of occurrence of it therein through hole.

The results of assessment on the basis of (2) and (3) a steel plate (h=1 mm) on the thermal action on its outer surface of long-term lightning current C- component are shown below in Table 4.

It should be noted, that the physics of the process in real lightning current sheet is more complicated than in the above calculation model. An important factor here is the consistent flow of the A- and C- current components. As a result, the wall is done preheating object A- component of the current. Therefore, obtained by [10], the results underestimate the value of the radius of the hole in the steel sheet for the received version of their action. We

can assume that the actual size of the hole in a sheet of two-component impact of natural lightning are between the values of the diameters calculated according to the methods discussed above.

Table 4

Results of assessment of the thermal action of long-term *C*- lightning current component on the flat steel sample of thickness h=1 mm [10]

q_C, C	I_{mC}, A	T_C=T_{long}=t_0, ms	Diameter $2r_c$ of the melted hole, mm	Average current, A
10*)	500	40	2.72	250
20*)	1000	40	4.06	500
40[1)]	800	100	4.96	400
125	500	500	6.40	250
200	800	500	7.72	400
350[2)]	1400	500	9.68	700

Note.

*) The probability of exceeding the tolerable in the plasma channel lightning storm magnitude charge q_C of 10 C and 20 C, respectively, as determined by 50 % and 20 % ([6], see Fig. A.5);

1) Excess of q_C amount of charge over 40 C transported downward lightning negative polarity, has a probability of less than 5 % (see [6], Table A.1);

2) Excess of the value of the lightning charge q_C over 350 C transported by the lightning of positive polarity, has a probability of less than 5 % (see [6], Table A.1).

3. The test circuit and the electrical parameters of high-power high-voltage generators of PCG-*A* and PCG-*C*. Fig. 2 is a schematic diagram of the type of generator УИТОМ-1 used in the experimental studies on electrothermal lighting resistibility of test specimens (TS) of the selected steel roofing technical facilities. From this scheme it is clear that the structure of two separate and parallel operating one electrical load type УИТОМ-1 generator included TS of pulse current generator (PCG), one of which PCG-*A* simulates pulse *A*- component of an artificial lightning current and other PCG-*C* – long-term *C*- component of artificial lightning current. We point out that their own electrical parameters of the discharge circuit generator HIT-A up [5]: resistance R_A≈0.057 Ω; inductance L_A≈2,5 μH; capacity C_A ≈333 μF. Own the electrical parameters of the discharge circuit generator PCG-*C* were equal to [5]: resistance R_C≈4.74 Ω; inductance L_C≈11.43 mH; capacitance C_C≈45.36 mF. Generator PCG-*A* was compiled on the basis of 111 parallel-connected high-voltage pulse capacitors such as ИК-50-3 (rated voltage of ±50 kV; nominal capacity 3 μF) and PCG-C generator - based on 324 parallel connected high-voltage pulse capacitors ИМ2-5-140 (nominal voltage ±5 kV; nominal capacity 140 μF) [5, 11]. The discharge circuit generator PCG-*A* three-electrode mounted air switch F_1 with massive steel electrodes, and the discharge circuit PCG-*C* generator – air-electrode switch F_2 with graphite electrodes.

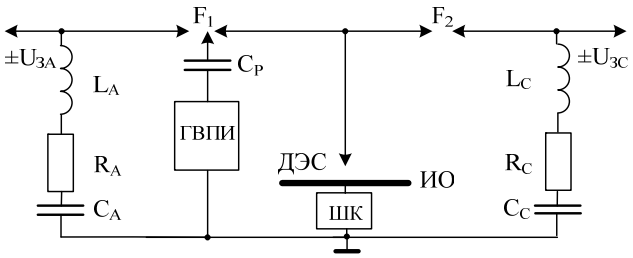

Fig. 2. Principal electrical circuits of high-current discharge circuits of generators PCG-*A* and PSG-*C* to form a roof in steel sample pulse *A*- and long-term *C*- artificial lightning current components (ГВПИ – generator of high-voltage igniting microsecond pulse amplitude voltage of ± 100 kV; F_1, F_2 – respectively, three and two-electrode spark high-voltage overhead switches PCG-*A* and PSG-*C*; C_p≈180 pF – luggage capacity on the pulse voltage up to ± 120 kV in the circuit of ГВПИ controlling the actuation of the spark switches F_1 and F_2; ДЭС – two-electrode system; ИО – roof test specimen; ШК – shunt coaxial type ШК-300 for measurement of artificial lightning impulse current amplitude from ±10 to ±300 A kA; $\pm U_{3A}$, $\pm U_{3C}$ – charge voltages respectively of PCG-*A* and PSG-*C*; L_A and L_C, R_A and R_C, C_A and C_C – respectively own inductances, active resistances and capacitances of discharged circuits of PCG-*A* and PCG-*C*) [8]

High-voltage switches F_1 and F_2 are high voltage products of own production [12]. Flat steel sample according to Fig. 2 firmly fixed on the desktop, a powerful generator of УИТОМ-1 between the massive aluminum electrodes that are connected to the bit generator circuits PCG-*A* and PSG-*C*. In the test circuit as shown in Fig. 2 for playback on plasma channel TS artificial lightning using air two-electrode system (TES), provided with a thin electrically exploding wire (EEW). As an EEW in accordance with [3, 4], a copper wire with a diameter of 0.2 mm and a length l_e=(37-50) mm. Fig. 3 shows in enlarged form the TES of the generator desktop УИТОМ-1. The air gap between the top h_a a massive cylindrical electrode TES and massive flat bottom electrode – TS could range from 27 to 14 mm. Air gap h_a in TES between EEW and TS remained unchanged and equal to about 1 mm.

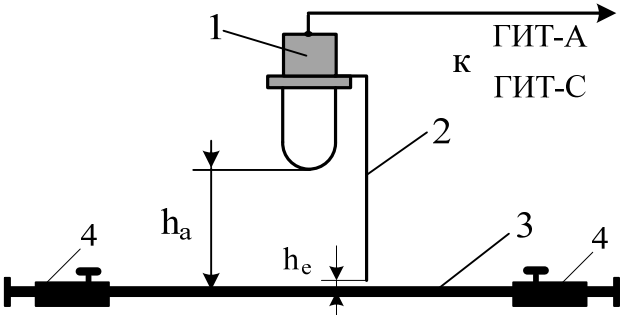

Fig. 3. Enlarged schematic representation of TES used in high-current discharge circuit generators PCG-*A* and PSG-*C* in the preparation of flat steel TS at pulse *A*- and long-term *C*- current component of an artificial lightning (1 – upper massive cylindrical steel electrode, 2 – thin copper EEW; 3 – lower the massive flat steel electrode (TS); 4 – solid aluminum electrodes are designed to secure the TS; h_a – the length of the air gap in the TES; h_e – the length of the air gap between the lower edge of the circular copper EEW and the outer flat surface of the TS) [8]

Fig. 4 is a perspective view of used TES.

Fig. 4. General view of the TES with copper EEW desktop of generators PCG-*A* and PSG-*C* when tested in their discharge circuits TS thin steel roof on electrothermal resistance to direct impact on them of pulse *A*- and long-term *C*- artificial lightning current components with a normalized according to [3, 4] ATP (l_e=37-50 mm) [8]

Charge voltages of high-voltage capacitors generators PCG-*A* and PSG-*C* to perform the planned experiments selected negative polarity, and the modules, respectively, their levels do not exceed U_{3A}≤25 kV and U_{3C}≤4.2 kV. Selecting the polarity of the charging voltages U_{3A} and U_{3C} determines the need for physical modeling of the most severe in terms of electrothermal conditions described in the TES and, respectively, in the area round the binding of a high cylindrical plasma channel with artificial lightning current on the outer surface of the flat steel roof TS technical facilities. To prevent mechanical damage to the capacitor banks generators PCG-*A* and PSG-*C* and provide the required safety conditions and safety for maintenance powerful generator type УИТОМ-1 personnel in the emergency mode of his work (for example, in electrical breakdown of insulation of at least one of the 435 these capacitors in their charge or discharge) all high-voltage outputs are used capacitors generators PCG-*A* and PSG-*C* protective resistance were installed, made from high-voltage constant bulk graphite-ceramic resistors type ТВО-60 for DC voltage ±25 kV [5, 13]. Moreover, in the terminal of the capacitor-type ИК-50-3 were installed protective resistors type ТВО 60-24 Ω (rigid assembly of four parallel connected resistors), and ИМ2-5-140 type capacitor terminals – one protective resistor type ТВО-60-100 Ω. Parallel operation of generators PCG-*A* and PSG-*C* on steel roof of the TS according to the diagram in Fig. 1 simultaneous actuation of high-voltage three-electrode-managed air switch F_1 with massive hemispherical steel main electrodes at the rated voltage of ±50 kV [12] and the high-voltage two-electrode air switch F_2 with massive rectangular graphite electrodes containing a flat working surface, a rated voltage of ±10 kV [12]. In turn, the synchronous operation of switches F_1 and F_2 performed by feeding through the separating capacity C_p to switch F_1 average spherical steel electrode set fire by a generator of high-voltage pulses (GHVP) of microsecond duration voltage pulse amplitude to ±100 kV [5, 12]. In the breakdown by GHVP one of the two air gaps switch F_1 and its subsequent activation occurs surge voltage to a TES with TS leads to virtually simultaneous with it and triggering the switch F_2. After tripping switches F_1 and F_2 due to discharge pre-charged high-voltage capacitors generators PCG-*A* and PSG-*C* through TS of steel roofing technical facilities begin to flow simulated lightning current pulses required by [3, 4] ATP. It should be noted that the nominal value of the stored electrical energy in the power generators PCG-*A* and PSG-*C* are respectively 416 and 567 kJ [5, 8, 13].

Measuring ATP of pulsed *A*- and long-term *C*-artificial lightning current component in the identity of the roof steel was carried out with the help of attorneys metrological service measuring coaxial shunt type ШК-300 [14], has for these currents, respectively, conversion factors K_A≈10417 A/V and K_C≈5219 A/V and digital storage oscilloscope Tektronix TDS 1012 type.

4. Results of tests of the roof steel samples for resistance to pulsed *A*- and long-term *C*- artificial lightning current component. Fig. 5 shows a general view of the desktop with powerful TES generator УИТОМ-1 and is rigidly fixed to it a flat roof TS steel thickness h=1 mm in the grooves of massive aluminum electrodes that are included in the high-current discharge circuit of high-voltage generators of PCG-*A* and PSG-*C*.

Fig. 5. External view of Ts of steel roof fixed in TES with EEW desktop УИТОМ-1 type generator, to direct exposure to high-voltage generators of PCG-*A* and PSG-*C* of pulsed *A*- and long-term *C*- artificial lightning current component (h_a=27 mm; l_e=50 mm)

The following two types of experiments to determine the electrothermal lighting resistibility identical TS steel roofs have been received for the same values of charging voltage in the PCG-*A* and PSG-*C* (U_{3A}=-25 kV; U_{3C}=-4.2 kV), the air gap h_e≈1 mm and two values of the air gap h_a, equal to 27 and 14 mm.

4.1. Results of experiments at h_a=27 mm. Fig. 6 shows the waveform of pulsed *A*- component of artificial

lightning current flowing in the identity of the roof steel technical facilities.

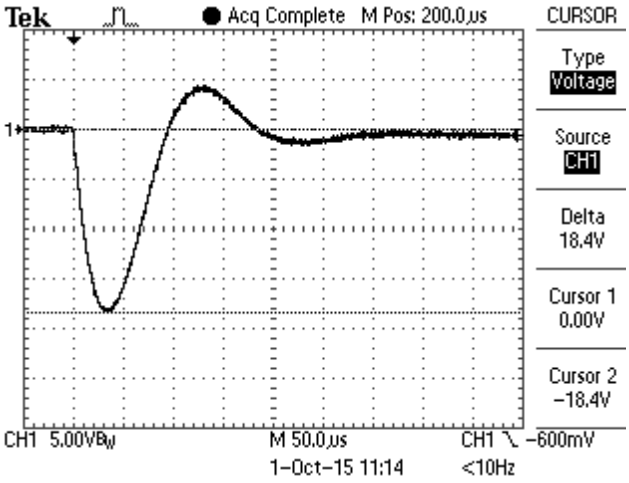

Fig. 6. Waveform of pulsed *A*- component of artificial lightning current acting on the TS of the roof

From decoding of the waveform it follows that for this case the amplitude of the first pulse *A*- component of artificial lightning current TS steel roof was $I_{1mA}\approx$–192 kA. This amplitude decaying exponentially oscillating current component corresponds to the time t_{mA}, equal to 34 µs. The duration of the first half-wave τ_{1A} current in this case was about 94 µs, and the total duration of the current components τ_{pA} simulated lightning - about 500 µs. Fig. 7 is a waveform of *C*- aperiodic long-term artificial lightning current amplitude components $I_{mC}\approx$ –804 A, flowing in the id stainless steel roof (h=1 mm). It can be seen that the duration of this component τ_C lightning surge current at $0.5\cdot I_{mC}$ was equal to about 160 ms, and its complete length τ_{pC} – about 0.516 s. t_{mC} time corresponding I_{mC} amplitude equals to 9 ms.

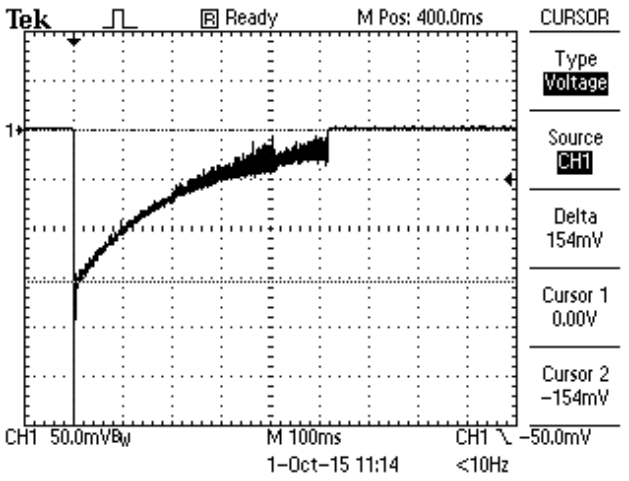

Fig. 7. Waveform of long-term *C*- component of artificial lightning current acting on the TS of the roof

According to Fig. 6 on the curve of the long-term *C*- components of artificial lightning current, especially in the final stages of its course, clearly visible multiple superimposed oscillations due to combustion instability of TS pulse arc of the roof in the air gap length h_a=27 mm. At the current time t, equal to $\tau_{pC}\approx$0.516 s, given the instability of the arc leads to the edge of the plasma channel and an end to the long-term *C*- component of the current in the tested TS of the steel roof. Decoding the waveform in Fig. 6 shows that over time the amount of electricity from $\tau_{pC}\approx$0.516 s, elapsed in the discharge circuit of the generator PSG-*C* through the TS of the roof, was in this case the absolute value of about 178 C. This charge corresponds to the average value of current used in current components in the TS equal $i_{CC}\approx q_C/\tau_{pC}\approx$−345 A.

Figures 8 and 9 show the outer appearances and back surfaces of the TS steel roof after co-exposure to the pulsed *A*- and long-term *C*- artificial lightning current component with the ATP, the relevant data waveforms in Fig. 6 and 7. It can be seen that the penetration through the wall of the roof TS stainless steel thickness h=1 mm, in this case (h_a=27 mm) has not occurred. Rounded binding zone on the outer surface of the steel roof TS of pulsed *A*- component of simulated lightning current was the largest dimension of up to 60 mm. The depth of the crater formed in this area does not exceed 50 µm. The circular zone of long-term *C*- binding prolonged artificial lightning current local melting of the components occurred TS steel wall material of the roof, having a melting point of about 1455 °C [7, 15]. The diameter of the melting zone as shown in Fig. 8 and 9 does not exceed 23 mm. On the back surface of the steel roof of the TS clearly manifested «discoloration» the action of its material high temperature pulsed Joule heating.

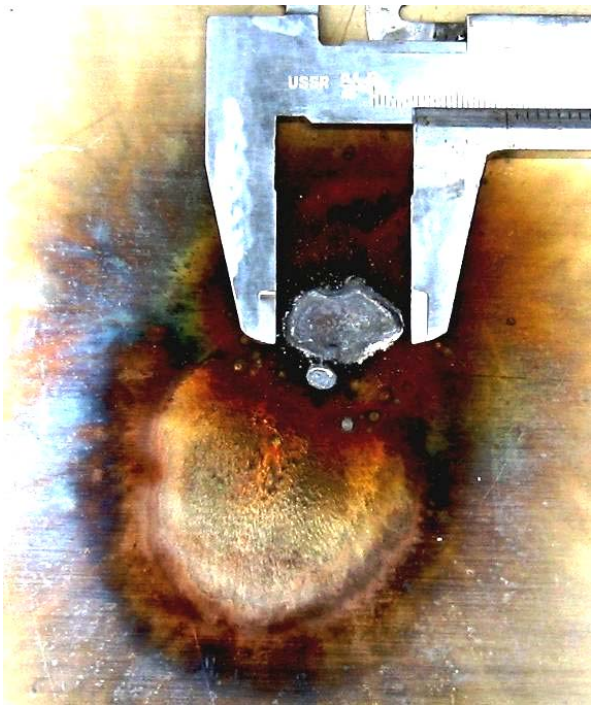

Fig. 8. General view of the outer surface of the steel roof TS circular hearth direct exposure to the pulsed *A*- and long-term *C*- artificial lightning current component with a normalized according to the requirements [3, 4] ATP

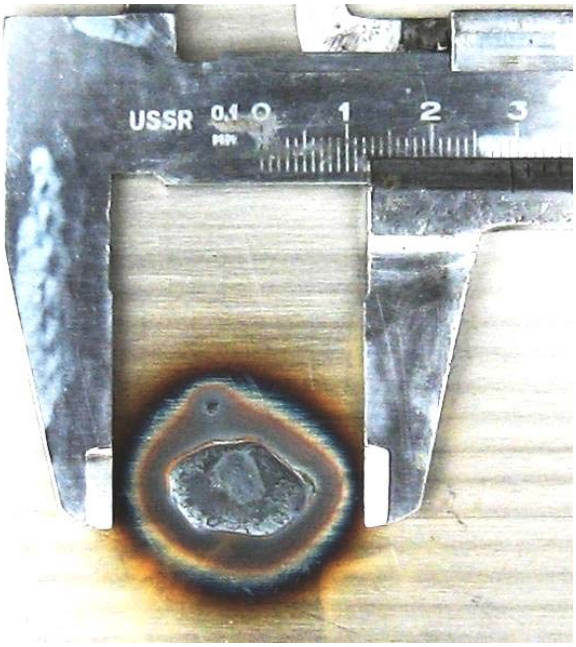

Fig. 9. General view on the rear surface of the TS steel roof rounded hearth direct exposure to the pulsed *A*- and long-term *C*- artificial lightning current component with a normalized according to the requirements [3, 4] ATP

4.2. Results of experiments at h_a=14 mm. Figures 10 and 11 show waveforms respectively for pulsed *A*- and long-term *C*- prolonged artificial lightning current components obtained with respect to the test steel roof of the TS electrothermal lighting resistibility decreases in TES value h_a to 14 mm. ATP of the pulsed components of the simulated lightning current at the same time fully consistent with the ATP this current component of the lightning discharge, shown in Fig. 6. With regard to ATP of the long-term *C*- component of the current simulated lightning, in this case (h_a=14 mm; l_e=37 mm) were changed only their three parameters: total duration i_C current flow decreased to τ_{pC}≈0.448 s; elapsed charge has decreased to a value of q_C≈165 C; average current increased to the level of i_{CC}≈ –367 A. Despite these changes in the long-term ATP of the long-term *C*- components of artificial lightning current, in this case occurred keyhole TS roof wall stainless steel with thickness h=1 mm. Diameter $2r_c$ penetration holes in TS was 12 mm (Fig. 12).

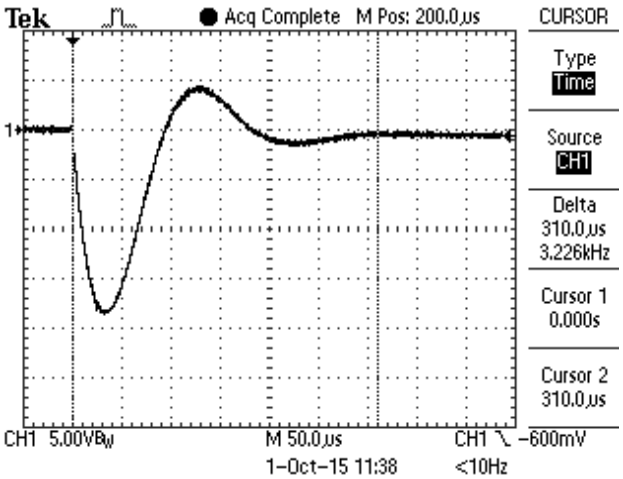

Fig. 10. Waveform of the pulsed *A*- component of artificial lightning current acting in high-current discharge circuit high-voltage generator PCG-*A* on flat steel roof of thickness of h=1 mm (I_{1mA}≈–192 kA; t_{mA}≈34 µs; τ_{pA}≈500 µs; J_A≈1.9·10^6 A^2·s)

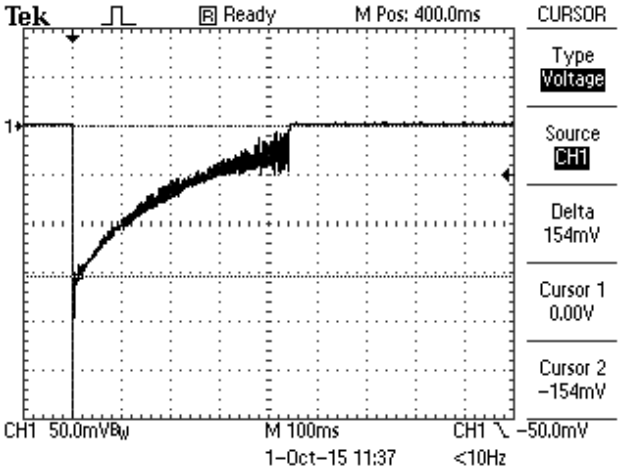

Fig. 11. Waveform of the long-term *C*- component of artificial lightning current acting on the flat roof of the TS steel of thickness of h=1 mm (I_{mC}≈–804 A; t_{mC}≈9 ms; τ_C≈160 ms; τ_{pC}≈0.448 s; q_C≈–165 C; i_{CC}≈–367 A)

Obtained when h_a=14 mm experimental results concerning the keyhole simulated lightning current of the test thin-walled sample steel roof technical facilities, it can be explained by the fact that a decrease in the length of the air gap h_a in TES (respectively, and the length l_e for EEW) desktop type used generator УИТОМ-1 comes stabilization zones binding on the outer surface of the TS steel roof of plasma channels for long-term *C*- and pulsed *A*- artificial lightning current component. In addition, the decrease in the value h_a prevents branching (division) in the air cylinder configuration corresponding plasma channels for high-voltage electrical pulse and arcs (trace smelting from such channel separation for simulated *C*- current components of lightning just present in Fig. 8 and 9) which also contributes to the local concentration of heat energy generated in the material studied stainless steel roofing samples.

Fig. 12. External view of the area with a diameter of about 12 mm of penetration through the flat wall TS steel roof (h=1 mm; h_a=14 mm) by a direct action on long-term C- component of the current artificial lightning and rounded zone diameters up to 58 mm in its surface melting from direct action on TS of pulsed A- components of with standardized requirements for [3, 4] ATP

In favor of this physical explanation of penetration through the wall of the test thin-walled steel roof TS used by us pulse currents with a decrease in the length of the air gap in the TES h_a (even with a decrease in leaked through the TS of the electric charge for a long-term C-artificial lightning current component from 178 to 165 C) show results followed by a series of experiments carried out on a powerful generator type УИТОМ-1 study at TS h_a=14 mm. Figures 13 and 14 show the corresponding waveform for use in this case pulse current component of artificial lightning. If the curve for the pulse current component A simulated lightning in the latter case, repeats similar curves for this current component of artificial lightning, shown in Fig. 6 and 10, the curve for long-term C- lightning current component are significantly different from those of the current curves shown in Fig. 7 and 11. These differences mainly relate to more stable combustion over TES in high TS i_C pulsed arc with a current in the air gap length h_a=14 mm. One of the signs of the process flow of the arc is the virtual absence of the curve aperiodic current i_C imposed considerable amplitude fluctuations (see Fig. 14). The consequence of this electromagnetic process is increased the total duration τ_{pC} flow through pulse current TS steel roof i_C, reaching the numerical value of 0.736 s. This implies also an increased amount of electricity $q_C \approx -187$ C, elapsed through a rounded zone of the plasma channel binding long-term C- component of artificial lightning current on the outer surface of the TS.

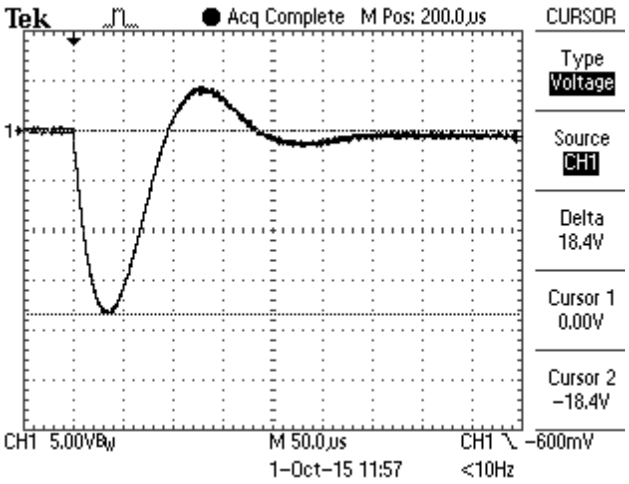

Fig. 13. Waveform of the pulsed A- component of simulated lightning current acting in high-current discharge circuit PCG-A high-voltage generator on a flat thin-walled steel roof IO of thickness of h=1 mm ($I_{1mA} \approx -192$ kA; $t_{mA} \approx 34$ µs; $\tau_{pA} \approx 500$ µs; $J_A \approx 1.9 \cdot 10^6$ A^2·s)

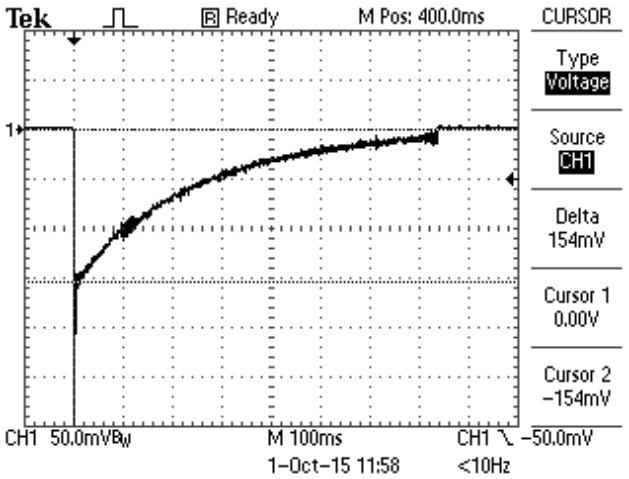

Fig. 14. Waveform of the long-term C- component of simulated lightning current acting in high-current discharge circuit PCG-C high-voltage generator on a flat thin-walled steel roof IO of thickness of h=1 mm ($I_{mC} \approx -804$ A; $t_{mC} \approx 9$ ms; $\tau_C \approx 160$ ms; $\tau_{pC} \approx 0.736$ s; $q_C \approx -187$ C; $i_{CC} \approx -254$ A)

Fig. 15 shows the appearance of the direct results of the joint impact on the flat thin-walled (h=1 mm; h_a=14 mm) of the TS roof stainless steel pulsed A- and long-term C- artificial lightning current component normalized by [3, 4], the ATP which led to keyhole steel wall TS. $2r_{mA}$ diameter of the surface (to a depth of no more than 50 µm) electrothermal exposure chamber on the outer surface of the flat roof on steel TS from pulsed A- simulated lightning current components made with up to 59 mm. The diameter of the holes in the area of penetration through the wall of the test sample from the roof of the electrothermal effect on her long-term component of the current long-term C- simulated lightning was 15 mm.

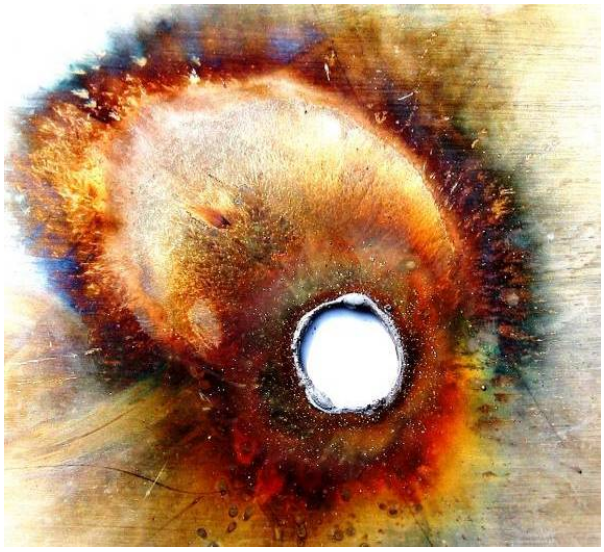

Fig. 15. External view of rounded zones of thermal influence on the flat roof of the TS steel of pulsed *A*- and long-term *C*- artificial lightning current components with standardized requirements for [3, 4] ATP accompanied keyhole TS wall (h=1 mm; h_a=14 mm)

5. Comparison of the results of calculation estimations and performed experiments. This comparison is conducted for the case of a direct action on experimental walled (h=1 mm), the samples of stainless steel 12X18H10T *C*- current component shown in Table 5 (the experiments were performed at the air gap length in TES h_a=14 mm).

Table 5

Comparative data for the results of the executed calculations and experiments for evaluating thermal lighting resistibility of steel samples

Значение заряда q_c, С	Diameter of the melted hole in the steel sample wall (h=1 mm), mm		
	Experiment	By formula (1)	Numerical method [10]
165	12.0	18.0	7.1
187	15.0	20.8	7.7

From Table 5 it follows that the calculated results of the evaluation electrothermal lighting resistibility of steel specimens (h=1 mm) using (1) satisfactory (with an accuracy of up to 28%) agree with the results of the experiments.

Conclusions.

1. The results obtained at the Research and Design Institute «Lightning» of the NTU «KPI» computational and experimental evaluation studies electrothermal resistance experienced flat sample size in terms 500×500 mm stainless steel 1 mm thick to the direct impact on them in the air of pulsed *A*- and long-term *C*- artificial lightning current components with standardized ATPs according to the applicable requirements of the US regulations SAE ARP 5412 and SAE ARP 5416 indicate that we investigated thin-walled steel samples can be exposed keyhole. The diameter of the through-hole penetration in the investigated samples of steel round anchor zone on the outer surface of the plasma channel of long-term *C*- components of simulated in the laboratory lightning current can reach 15 mm.

2. A significant influence on the results of the electro-thermal effects of artificial lightning plasma channels with *A*- and *C*- components of the pulse current at the steel studied experienced technical facilities provide examples of electrical processes of binding the corresponding plasma channels on their outer surface and burning them on a high-voltage pulse of the arc in the air gap TES used in the experiments, a powerful high-voltage generator type УИТОМ-1 artificial lightning current.

3. To prevent possible flashpoint of flammable liquids and materials, placed under the bottom of the thin-walled steel liner with these characteristics, is striking in the open air directly blows high-lightning, it requires the development of specific technical measures that increase the fire safety of such technical facilities to act on them large pulsed lightning currents.

REFERENCES

1. Yuman M.A. *Molniya* [Lightning]. Moscow, Mir Publ., 1972. 327 p. (Rus).

2. Kravchenko V.I. *Molniya. Elektromahnitny faktory i porazhayushchie vozdeystviya na tekhnycheskie sredstva* [Lightning. Electromagnetic factors and their impact on the striking technical objects]. Kharkov, NTMT Publ., 2010. 292 p. (Rus).

3. *SAE ARP 5412: 2013. Aircraft Lightning Environment and Ralated Test Waveforms*. SAE Aerospace. USA, 2013. pp. 1-56.

4. *SAE ARP 5416: 2013. Aircraft Lightning Test M*ethods. SAE Aerospace. USA, 2013. pp. 1-145.

5. Baranov M.I., Koliushko G.M., Kravchenko V.I., Nedzel'skii O.S., Dnyshchenko V.N. A Current Generator of the Artificial Lightning for Full-Scale Tests of Engineering Objects. *Pribory i tehnika eksperimenta − Instruments and Experimental Technique*, 2008, no.3, pp. 401-405. **doi: 10.1134/s0020441208030123**.

6. IEC 62305-1: 2010 «Protection against lightning. Part 1: General principles». Geneva, IEC Publ., 2010.

7. Available at: http://www.sgkarkas.ru/spravochnik/marochnik_stalej/12h18n10t (accessed 15 May 2013). (Rus).

8. Baranov M.I. *Izbrannye voprosy elektrofiziki. Tom 2, Kn. 2: Teoriia elektrofizicheskikh effektov i zadach* [Selected topics of Electrophysics. Vol.2, Book 2. A theory of electrophysical effects and tasks]. Kharkiv, NTU «KhPI» Publ., 2010. 407 p. (Rus).

9. Karslou G., Eger D. *Teploprovodnost' tverdykh tel / Per. s angl.* [Heat conductivity of solids / Transl. from Eng.]. Moscow, Nauka Publ., 1964. 487 p. (Rus).

10. Dronov V.N., Serkov A.A. *Komp'iuternaia programma dlja rascheta struktury elektrotermicheskogo vozdeistvija toka molnii na metallicheskuju obshivku / Svidetel'stvo o registratsii avtorskogo prava № 30557 ot 06.10.2009. Vydano gosudarstvennoi sluzhboi intellektual'noi sobstvennosti Ukrainy* [Computer program for the calculation of structure of electro-thermal action of current of lightning on the metallic edging / Testifying to registration of copyright no.30557 from 06.10.2009. It is given out government service intellectual property of Ukraine]. (Rus).

11. Berzan V.P., Gelikman B.Yu., Guraevsky M.N., Ermuratsky V.V., Kuchinsky G.S., Mezenin O.L., Nazarov N.I., Peregudova E.N., Rud' V.I., Sadovnikov A.I., Smirnov B.K., Stepina K.I. *Elektricheskie kondensatory i kondensatornye ustanovki. Spravochnik* [The electrical capacitors and condenser options. Directory]. Moscow, Energoatomizdat Publ., 1987, 656 p. (Rus).

12. Baranov M.I., Koliushko G.M., Kravchenko V.I., Nedzel'skiy O.S. High-voltage high-current generator air gaps of the current artificial lightning. *Pribory i tekhnika eksperimenta – Instruments and experimental techniques*, 2008, no.6, pp. 58-62. (Rus).

13. Baranov M.I., Rudakov S.V. Development of new charts of capacitance-resistance defense of high-voltage capacitors of powerful capacity stores of energy from emergency currents. *Elektrotekhnika i elektromekhanika – Electrical engineering & electromechanics*, 2015, no.6, pp.47-52. **doi: 10.20998/2074-272X.2015.6.08**. (Rus).

14. Baranov M.I., Kravchenko V.I. Electrothermal resistance wire and cable to the aircraft to the striking action pulsed current lightning. *Elektrichestvo − Electricity*, 2013, no.10, pp. 7-15. (Rus).

15. Kuhling H. *Spravochnik po fizike. Per. s nem*. [Dictonary on Physics. Translated from German]. Moscow, Mir Publ., 1982. 520 p. (Rus).

Received 23.02.2016

M.I. Baranov[1], *Doctor of Technical Science, Chief Researcher,*
V.V. Kniaziev[1], *Candidate of Technical Science, Senior Research Scientist,*
V.I. Kravchenko[1], *Doctor of Technical Science, Professor,*
S.V. Rudakov[2], *Candidate of Technical Science, Associate Professor,*
[1] Scientific-&-Research Planning-&-Design Institute «Molniya», National Technical University «Kharkiv Polytechnic Institute», 47, Shevchenko Str., Kharkiv, 61013, Ukraine,
phone +380 57 7076841, e-mail: eft@kpi.kharkov.ua
[2] National University of Civil Protection of Ukraine, 94, Chernyshevska Str., Kharkiv, 61023, Ukraine,
phone +380 57 7073438, e-mail: serg_73@i.ua

How to cite this article:
Baranov M.I., Kniaziev V.V., Kravchenko V.I., Rudakov S.V. Results of calculation-experimental investigations of electro-thermal resistibility of sheet steel samples to action of rationed components of pulsed current of artificial lighting. *Electrical engineering & electromechanics*, 2016, no.3, pp. 40-49. doi: 10.20998/2074-272X.2016.3.07.

UDC 621.316.99 **doi: 10.20998/2074-272X.2016.3.08**

I.V. Nizhevskyi, V.I. Nizhevskyi

A TECHNIQUE OF MEASURING OF RESISTANCE OF A GROUNDING DEVICE

Introduction. Measurement of resistance of the grounding device (GD) by means of a three-electrode system. This requires not only the right choice of installation locations of measuring electrodes, but also the determination of the point of zero potential. Implementation of these requirements quite time-consuming, and in some cases impossible. Aim. Develop a new technique for measuring the electrical resistance of the GD. Task. The method of measuring the resistance of the GD with the help of a three-electrode setup is necessary to exclude the determination of the point of zero potential. Method. Mathematical modeling and calculation engine. Results. A three-electrode system for measuring the resistance of grounding devices (GD) for various purposes is considered. On the basis of Maxwell equations a theoretical substantiation of a new technique for measuring the resistance of any GD of any construction in random soil structure has been proposed. An equation system of the sixth order has been obtained, its solution makes it possible to measure its own mutual resistance in the three-electrode installation with sufficiently high accuracy. Peculiarities of drawing up a calculation scheme of substitution of a three-electrode installation with lumped parameters: self and mutual impedance. Use of the principle of reciprocity eliminates the need of finding a point of zero potential which is a rather difficult task. The technique allows to minimize the spacing of measuring electrodes outside the GD, which substantially reduces the length of wiring of the measurement circuit and increases the «signal-to-interference» ratio and also removes the restrictions on the development of the territory outside the GD being tested. Conclusion. The procedure allows to evaluate the self and mutual impedance grounding all the electrodes in a three-electrode measuring installation of the grounding resistance of the device without finding the point of zero potential. References 12, tables 2, figures 11.

Key words: **grounding device, resistance measurement, three-electrode installation, minimum spacing of measuring electrodes, technique of measuring, substitution circuit.**

Рассмотрена трехэлектродная установка для измерения сопротивления заземляющих устройств (ЗУ) различного назначения. На основе использования системы уравнений Максвелла предложено теоретическое обоснование методики измерения сопротивления ЗУ любой конструкции в произвольной структуре грунта. Получена система уравнений шестого порядка, решение которой позволяет определить собственные и взаимные сопротивления в трехэлектродной установке с достаточно высокой точностью. Рассмотрены особенности составления расчетной схемы замещения трехэлектродной измерительной установки с сосредоточенными параметрами: собственными и взаимными сопротивлениями. Используя принцип взаимности, исключена необходимость отыскания точки нулевого потенциала, представляющего весьма трудоемкую задачу. Методика позволяет обеспечить минимально возможный разнос измерительных электродов за пределами ЗУ, что существенно уменьшает длину соединительных проводов схемы измерения и увеличивает отношение «сигнал–помехи», а также снимает ограничения по застройке территории за пределами исследуемого ЗУ. Библ. 12, табл. 2, рис. 11.

Ключевые слова: **заземляющее устройство, измерение сопротивления, трехэлектродная установка, минимальный разнос измерительных электродов, методика, схема замещения.**

Introduction. Fundamental works of famous scientists: A.L. Vainer [1], S.I. Kostruba [2], A.B. Oslon [3] Iu.V. Tselebrovskii [4], A.I. Yacobs [5], and others deal with problems of measurement of electrical parameters of the earth and grounding devices (GD). In their works domestic and foreign researchers note that one of the main problems is that the exact measurement of resistance of GD for various purposes.

Currently, widespread is a three-electrode measuring device for measuring the resistance of the GD. One of the main problems to be solved to get to this setting, sufficiently accurate results, is as specified in [6], the right choice of places measuring electrode, i.e. correct placement at which the measured value is accompanied electrodes different from its true value by not more than a certain amount, which is called acceptable error of measurement. It is usually assumed that at the measurement of the GD resistance error of about 10% in either direction is acceptable [5].

Measurement of resistances of large GD in a uniform soil is presented in [6] which describes the calculation method defined-division optimal placement of measuring electrodes when measuring resistance of large GD permitting the electrodes placement at short distances by GD. However, it is noted that the calculations with the help of earth considered models have only limited application due to their external fields.

Analysis of Tagg methods for measurement of earth resistance given in [7] showed that Tagg method is not suitable in soils with increasing the depth of soil resistivity.

Besides, in the conclusions of [8] it pointed out that there is a fundamental ability to accurately measure of the GD resistance for any character of the soil heterogeneity and any size and configuration of GD without the use of computational programs which also shows the realization of this possibility. However, unfortunately, in this case it

will be necessary to determine the location of the potential electrode by finding the point of zero potential on-site measurements.

Mathematical modeling of the GD resistance measurement process for current of industrial frequency in multilayer soil is presented in [9] which describes an algorithm for calculating the GD resistance measurement errors of electrical installations in multilayer soils at various locations of the measuring electrodes and is an example of building an equal error lines for GD complex shapes in a four-layer ground. Unfortunately, as the authors note [9], choose a layout of electrodes, in which the measured GD resistance equals true, experimentally in measurements on the ground is impossible.

The goal of the work is theoretical substantiation of methods of measuring the GD resistance by means of a three-electrode measuring setup with any character of soil heterogeneity of any size and configuration of GD and the random placement of the measuring electrodes.

Theoretical justification of a developed GD resistance measurement technique. Three-electrode system for measuring the resistance of memory for various purposes in the general case is a multi-electrode system. A calculation of multi-electrode systems in a linear conductive medium of any structure, as noted in [9], based on a system of equations proposed by Maxwell [10].

In this regard, we first consider the example of the calculated equivalent circuit when placing passive grounding in the current field of active GD. Fig. 1 shows the elements of the equivalent circuit: R_1 is the active GD, R_2 is the passive GD, R_{12} is the mutual resistance.

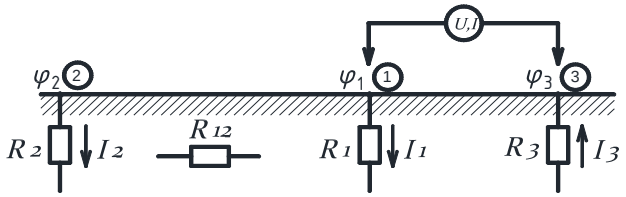

Fig. 1. Mutual influence of active (1) and passive (2) GD

We assume that the current source I_1 has the second pole (R_3), being located so that its field has no effect on the potential at point 2. Potential in point 2 (φ_2) is determined as $I_1 \cdot R_{12}$ then from passive electrode R_2 current I_2 flows into the ground. Source (of current) loaded by additional current I_2; if the source is defined as a «source of voltage», the potential of point 1 (φ_1) is reduced. In the case of «source voltage», power load increases due to the summation of the currents I_1 and I_2. The presence of the two currents (I_1 and I_2) allows the use of already known system Maxwell equations:

$$\begin{cases} \varphi_1 = I_1 R_1 + I_2 R_{12}; \\ \varphi_2 = I_1 R_{12} + I_2 R_2. \end{cases} \quad (1)$$

We note certain limitations in determining the (pilot) of mutual resistance: from the experience of two grounding resistance R_{12} is indefinable. The desire to determine all three resistances is realized when working with a system of three mutually influencing groundings.

Maxwell equations define the potential field communication, whereas to simplify calculations it is more convenient to use the equivalent circuit with some (φ, I, R) parameters.

On the example of two GD streamlined by the same current source (U, I) in a series chain (Fig. 2), consider the options of the equivalent circuit.

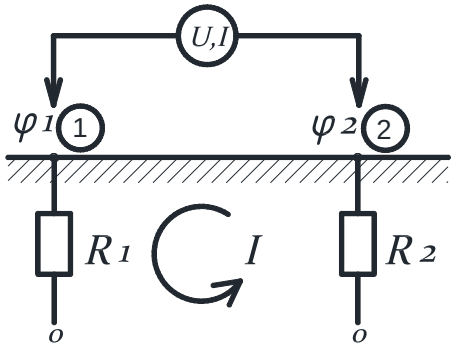

Fig. 2. The system of two GD at their series connection

Following the electrostatic analogy and Maxwell equations we have

$$\begin{cases} \varphi_1 = IR_1 - IR_{12}; \\ \varphi_2 = -IR_{12} + IR_2. \end{cases} \quad (2)$$

On the base of equations (2) we can write

$$\begin{aligned} \varphi_1 + \varphi_2 = U = I\left(R_1 - R_{12} + R_2 - R_{12}\right) = \\ = I\left(R_1 + R_2 - 2R_{12}\right) = IR_{equ}. \end{aligned} \quad (3)$$

Following equation (3) the equivalent circuit has a form (Fig. 3).

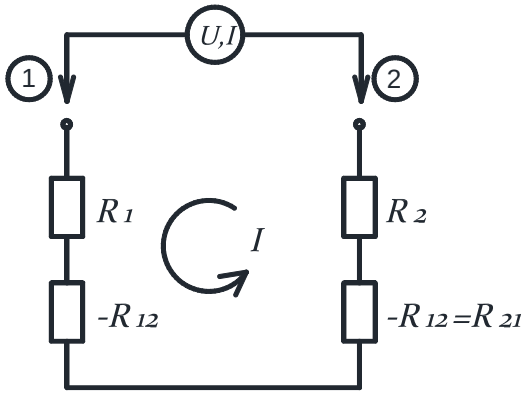

Fig. 3. A variant of the equivalent circuit for series connected GD

The circuit shown in Fig. 3 is suitable for mathematical modeling, but not for the physical model because of the negative resistances R_{12}. The physical analogue for the circuit in Fig. 3 we present in the form of a diagram on Fig. 4.

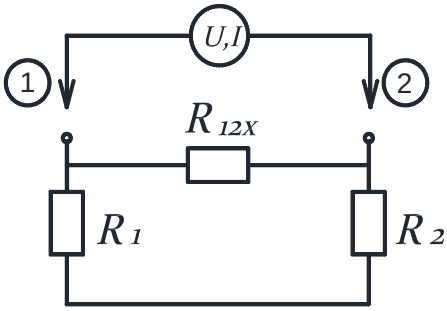

Fig. 4. Calculated analogue of the equivalent circuit

By equality of input resistance of circuit on Fig. 3 and Fig. 4 we have:

$$R_1 + R_2 - 2R_{12} = \frac{(R_1 + R_2)R_{12X}}{R_1 + R_2 + R_{12X}}. \quad (4)$$

After arrangement of summands we obtain

$$2R_{12X}R_{12} = (R_1 + R_2)^2 - 2R_{12}(R_1 + R_2), \quad (5)$$

and from here we obtain

$$R_{12X} = \frac{(R_1 + R_2)^2}{2R_{12}} - R_1 - R_2, \quad (6)$$

or obtain a relation between resistances R_{12} (see formula (5)) and R_{12X}:

$$R_{12} = \frac{(R_1 + R_2)^2}{2(R_1 + R_2 + R_{12X})}. \quad (7)$$

We take into account that mutual resistance R_{12} less than the smaller of resistances R_1 or R_2 and $R_{12X} > 0$.

Using the model for the Fig. 4 in the calculations permits to find the value R_{12X} in view of the expression (7) makes it possible to determine the relative resistance R_{12X}; accounting effect of R_{12} (with the appropriate sign) should be carried out according to Fig. 3.

Measurements at two GD (see Fig. 2) by the input source (U, I) do not allow to decipher the values of R_1, R_2 and R_{12} as well as the potential φ_1 and φ_2. We introduce the third electrode to the point 3, as shown in Fig. 5, and consider three experiments: A, B and C.

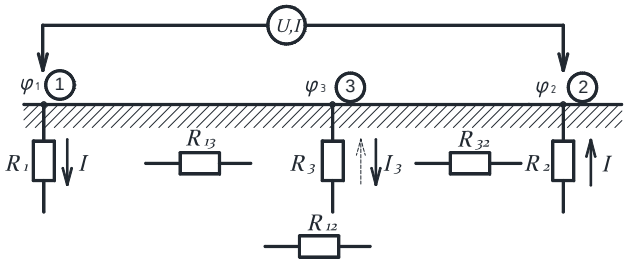

Fig. 5. A three-electrode system of GD, experiment A

In the experiment A the active electrodes 1 and 2, streamlined common current I from the source, create a potential field for the passive electrode 3, which determines the potential of the latter:

$$\varphi_3 = R_{13}I - R_{32}I = I(R_{13} - R_{32}) = IR_{3E}. \quad (8)$$

There are U_{13} and U_{32} voltage. For example, when $U_{32} < U_{13}$ and influence of the electrode 2 on the formation of φ_3 increase over the electrode 1. Under the influence of φ_3 in the electrode 3 the current $I_3 = \varphi_3/R_3$ flows. In the case of $U_{32} < U_{13}$ current I_3 has same direction as the current in resistance R_2; direction of current I in the electrode 1 is assumed positive, and in electrode 2 – negative.

The presence of current I_3 should be considered for active electrodes 1 and 2 through the respective mutual resistance in Maxwell equations. Taking into account the expressions (8) for the active electrode 1, the summand appears

$$-I_3R_{13} = -I\frac{(R_{13} - R_{32})}{R_3}R_{13},$$

and potential of the electrode 1 is determined as

$$\varphi_1 = R_1I - R_{12}I - I\frac{(R_{13} - R_{32})}{R_3}R_{13} = \\ = I\left[R_1 - R_{12} - \frac{(R_{13} - R_{32})R_{13}}{R_3}\right] = IR_{1E}. \quad (9)$$

Analogously, we obtain potential for the active electrode 2:

$$\varphi_2 = I\left[R_2 - R_{12} + \frac{(R_{13} - R_{32})R_{32}}{R_3}\right] = IR_{2E}. \quad (10)$$

Potentials φ_1, $\varphi_2$and φ_3 according equations (8), (9) and (10) are expressed by source current I and values of resistors (own R_s (R_1, R_2 and R_3) and mutual R_{vz} ($R_{12} = R_{21}$, $R_{13} = R_{31}$ and $R_{23} = R_{32}$)).

Voltage measurement between passive 3 and active 1 and 2 electrodes determines respectively

$$U_{13} = \varphi_1 - \varphi_3;$$

$$U_{32} = \varphi_3 - \varphi_2.$$

As a result,

$$U_{13} = I(R_{1E} - R_{3E}) \text{ and } \frac{U_{13}}{I} = R_{1E} - R_{3E}, \quad (11)$$

$$U_{32} = I(R_{3E} - R_{2E}) \text{ and } \frac{U_{32}}{I} = R_{3E} - R_{2E}. \quad (12)$$

Voltages measurement U_{13}, U_{32} at current I determines left-hand sides of two coupling equations with six resistors according to (11) and (12).

The next two equations we obtain as measured input current between points 1 and 3. In this case, according to Fig. 6, we consider experiment B.

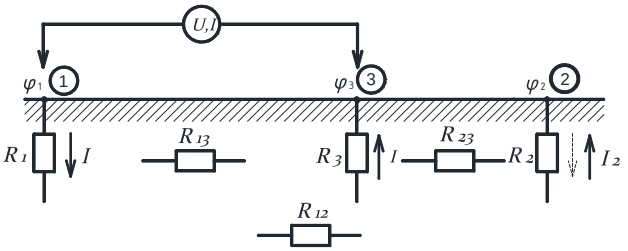

Fig. 6. Connection of the source (U, I) in the experiment B

Voltages U and current I are «own» for this experiment, i.e. they different from the values in the experiment A. Measuring voltages U_{32} and U_{12} allows to determine, for example $U_{32} < U_{12}$ a then to assume current in the resistance R_2 coinciding with the direction of current in the resistance R_3.

For the passive electrode 2 we have potential

$$\varphi_2 = I\left(R_{23} - R_{12}\right) = IR_{2E},$$

and flowing from its current

$$I_2 = I\frac{\left(R_{23} - R_{12}\right)}{R_2}.$$

For the active electrode 1 we determine potential by expression

$$\varphi_1 = I\left[R_1 - R_{13} - \frac{\left(R_{23} - R_{12}\right)R_{12}}{R_2}\right] = IR_{1E}.$$

Taking into account mutual influences, for active electrode 3 we have potential

$$\varphi_3 = I\left[R_3 - R_{13} + \frac{\left(R_{23} - R_{12}\right)R_{23}}{R_2}\right] = IR_{3E}.$$

As a result, we obtain voltages available for measurements

$$U_{12} = \varphi_1 - \varphi_2 = I\left(R_{1E} - R_{2E}\right) \text{ or } \frac{U_{12}}{I} = \left(R_{1E} - R_{2E}\right) \quad (13)$$

and voltages

$$U_{32} = \varphi_3 - \varphi_2 = I\left(R_{3E} - R_{2E}\right) \text{ or } \frac{U_{32}}{I} = \left(R_{3E} - R_{2E}\right). \quad (14)$$

In the experiment C the source (U, I) is connected between points 3 and 2 as shown in Fig 7.

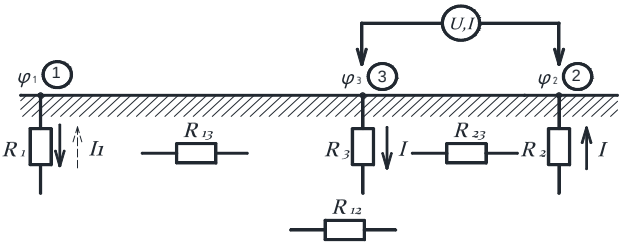

Fig. 7. Connection of the source (U, I) in the experiment C

Measuring voltages U_{13} and U_{12} allows in the case, for example $U_{13} > U_{12}$ assume the potential φ_1 near to potential φ_2 and currents for points 1 and 2 have the same direction.

We express potential of passive electrode 1:

$$\varphi_1 = -IR_{12} + IR_{13} = I\left(R_{13} - R_{12}\right) = IR_{E1}.$$

Current I_1 in the resistance R_1 we determine by formula:

$$I_1 = I\frac{\left(R_{13} - R_{12}\right)}{R_1}.$$

Potentials of active electrodes 3 and 2 are respectively determined by formulae:

$$\varphi_3 = I\left(R_3 - R_{32} - \frac{\left(R_{13} - R_{12}\right)}{R_1}R_{13}\right) = IR_{E3}$$

and

$$\varphi_2 = I\left(R_2 - R_{32} + \frac{\left(R_{13} - R_{12}\right)}{R_1}R_{12}\right) = IR_{E2}.$$

Because of in this experiment we measure voltages

$$U_{12} = \varphi_1 - \varphi_2 = I\left(R_{E1} - R_{E2}\right)$$

and

$$U_{13} = \varphi_1 - \varphi_3 = I\left(R_{E1} - R_{E3}\right),$$

then finally we obtain next two equations:

$$\frac{U_{12}}{I} = \left(R_{E1} - R_{E2}\right) \quad (15)$$

and

$$\frac{U_{13}}{I} = \left(R_{E1} - R_{E3}\right). \quad (16)$$

So, above consideration determines amount of tests (measurements) in three experiments (A, B, C).

Input of the source (U, I) in points 1 and 2 (experiment A) and measuring voltages U_{13A} and U_{32A} at current I_A, gives a possibility to calculate input resistances

$$\frac{U_{13A}}{I_A} = R_{(1-3)A}$$

and

$$\frac{U_{32A}}{I_A} = R_{(3-2)A}.$$

Such resistances are left-hand sides of equations:

- from equations (8), (9) and (11) we obtain

$$R_{(1-3)A} = \left[\left(R_1 - R_{12}\right) - \frac{\left(R_{13} - R_{32}\right)R_{13}}{R_3}\right] - \left(R_{13} - R_{32}\right), \quad (17)$$

- from equations (8), (10) and (12):

$$R_{(3-2)A} = \left[\left(R_2 - R_{12}\right) + \frac{\left(R_{13} - R_{32}\right)R_{32}}{R_3}\right] + \left(R_{32} - R_{13}\right). \quad (18)$$

Experiment B, input of the source (U, I) in points 1 and 3 and measuring voltages U_{32B} and U_{12B} at current I_B.

Taking into account above-mentioned (expressions (13) and (14)) we obtain

$$R_{(1-2)B} = \frac{U_{12B}}{I_B} = \left[\left(R_1 - R_{13}\right) - \frac{\left(R_{23} - R_{12}\right)R_{12}}{R_2}\right] - \left(R_{23} - R_{12}\right); \quad (19)$$

$$R_{(3-2)B} = \frac{U_{32B}}{I_B} = \left[\left(R_3 - R_{13}\right) + \frac{\left(R_{23} - R_{12}\right)R_{23}}{R_2}\right] - \left(R_{23} - R_{12}\right). \quad (20)$$

Experiment C, input of the source (U, I) in points 3 and 2, measuring voltages U_{13C} and U_{12C} at current I_C.

Taking into account expression (15) we obtain

$$\frac{U_{12C}}{I_C} = \left(R_{12} - R_{13}\right) + \left[R_2 - R_{32} + \frac{\left(R_{13} - R_{12}\right)R_{12}}{R_1}\right] = R_{(1-2)C}, \quad (21)$$

and from expression (16) we have

$$\frac{U_{13C}}{I_C} = (R_{12} - R_{13}) + \left[R_3 - R_{32} - \frac{(R_{13} - R_{12})R_{13}}{R_1} \right] = \quad (22)$$

$= R_{(1-3)C}$.

Finally, we obtain a system of six equations (17) – (22) with six unknowns (R_1, R_2, R_3, R_{12}, R_{13}, R_{23}) at known from measurements resistances values $R_{(1\text{-}3)A}$, $R_{(3\text{-}2)A}$, $R_{(1\text{-}2)B}$, $R_{(3\text{-}2)B}$, $R_{(1\text{-}2)C}$, $R_{(1\text{-}3)C}$.

Solution of the obtained system of six equations with six unknowns is carried out by the code realized in the Mathcad environment.

Some peculiarities of measuring GD resistance. It is useful to add the following to the presented technique. In the case of applying the method to an electrode of zero potential φ_p, for example, a linear circuit «object with R_g – current electrode R_c» and experimentally determined location and potential of the last electrode R_g they achieve the condition

$$\varphi_p = 0 = \alpha_{gp} I - \alpha_{cp} I \quad (23)$$

at series connection of R_g and R_c with source (U, I) – see Fig. 2.

In general case, the potential φ_p by equation (23) is not zero, but there are the potentials of the current I to the electrodes R_g and R_c. Then, if there is some conductivity (to ground) potential electrode when at $\varphi_p \neq 0$ and a current I_p flowing between the electrodes in the circuit voltage dissipated:

$$\begin{cases} \varphi_g - \varphi_p = U_{g-p}; \\ \varphi_c - \varphi_p = U_{c-p}, \end{cases} \quad (24)$$

in accordance with expression

$$\varphi_p = \alpha_{gp} I - \alpha_{cp} I + \alpha_{pp} I_p = U_{g-p} - U_{c-p} + U_p, \quad (25)$$

where α_{pp} is the own potential coefficient of the GD of the potential electrode.

Voltage $U_{g\text{-}p}$ can $U_{c\text{-}p}$ can be measured under the condition of the measuring circuit is negligibly small influence on the current distribution of conductivity in the investigated system (electrodes R_g, R_p and R_c).

At known current I and measured voltage $U_{g\text{-}p}$ by expression

$$U_{g-p} = \alpha_{gp} I, \quad (26)$$

we estimate the value of α_{gp}.

In this system three grounding (Fig. 5) similar to the calculations of the type (26) allow us to determine (based on designations in Fig. 5) mutual resistance R_{12}, R_{13}, R_{23}.

Known values are now possible to consider the mutual resistances for determining own resistances three equations, for example, (17) – (19) or another combination of the equations forming the reciprocal of resistances after introducing in the third order system.

The above approach to the definition of the self and mutual impedances in the case of three of earth is based on the mutual influence of natural elements of earth of a particular group. Great opportunities for research give equivalent circuit and methods of calculation of electrical circuits. It is obvious that communication should form the equation in the case of three GD of the sixth-order equations (the number of mutual and inherent resistance).

Formally, especially solutions of the sixth-order equations can be estimated at solutions for the equivalent circuit with the desired resistors. Estimated scheme (also used for physical modeling) for a group of earth discussed below.

We distinguish for example a group of three GD as shown in Fig. 8.

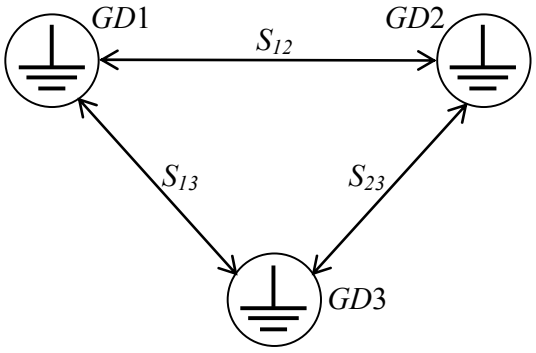

Fig. 8. Placement variant (in plane) of GD group with distances S one from another

Lack of electrical (conductive) links between them necessarily checked.

By definition – every memory can be characterized by some «own» resistance R_s (as if there is no effect of «neighbors») and the effect of the mutual resistance R_{vz}.

By the way, the traditional situation (as reflected in the instructions, guidance documents, and others) of measurement, for example, R_{GD1} is consistent with Fig. 8 at GD2 (or GD3) – current electrode and GD3 (GD2), respectively – potential. Moreover, it is recommended to ensure the lowest possible mutual impedance (in fact – interference) through a search for a comfortable position for GD2 and GD3, either through an increase in distance. Obviously recommendations of RD [11, 12] in their implementation involve estimation of own resistance of GD1.

We will seek to simplify (v. RD) for proper R_{GD1}, namely through the definition of (quantitative) of R_s and R_{vz} in the circuit according to Fig. 8. The proposal removes the requirement to remove the RD current electrode from R_{GD1} (unknown); simplified measurement of their capacity to R_{GD1}.

For three (electrically not connected) GD located in some way in the area (Fig. 8) the use of electrostatic analogy, taking into account the transformations (6) and (7) allows you to submit a design scheme of substitution in the form shown in Fig. 9. We note that the initial measurements are three points accessible: 1, 2, 3.

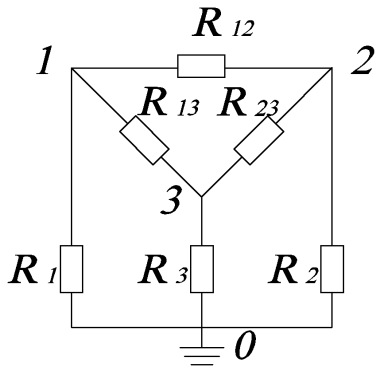

Fig. 9. Calculated equivalent circuit for the group of three GD

Some source (U, e.g. transformer) is connected alternately to the two points of the system and we measure the applied voltage and the voltage of the third point on the two connected to the source. Separate experiments (I, II and III) are shown in Fig. 10 and designated as *a*, *b* and *c* respectively.

The corresponding voltage (U_{12}, U_{13}, U_{32},) in different experiments are different by values.

Under laboratory conditions, the equivalent circuit model is studied (see Fig. 9) with certain parameters, which are shown in Table 1.

Table 1

Resistors values for the circuit on Fig. 9

Resistor	R_1	R_2	R_3	R_{12}	R_{13}	R_{23}
Value, Ω	10	20	5	5	3	3

Results of measurements are presented in Table 2.

Table 2

Measurements of voltages in the equivalent circuit model on Fig. 9 in accordance with Fig. 10

Source connect	U_{12}, V	U_{23}, V	U_{13}, V	φ_1, V	φ_2, V	φ_3, V
Test I, U_{12}	2.75	1.42	1.33	1.18	1.6	0.18
Test II, U_{23}	1.47	2.31	0.83	0.28	1.77	0.55
Test III, U_{13}	1.4	0.82	2.24	1.5	0.09	0.74

Voltages on the «own» resistance measured with respect to the point of «0», designated by the appropriate φ.

The ratios of measured voltage systems are described by systems:

$$\text{Fig. 10,}a \quad \begin{cases} U_{12} = \varphi_1 + \varphi_2; \\ U_{23} = \varphi_2 - \varphi_3; \\ U_{13} = \varphi_1 + \varphi_3; \end{cases} \tag{27}$$

$$\text{Fig. 10,}b \quad \begin{cases} U_{12} = \varphi_2 - \varphi_1; \\ U_{23} = \varphi_2 + \varphi_3; \\ U_{13} = \varphi_1 + \varphi_3; \end{cases} \tag{28}$$

$$\text{Fig. 10,}c \quad \begin{cases} U_{12} = \varphi_1 - \varphi_2; \\ U_{23} = \varphi_2 + \varphi_3; \\ U_{13} = \varphi_1 + \varphi_3. \end{cases} \tag{29}$$

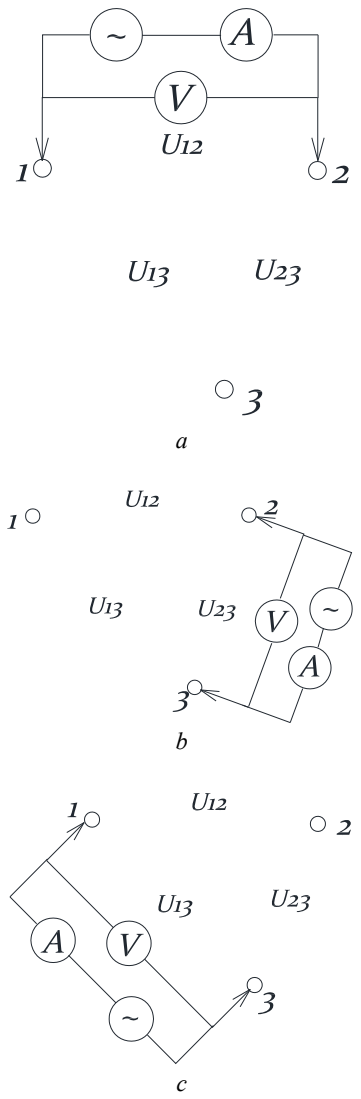

Fig. 10. Connection of the source and measured voltages in the group of GD on Fig. 8

Some equalities in (27) – (29) are satisfied with the approximate measurements of voltages

Formally, the system, for example, (27) has three equations with three unknowns φ_1, φ_2 and φ_3. However, the system is unsolvable by elementary exception of one of unknowns and further solution of two equations with two to remain unknowns.

However, we note that (according to the measurements, calculations) assessment of values φ in systems (27) – (29) is sufficient to obtain the desired resistance of all six unknown resistances (three of their own, the three mutual).

Additional investigations on the territory of the placement of grounding devices GD1, GD2 and GD3 are to remove the gradient curves in an easy direction to connect the variants of Fig. 10. We suppose that t two GD switches at the earth's surface to an applied voltage (Fig. 11,*a*) is formed the U_x potential field, including any and l lines on the surface of earth between the GD edges (Fig. 11,*b*).

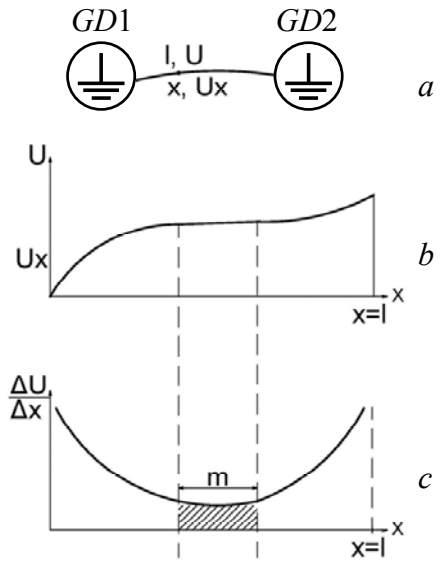

Fig. 11. Potential field between two GD and a gradient curve

The curve (potential) in Fig. 11,*b* corresponds to the gradient curve $\Delta U_x / \Delta x$ (see Fig. 11,*c*). ΔU_x measurements appear to be relatively simple: the input terminals of a voltmeter connected to the electrodes with a length Δx spacing interchanges along the line *l* of the template.

The voltage measured by the voltmeter (one terminal – in the soil at the site *m*, the second (by turn) in point 1 and point 2) assess φ_1 and φ_2. Like the majority of measurements for the GD, the method considered for φ_1, φ_2 is approximate.

Knowledge of φ_1, φ_2 determines the φ_3 value for the system (27); from the values of φ_1 and φ_2 we find φ_1 in (28); from the values of φ_1 and φ_3 we found φ_2 in (29). The subsequent calculation of the possible conductivity (resistance) for the circuit according to Fig. 9 is discussed above.

The code which implements the methodology set out in the paper allows on the basis of the relevant electrical measurements to evaluate not only the resistance of the grounding of electrical devices, but also as its own and mutual resistance grounding all the electrodes in a three-electrode setup measuring the resistance of the grounding device. Also, there is no need to distribute the measuring electrodes longer distances and therefore use large wire length measuring circuit in a three-electrode system. Furthermore, the proposed method is no limitation in the arrangement of the measuring electrodes due to local conditions, even in the case of densely built-up area outside of the investigated GD. Finally, most importantly – there is no need to find the point of ground potential at the measurement electrode or the potential for counting zero error boundaries representing a time-consuming process.

The results of experimental investigations of a three-electrode setup of measuring GD resistance in the electrolytic bath of the National Technical University «Kharkiv Polytechnic Institute» showed that the proposed method provides a fairly accurate results in all cases, measurement of resistance of grounding of electrical devices.

Conclusions.

1. Firstly is a theoretical foundation of the new technique of measuring the resistance of the GD with the help of a three-electrode measuring setup with any character of soil heterogeneity, of any size and configuration of grounding devices and random placement of the measuring electrodes, which, in essence, is universal is presented.

2. On the basis of the investigations carried out it is found that the developed method has the following advantages:

- it permits to evaluate own and mutual resistances of GD of all the electrodes in a three-electrode setup measuring the resistance of the grounding device;
- there is no need for spacing measurement electrodes over long distances in the measuring circuit of a three-electrode unit;
- there are no restrictions in the arrangement of the measuring electrodes due to local conditions, even in the case of dense building areas outside of the investigated GD;
- there is no need for searching the point of zero potential in the place of measuring for the potential or in the calculation of zero error boundary representing a time-consuming process.

REFERENCES

1. Vainer A.L. *Zazemleniia* [Grounding]. Kharkov, GNTI Ukrainy Publ., 1938. 287 p.

2. Kostruba S.I. *Izmerenie elektricheskikh parametrov zemli i zazemlyayushchikh ustroistv* [Measurement of electrical parameters of the earth and ground grids]. Moscow, Energoatomizdat Publ., 1983. 168 p. (Rus).

3. Oslon A.B. Grounding devices on power lines and high voltage substations. *Results of science and tech. VINITI. Ser. el. stations, networks and systems*. Moscow, VINITI Publ., 1966, pp. 65-184. (Rus).

4. Kats E.L., Men'shov B.G., Tselebrovskii Iu.V. Grounding devices of electrical installations of high and low voltage. *Results of science and tech. VINITI. Ser. el. station and networks*. Moscow, VINITI Publ., 1989, vol. 15, 158 p. (Rus).

5. Burgsdorf V.V., Yakobs A.I. *Zazemlyayushchie ustroystva elektroustanovok* [Grounding device of electrical installations]. Moscow, Energoatomizdat Publ., 1987. 400 p. (Rus).

6. Oslon A.B., Kostruba S.I. Measuring the resistance of large grounding devices. *Electrichestvo – Electricity*, 2006, no.8. pp. 49-56. (Rus).

7. Oslon A.B. Tagg methods analysis for measuring grounding resistance. *III Rossiiskaia konferentsiia po zazemliaiushchim ustroistvam: Sbornik dokladov* [3rd Russian Conf. on Grounding Devices: Collected Papers]. Novosibirsk, Russia, 27-31 October 2008, pp. 111-120. (Rus).

8. Oslon A.B., Tselebrovskii Iu.V. The intersection of the potential curves and the resistance of the grounding device *III Rossiiskaia konferentsiia po zazemliaiushchim ustroistvam: Sbornik dokladov* [3rd Russian Conf. on Grounding Devices: Collected Papers]. Novosibirsk, Russia, 27-31 October 2008, pp. 121-130. (Rus).

9. Oslon A.B., Kostruba S.I. Mathematical modeling of the process of grounding resistance measurement current of industrial frequency in multilayer soil. *Electrichestvo – Electricity*, 2008, no.5, pp. 12-17. (Rus).

10. Neiman L.R., Kalantarov P.L. *Teoreticheskie osnovy elektrotekhniki. Ch. 3* [Theoretical Foundations of Electrical Engineering. Part 3]. Moscow, Leningrad, Gosenergoizdat Publ., 1948. 343 p. (Rus).

11. *RD 153-34.0-20.525-00. Metodicheskie ukazaniia po kontroliu sostoianiia zazemliaiushchikh ustroistv elektroustanovok* [RD 153-34.0-20.525-00. Guidelines for the control of state-earthlings electrical devices]. Moscow, SPO ORGRES Publ., 2000. 64 p. (Rus).

12. *SOU 31.2-21677681-19:2009. Viprobuvannya ta kontrol' pristroyiv zazemlennya elektroustanovok. Tipova instruktsiya* [SOU 31.2-21677681-19:2009. Test and control devices, electrical grounding. Standard instruction.]. Kyiv, Minenergovugillya Ukrayiny Publ., 2010. 54 p. (Ukr).

Received 27.12.2015

I.V. Nizhevskyi[1], *Engineer,*
V.I. Nizhevskyi[1], *Candidate of Technical Science, Associate Professor,*
[1] National Technical University «Kharkiv Polytechnic Institute», 21, Frunze Str., Kharkiv, 61002, Ukraine
phone +380 57 7076977,
e-mail: nivich1@mail.ru

How to cite this article:
Nizhevskyi I.V., Nizhevskyi V.I. A technique of measuring of resistance of a grounding device. *Electrical engineering & electromechanics*, 2016, no.3, pp. 50-57. doi: 10.20998/2074-272X.2016.3.08.

UDC 621.311 **doi: 10.20998/2074-272X.2016.3.09**

G.A. Senderovich, A.V. Diachenko

A METHOD FOR DETERMINING LOCATION OF VOLTAGE FLUCTUATIONS SOURCE IN ELECTRIC GRID

Purpose. The purpose of work is development of a method of definition of the location of a source of fluctuations of voltage. Methodology. The reasons of emergence of fluctuations of voltage at an arrangement of a source both in power lines, and in the consumer's networks, are connected with changes of consumption and active and reactive capacities. As criterion for definition of the location of a source of fluctuations of voltage we choose change of size of the active power received by reception substation on equivalent communication with system. The source of fluctuations of voltage is external for the consumer if emergence of fluctuations of voltage leads to the coordinated changes of tension and consumed in the area of active power that corresponds to a condition of the positive regulating effect of active loading on voltage (1). The source of fluctuations of voltage is internal for the consumer if emergence of fluctuations of voltage leads to counter changes of tension and consumed in the area of active power that resembles a condition of the negative regulating effect of active loading on voltage superficially (6). Results. The method of definition of the location of a source of fluctuations of voltage in an electric network which, works by the principle of an assessment of correlation of change of power and tension in a power supply network is developed. The method allows to consider shift between extrema of curves of change of voltage of U(t) and power of $P_{load}(t)$. Originality. The method of definition of an arrangement of a source of fluctuations of voltage is developed. Practical value. The answer to this question where the source of fluctuations of voltage (in the territory of the consumer is located or in an external network) confirmed with the determined calculation, can form a basis of the expert opinion for the solution of legal disputes at an assessment of the damages caused by poor quality of electric energy. References 5, figures 4.

Key words: **quality of the electric power, indicators of quality of the electric power, fluctuation of voltage, source of fluctuation of voltage, curve of change of voltage, curve of change of active power, definition of responsibility.**

Предложен метод корреляции колебаний мощности и напряжения, который позволяет определять место расположения источника колебаний напряжения в системе электроснабжения. Библ. 5, рис. 4.

Ключевые слова: **качество электроэнергии, показатели качества электроэнергии, колебания напряжения, источник колебания напряжения, кривая изменения напряжения, кривая изменения активной мощности, определения ответственности.**

Introduction. In terms of defining the subjects participating in the responsibility for violation of requirements of power quality (PQ) in determining the source of voltage fluctuations (VF) in the system of power supply to consumers, with a light load, the main issue is the location of the VF source: on the territory of the consumer or in the external network. The answer to this question, confirmed by a deterministic calculation, can be the basis of expert opinion to resolve legal disputes in the assessment of damages caused by the poor quality electrical energy.

We are talking about systematic VF which are recurring in nature, and which may be at some interval measuring time T to characterize by the number of voltage changes m, voltage repetition changes rate $F_{\delta Ut}$ and other indicators relevant VF [1].

Sources of VF are powerful power-consuming equipment with a pulse, sharply changing nature of consumption of active and reactive power: arc and induction furnaces; electric welding machines; electrical motors during starting.

Problem definition. From the consumer's point of view the VF source may be placed in its electric networks or networks of other users. In the first case, if the systematic VF exceed the allowable value, the consumer must take action to reduce the level of fluctuations. In the second one – VF at consumer external factor identified as coming to him through the networks of electricity supplier. In this case, responsible for carrying out measures to reduce the level of the VF is a supplier.

The goal of the work is the development of a method for determining the location of the VF source.

The information necessary for determining the position of the VF source can be obtained by analyzing the parameters of the current mode of the power supply. As it is known, the regulatory effect of the active load voltage is almost always positive [2]

$$\partial P_{load} / \partial U > 0 . \quad (1)$$

Therefore, reducing the voltage decrease caused by external factors will reduce the load active power. Accordingly, an increase in voltage caused by external factors, will lead to an increase in the load active power. With regard to reactive power, the regulatory effect of the reactive load voltage is also positive ($\partial Q_{load} / \partial U > 0$) if the voltage exceeds a critical value ($U > U_{cr}$). With deep voltage brownouts ($U < U_{cr}$) regulating effect of reactive load voltage becomes negative ($\partial Q_{load} / \partial U < 0$). Taking into account that for the tires 110 kV critical voltage can reach values of the order $0.8U_{nom}$ [2], the use of reactive power change as a criterion must be confirmed by additional research.

If the voltage change is caused by internal factors, then the object in question the voltage drop do not cause changes in other parameters of the regime, but the consequence.

Results of investigations. We represent the power supply of the consumer in the form of equivalent circuit (Fig. 1) in which $\underline{E}_{syst}$ is the equivalent EMF of the system; $\underline{U}$ is the voltage on the busbars of the receiving substation; $\underline{Z}_{\text{syst}}$ is the equivalent resistance of the connection with the system; $\underline{Z}_{load}$ is the equivalent resistance of the load of the enterprise.

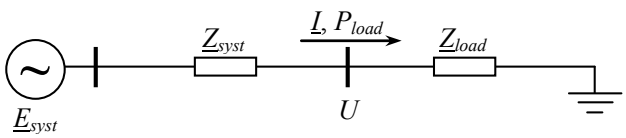

Fig. 1. Equivalent circuit of the customer power supply

Changing of the voltage $\underline{U}$ on the tires of the receiving substation caused by external to the electrical network of the consumer exposure, it can be seen as a consequence of changes in the EMF of the system $\underline{E}_{syst}$. On the assumption of the immutability of the load resistance (Z_{load} = const) E_{syst} reduction reduces the current I on the load lines and power consumer P_{load}, raising $\underline{E}_{syst}$ – to increase of I and P_{load}. In fact, when changing the voltage U the load resistance Z_{load} may vary somewhat, but in general, this change corresponds to a positive regulatory effect of active load by voltage [4, 5].

If the source of the VF is located in the electrical network of the consumer, the voltage $\underline{U}$ changes in the tires of the receiving substation is due to varying load at constant EMF of the system ($\underline{E}_{syst}$ = const). The voltage U is determined by the loss of voltage on resistance of the connection with the system Z_{syst} [5]. If we neglect the transverse component of the voltage drop, which is typical of the distribution networks, we can write:

$$U = E_{syst} - \frac{P_{load} \cdot r_{syst} + Q_{load} \cdot x_{syst}}{U}, \qquad (2)$$

where P_{load}, Q_{load} are the powers of active and reactive consumer's load.

In accordance with (2) a prerequisite to reduce the voltage U tire receiving substation at $\underline{E}_{syst}$ = const is to increase the voltage loss in the equivalent connection with the system and, hence, the numerator in the fractional part of the formula:

$$\left[\left(P_{load} + \Delta P_{load}\right) \cdot r_{syst} + \left(Q_{load} + \Delta Q_{load}\right) \cdot x_{syst}\right] - \left(P_{load} \cdot r_{syst} + Q_{load} \cdot x_{syst}\right) > 0, \qquad (3)$$

where $\Delta P_{load} + j\Delta Q_{load}$ is the increment of power caused VF

The increase of U will be observed in the case when the inequality (3) will change its sign. This is possible if the power increments will be negative ($\Delta P_{load}<0$; $\Delta Q_{load}<0$).

This implies changes in the conditions of the power load, causing the VF. At a negative voltage change ΔU:

$$\begin{cases} \Delta U < 0; \\ \Delta P_{load} \cdot r_{syst} + \Delta Q_{load} \cdot x_{syst} > 0, \end{cases} \qquad (4)$$

At a positive voltage change ΔU:

$$\begin{cases} \Delta U > 0; \\ \Delta P_{load} \cdot r_{syst} + \Delta Q_{load} \cdot x_{syst} < 0. \end{cases} \qquad (5)$$

Condition (5) is necessary for the emergence of the VF at the source location in the networks of the consumer, but is not sufficient. Conclusion sufficient conditions for the task is not required, since the aim is not to establish the fact of VF (VF is fixed by measurement), and the definition of the source location.

The causes of VF at the location of the source in the power network, and the network user, are associated with changes in consumption and active and reactive power. As a criterion for determining the place of supply VF location chosen change in the active power received by the receiving substation for connection with an equivalent system.

VF source is *external* to the consumer, if the occurrence of the VF resulting in consistent voltage changes and consumed active power line that corresponds to the condition of a positive regulator of active load voltage effect (1).

VF source is *internal* to the consumer, if the VF occurrence leads to changes in the counter-voltage and consumed active power line that resembles the condition of negative regulatory effect of active load by voltage:

$$\partial P_{load} / \partial U < 0. \qquad (6)$$

Conditions (1) and (6) correspond to the static load characteristics and can be used in the absence of load the motor component of the consumer. In general, with the dynamic characteristics of the engines, the criteria for determining the location of the source VF requires clarification as voltage curves of the $U(t)$ and active power $P_{load}(t)$ may have a time shift t. k_d factor which takes into account dynamic characteristics unlike the static, usually in the range k_d = 0.7÷1 [3]. The physical meaning of the coefficient – the ratio of acceleration (or deceleration) durations $k_d = t_{st}/t_{dyn}$ defined by static (t_{st}) and dynamic (t_{dyn}) characteristics. At the conditions of regular VF in distribution networks when the swing changes δU_t voltage is not so large to cause equipment failures, and constant inertia is much lower than on the interconnections, should expect k_d values close to unity. At the same time, at intervals averaging close to extrema instead of criterion (1) the criterion (6) may be falsely recorded. The probability of error increases with the frequency of recurrence $F_{\delta Ut}$ of voltage changes.

To take into account for a possible shift between the extremes of the curves of changes of the voltage $U(t)$ and power $P_{load}(t)$ it is advisable to make a parallel analysis of these characteristics. We consider a characteristic of change in the rms of the voltage U on the consumer tires To simplify the analysis we assume that the curve $U(t)$ of voltage change is continuity of an arbitrary shape (Fig. 2).

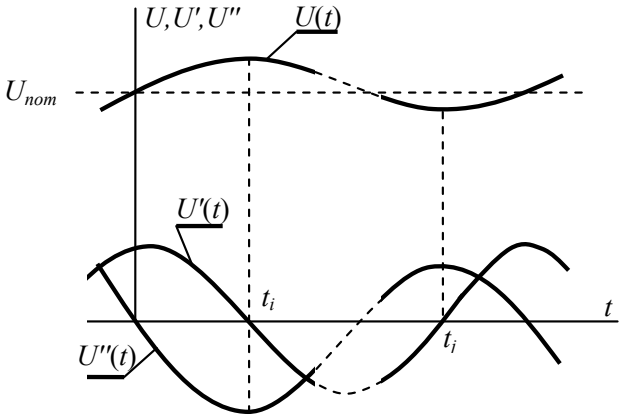

Fig. 2. Characteristics of voltage fluctuations $U(t)$, the first $U'(t)$ and the second $U''(t)$ voltage derivatives

The smoothed shape of oscillations, in varying degrees, it is assumed in any case, as the information is received will be the integration of Instant Mode parameters for the averaging interval τ. The minimum value of τ

should be sufficient to convert the instantaneous voltage u in the rms U (of the order of one period of the fundamental frequency).

In the considered problem we should focus on the averaging interval τ that according to GOST [1], complies with the requirements for other indicators of quality of electric energy, which are long-lasting changes in voltage characteristics (voltage asymmetry coefficients for reverse K_{2U} and zero K_{0U} sequences ratio distortion sinusoidal voltage curve K_U coefficient of the n-th harmonic component of voltage $K_{U(n)}$).

Whatever the curve of the voltage $U(t)$ at regular VF it is inherent in the existence of local extremes (see Fig. 2) availability of extremum conditions are known [4]. A *necessary condition of the extremum* of the function $U(t)$ at the point t_i is the fact that its derivative at this point $U'(t_i)$ is either zero or does not exist.

If at the point t_i the function $U(t)$ has an extreme, and this is the maximum, then going through the t_i point f the derivative changes sign from positive to negative; If at the point $t = t_i$ function $U(t)$ has a minimum – from minus to plus. If the derivative $U'(t)$ when passing through the point t_i does not change sign, the extremum at the point t_i is absent.

To estimate the extremum sign it is possible using the second derivative. If at the point t_i extremum is reached, and $U''(t_i) < 0$ then the point $t = t_i$ the function $U(t)$ has a maximum; if $U''(t_j) > 0$ then the point $t = t_j$ function $U(t)$ reaches a minimum.

Known methods of analysis of curves having local extrema can be used to estimate the power and voltage fluctuations, and in particular, to identify the source location of the VF according to the criteria (1), (6) and with the dynamic characteristics of the motor load.

We suppose that the curve of active power change $P(t)$ is similar to the voltage $U(t)$ curve and is not time shift ($\Delta t_{dyn} = t_{dyn} - t_{st} = 0$) defined by difference of static and dynamic characteristics (Fig. 3). Then local extremum of the curve $U(t)$ will corresponds to local extrema of the curve $P(t)$. At the points of extrema $t = t_i$, $t = t_j$ first derivatives must be equal to zero:

$$U'(t_i) = U'(t_j) = P'(t_i) = P'(t_j) = 0. \qquad (7)$$

If the source of the VF is in the system, maxima of $U(t)$ will correspond to the maxima of $P(t)$, minima – to minima (see Fig. 3,*a*). Signs of first derivatives $U'(t)$ and $P'(t)$ must be the same throughout the measurement time interval T:

$$\begin{aligned} signU'(t_i) &= signP'(t_i); \\ signU'(t_j) &= signP'(t_j). \end{aligned} \qquad (8)$$

The second derivatives at the points of extrema must match the sign:

$$\begin{aligned} signU''(t_i) &= signP''(t_i); \\ signU''(t_j) &= signP''(t_j). \end{aligned} \qquad (9)$$

If the source of the VF is in the customer network, maxima of $U(t)$ will correspond to the minima of $P(t)$, minima – to maxima (see Fig. 3,*b*). Signs of first derivatives $U'(t)$ and $P'(t)$ must be opposite throughout the measurement time interval T:

$$\begin{aligned} signU'(t_i) &= -signP'(t_i); \\ signU'(t_j) &= -signP'(t_j). \end{aligned} \qquad (10)$$

The second derivatives at the points of extrema must be opposite by sign:

$$\begin{aligned} signU''(t_i) &= -signP''(t_i); \\ signU''(t_j) &= -signP''(t_j). \end{aligned} \qquad (11)$$

Accounting for the dynamic characteristics of the motor load curve gives the power shift $P(t)$ with respect to the curve of voltage $U(t)$ at the time of the delay $\Delta t_{dyn} = t_{dyn} - t_{st}$ (Fig. 4). Accordingly, local extrema of the curve $P(t)$ will be shifted relative to the extrema of the curve $P(t)$ at the time of Δt_{dyn}. For this reason, in the shear zone relations shown above (see Fig. 3) can not be observed and criteria (1), (6) will not work.

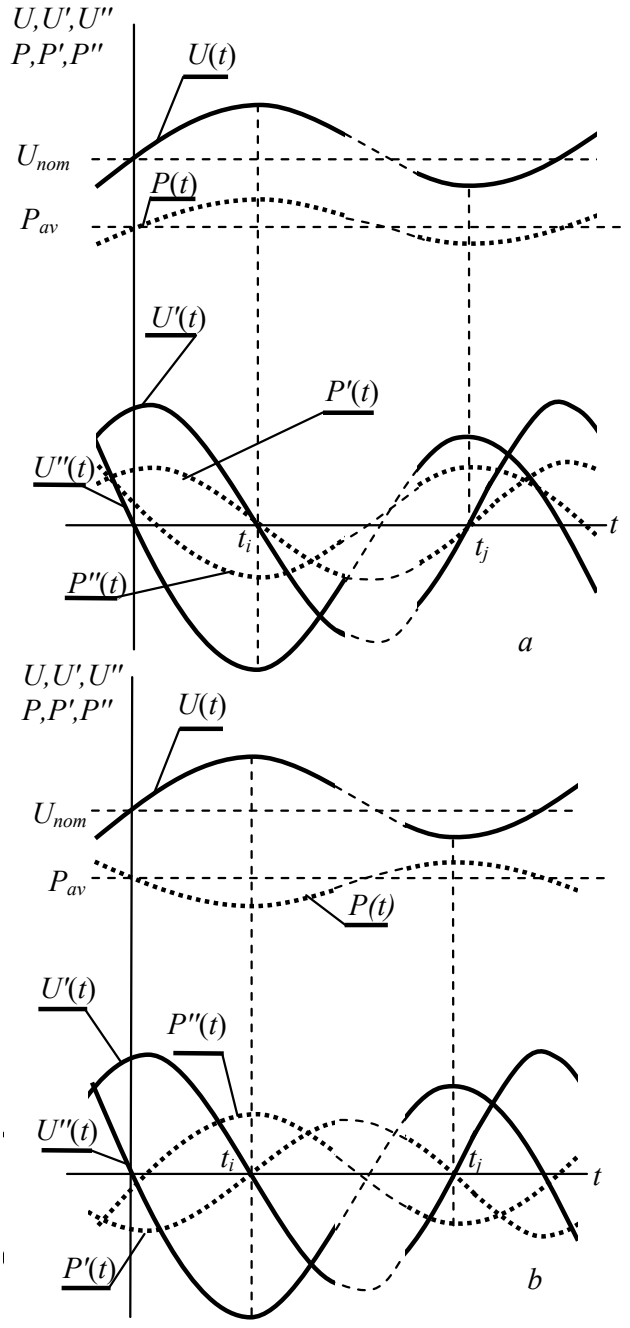

Fig. 3. Characteristics of fluctuation of voltage $U(t)$ and active power $P(t)$, their first $U'(t)$, $P'(t)$ and second $U''(t)$ and $P''(t)$ derivatives at the VF source placement:
a – in the power supply system; *b* – in the customer network

It should be noted that the shift can be observed by the consumer load motor at the location of the source of VF in the system. If the source of VF is located in the customer network the VF are the results of changes in load power (2). The constant of the electromagnetic transient in the power line distribution network is small, the shift can be ignored.

In general case, to determine the position of the source of the VF, apparently, should be carried out parallel analysis of the curves of voltage $U(t)$ and active power $P(t)$ over the entire time interval of the measurement T tracking and comparing features of their change.

In the practical analysis of information on the regime parameters coming from the registrar in the form of discrete recording of instantaneous values of current and voltage with discrete intervals, providing a given accuracy class, and, consequently, the final amount of measurements (e.g. ANTES AP-3F – 100 measurements per period). Use the information on the rms voltage and active power can be selected for the averaging interval τ. Methods of determining the place of location of the VF intends to use the basic signs of change (7)÷(11) of the power curve $P(t)$ with respect to the curve of voltage $U(t)$ at their the discrete implementation.

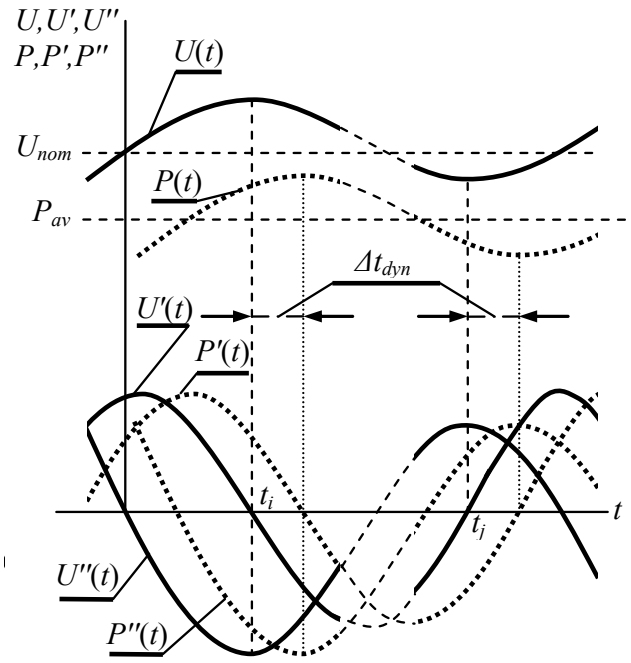

Fig. 4. Account of dynamic characteristics of the motor load

Conclusions.

1. A method for determining the location of the source of VF in the electrical network, which operates on the principle of evaluating the correlation of power and voltage changes in the power supply network is developed.

2. The method allows to take into account the shift between the extrema of the curves of changes of the voltage $U(t)$ and power $P_{load}(t)$.

REFERENCES

1. *GOST 13109-97. Elektricheskaya energiya. Sovmestimost' tehnicheskih sredstv elektromagnitnaya. Normy kachestva elektricheskoi energii v sistemah elektrosnabzheniya obschego naznacheniya* [State Standard 13109-97. Electrical energy. Technical equipment electromagnetic compatibility. Quality standards for electrical energy in general use power systems]. Minsk, IPK Publishing house of standards, 1998. 30 p. (Rus).

2. Idelchik V.I. *Elektricheskie sistemy i seti: Uchebnik dlia vuzov* [Electrical Systems and Grids: Textbook for high schools]. Moscow, Energoatomisdat Publ., 1989. 592 p. (Rus).

3. Venikov V.A. *Perekhodnye elektromekhanicheskie protsessy v elektricheskikh sistemakh: Ucheb. dlia elektroenerget. spets. vuzov* [Transitional electromechanical processes in electrical systems: Textbook for electric. specialist. high schools]. Moscow, High School Publ., 1985. 536 p. (Rus).

4. Bronshteyn I.N., Semendyayev K.A. *Spravochnik po matematike dlya inzhenerov i uchashchikhsya vuzov* [Mathematical handbook for engineers and university students]. Moscow, Nauka Publ., 1986. 723 p. (Rus).

5. Senderovich G.A., Diachenko A.V. The relevance of determining responsibility for violation of power quality in terms of voltage fluctuations. *Elektrotekhnika i elektromekhanika − Electrical engineering & electromechanics*, 2016, no.2, pp. 54-60. (Rus). **doi: 10.20998/2074-272X.2016.2.10.**

G.A. Senderovich[1], *Doctor of Technical Science, Professor,*
A.V. Diachenko[1], *Postgraduate Student,*
[1] National Technical University «Kharkiv Polytechnic Institute», 21, Frunze Str., Kharkiv, 61002, Ukraine,
phone +380 95 2098150,
e-mail: senderovichg@mail.ru, alex.7491@mail.ru

How to cite this article:
Senderovich G.A., Diachenko A.V. A method for determining location of voltage fluctuations source in electric grid. *Electrical engineering & electromechanics*, 2016, no.3, pp. 58-61. doi: 10.20998/2074-272X.2016.3.09.

UDC 621.31 **doi: 10.20998/2074-272X.2016.3.10**

Iu.A. Sirotin

ORTHOGONAL COMPONENTS OF THE THREE-PHASE CURRENT AT ASYMMETRICAL ACTIVE-REACTIVE LOAD IN 4-WIRE CIRCUIT

Purpose. For the unbalanced sinusoidal mode with asymmetric voltage in 3-phase 4-wire to receive the orthogonal 4-component decomposition of 3-phase current, are classified symmetry/asymmetry of active and reactive load elements separately. Methodology. The methodology is based on the vector approach, which with one voice allows to analyze the energy characteristics of a 4-wire and 3-wire circuits as balanced and unbalanced modes. At asymmetrical voltage the matrix representation methodology of the equivalent conductivities is used. Results. For 3-phase 4-wire network with a sinusoidal unbalanced mode with asymmetric voltage obtained 4-component orthogonal decomposition of the 3-phase current. The components have a clear electro-energetic sense and are classified irrespective by the load condition. Originality. The resulting decomposition current develops the theory Currents' Physical Components (CPC) for 4-wire circuit with asymmetric voltage. For the first time the unbalanced current is classified by activity and reactivity of asymmetry load elements. Practical value. Practical value of the obtained orthogonal decomposition current and the power equation is a possibility of their utilization for the increase both quality of delivery and quality of consumption of electrical energy. References 8, figures 1.

Key words: **three-phase circuit, active and reactive power, power shift, power equation, unbalanced current and mode**, **active-reactive asymmetrical load, asymmetrical voltage, currents' physical components (CPC)**.

Для 3– фазной схемы электроснабжения рассмотрен синусоидальный несимметричный режим. При несимметричном напряжении и ассиметричной активно–реактивной нагрузке для 4– проводной сети получено ортогональное разложение трехфазного тока. Четыре составляющие разложения классифицированы активностью/реактивностью и симметрией/асимметрией нагрузки и имеют однозначный электроэнергетический смысл. Для 4– проводной цепи с несимметричной нагрузкой при несимметричном напряжении полученное уравнение мощности развивает теорию токовых физических составляющих (Currents' Physical Components – CPC). Библ. 8, рис. 1.

Ключевые слова: **трехфазная цепь, активная и реактивная мощность, мощность сдвига, уравнение мощности, несбалансированный ток и режим, активно-реактивная несимметричная нагрузка, несимметричное напряжение, Currents' Physical Components (CPC).**

Introduction. Active-reactive unbalanced load not only consumes electrical energy (EE) of active power, but also the EE of inactive components of total power (TP) which leads to additional losses. An effective solution to the problem of reducing losses and increasing the accuracy of accounting EE is the combined use of compensating devices and differential accounting means consumption EE. However, even in a sinusoidal mode, taking into account existing means of measuring energy efficiency they measure EE due to only the *symmetry* of the load active and reactive elements (active power and reactive power of shift). In real conditions of asymmetry voltage components of TP due to the asymmetry of the active-reactive load elements lead to additional losses, however, are not measured are not counted and will not be compensated.

Problem definition. Compensation, measuring and accounting for components of TP are related, complementary objectives of effective EE consumption. These tasks are the same positions should be solved within the framework of the general theory of power using orthogonal decomposition of 3-phase current [1-6] The mutual orthogonal component decomposition can uniquely estimate the losses caused by them independently. Widely used power theory *Currents' Physical Components* (CPC) [2, 4-6] uses a methodology of orthogonal decomposition. At the sinusoidal unbalanced mode, 3-phase current comprises two orthogonal components: balanced and unbalanced. Balanced component (due to the symmetry of the active-reactive load elements) comprises orthogonally reactive current and active for three, and for a 4-wire circuit. The asymmetry of the active-reactive load elements, both in symmetric and asymmetric under voltage leads to unbalance current.

Unfortunately, even in a sinusoidal mode CPC theory developed either for 3-wire or 4-wire circuits with a symmetrical voltage [2, 4-6]. Thus, for 3-wire circuit is decomposed into two components with unbalanced voltage in the CPC power theory of unbalance current, using the method of symmetrical components [6], which is not shared by the asymmetry of the load active and reactive elements explicitly.

The goal of the work is for unbalanced mode with asymmetric voltage in 3-phase 4-wire to obtain orthogonal 4-component decomposition of the 3-phase current, are classified by symmetry/asymmetry of separate active and reactive load elements separately.

Periodic power processes. When considering a 3-phase 4-wire circuit we assume that the voltage in the phases are measured relative to the neutral (Fig. 1).

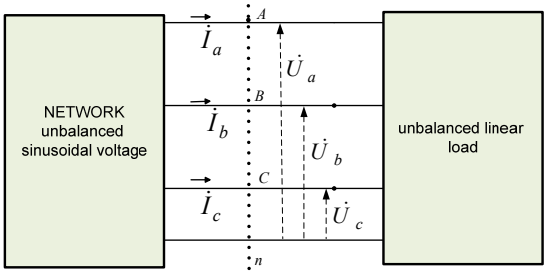

Fig. 1. 3-phase 4-wire power supply with unbalanced load – sinusoidal mode

At any time, instantaneous values (*i.v.*) of voltages (relative to a «neutral» conductor) and *i.v.* of currents in the phases are considered as 3-dimensional vectors (matrix columns) of an arithmetic 3-dimensional space $R^{(3)}$

$$\boldsymbol{u}(t)=\left[u_a(t)\ \ u_b(t)\ \ u_c(t)\right]^{\tau},\ \boldsymbol{i}(t)=\left[i_a(t)\ \ i_b(t)\ \ i_c(t)\right]^{\tau}, \quad (1)$$

hereinafter τ is the transposition sign.

Steady power mode in a 3-phase section <*A*, *B*, *C*> is determined by 3-D *T*-periodic curves of current and voltage:

$$\boldsymbol{u}(t)=\boldsymbol{u}(t+T),\ \boldsymbol{i}(t)=\boldsymbol{i}(t+T)\cdot$$

An ensemble of 3-D (3-phase) *T*-periodic vector curves

$$\boldsymbol{x}(t)=[x_a(t)\ \ x_b(t)\ \ x_c(t)]^{\tau},\quad t\in(v,v+T) \quad (2)$$

with finite root mean square (*rms*) value

$$\|\boldsymbol{x}\|=\sqrt{\frac{1}{T}\int_{v}^{v+T}\boldsymbol{x}(t)^{\tau}\boldsymbol{x}(t)dt}<\infty \quad (3)$$

form a Hilbert space

$$L_2^{(3)}(T)=\{\boldsymbol{x}(t),\quad t\in(v,v+T):\|\boldsymbol{x}\|<\infty\}. \quad (4)$$

For vector curves $\boldsymbol{x}(t)$, $\boldsymbol{y}(t)\in L_2^{(3)}(T)$ a scalar product (SP) is determined

$$<\boldsymbol{x},\boldsymbol{y}>=\frac{1}{T}\int_{v}^{v+T}\boldsymbol{x}(t)^{\tau}\boldsymbol{y}(t)dt=\frac{1}{T}\int_{v}^{v+T}(\boldsymbol{x}(t),\boldsymbol{y}(t))dt \quad (5)$$

as integral averaged of scalar products of *i.v.* in a 3-D space $R^{(3)}$.

In particular, for active power

$$<\boldsymbol{i},\boldsymbol{u}>=\frac{1}{T}\int_{v}^{v+T}\underbrace{\boldsymbol{i}(t)^{\tau}\boldsymbol{u}(t)dt}_{p(t)}=\frac{1}{T}\int_{v}^{v+T}(\boldsymbol{i}(t),\boldsymbol{u}(t))dt=P. \quad (6)$$

Instantaneous power

$$p(t)=\boldsymbol{i}^{\tau}\boldsymbol{u}=i_a(t)u_a(t)+i_b(t)u_b(t)+i_c(t)u_c(t) \quad (7)$$

equals to the electricity rate through the section <*A*, *B*, *C*>. In the space (4) the inequality of Cauchy-Schwarz is correct

$$<\boldsymbol{x},\boldsymbol{y}>\le\|\boldsymbol{x}\|\cdot\|\boldsymbol{y}\|. \quad (8)$$

In particular, active power does not exceed the apparent (total) power

$$P=<\boldsymbol{i},\boldsymbol{u}>\ \le\ \|\boldsymbol{u}\|\cdot\|\boldsymbol{i}\|.$$

Sinusoidal mode and 3-complexes. 3-D curves of *i.v.* sinusoidal processes of voltage and current

$$\boldsymbol{u}(t)=\sqrt{2}\Re e[\boldsymbol{U}e^{j\omega t}],\ \boldsymbol{i}(t)=\sqrt{2}\Re e[\boldsymbol{I}e^{j\omega t}]. \quad (9)$$

are *T*-periodic ($T\omega = 2\pi$) and fully determined by 3-complexes of voltage and current

$$\boldsymbol{U}=\begin{bmatrix}\dot U_a\\ \dot U_b\\ \dot U_c\end{bmatrix}=\begin{bmatrix}U_a e^{j\psi_a}\\ U_b e^{j\psi_b}\\ U_c e^{j\psi_c}\end{bmatrix},\ \boldsymbol{I}=\begin{bmatrix}\dot I_a\\ \dot I_b\\ \dot I_c\end{bmatrix}=\begin{bmatrix}I_a e^{j\varphi_a}\\ I_b e^{j\varphi_b}\\ I_c e^{j\varphi_c}\end{bmatrix}, \quad (10)$$

– vectors of complex *rms* of voltage and current.

3-complexes (10) are calculated by 3-D curves of *i.v.* of sinusoidal processes of voltage and current

$$\boldsymbol{U}=\frac{\sqrt{2}}{T}\int_{v}^{v+T}\boldsymbol{u}(t)e^{-j\omega t}dt,\ \boldsymbol{I}=\frac{\sqrt{2}}{T}\int_{v}^{v+T}\boldsymbol{i}(t)e^{-j\omega t}dt. \quad (11)$$

An ensemble of 3-form a 3-D complex space $C^{(3)}$ with a complex SP

$$(\boldsymbol{X},\boldsymbol{Z})=\boldsymbol{X}^{\tau}\boldsymbol{Z}^{*}=\dot X_a Z_a^{*}+\dot X_b Z_b^{*}+\dot X_c Z_c^{*}. \quad (12)$$

Hereinafter $*$ is a sign of complex conjugation. Thus, for rms

$$\|\boldsymbol{x}\|^2=\boldsymbol{X}^{\tau}\boldsymbol{X}^{*}=\sum\nolimits_m \dot X_m X_m^{*}=\sum\nolimits_m X_m^2=|\boldsymbol{X}|^2=X^2.$$

In particular,

$$\|\boldsymbol{u}\|=|\boldsymbol{U}|=U,\ \|\boldsymbol{i}\|=|\boldsymbol{I}|=I. \quad (13)$$

For a couple of sinusoidal processes $\boldsymbol{x}(t)$, $\boldsymbol{z}(t)\in L_2^{(3)}(T)$ the equality is correct

$$<\boldsymbol{x},\boldsymbol{z}>=\mathrm{Re}[\boldsymbol{X}^{\tau}\boldsymbol{Z}^{*}]=\mathrm{Re}[\boldsymbol{Z}^{\tau}\boldsymbol{X}^{*}]. \quad (14)$$

So, if 3-complexes are orthogonal then corresponding 3-D curves are orthogonal, too. The converse is not true.

From (14) it follows that at the sinusoidal mode active power is adequately represented in terms of 3-complexes of voltage and current

$$P=<\boldsymbol{i},\boldsymbol{u}>=\mathrm{Re}[\boldsymbol{I}^{\tau}\boldsymbol{U}^{*}]=\mathrm{Re}[\boldsymbol{U}^{\tau}\boldsymbol{I}^{*}]. \quad (15)$$

The temporal shift of 3-D curve of *i.v.* of sinusoidal voltage $\boldsymbol{u}_{\perp}(t)=\boldsymbol{u}(t-T/4)$ is equivalent to a rotation of the 3-complex of voltage in the space $C^{(3)}$ to 90°

$$\boldsymbol{u}_{\perp}(t)=\sqrt{2}\Re e[\boldsymbol{U}_{\perp}e^{j\omega t}]=\sqrt{2}\Re e[-j\boldsymbol{U}e^{j\omega t}]. \quad (16)$$

Here $\|\boldsymbol{u}_{\perp}\|=\|\boldsymbol{u}\|$. Because of

$$<\boldsymbol{u}_{\perp},\boldsymbol{u}>=\Re e[-j\boldsymbol{U}^{\tau}\boldsymbol{U}^{*}]=\Re e[-j|\boldsymbol{U}|^2]=0,$$

3-D curves of voltages are orthogonal ($\boldsymbol{u}\perp\boldsymbol{u}_{\perp}$).

Integral determination of reactive power (known as power of shift) is represented in terms of 3-complexes of voltage and current

$$Q=<i,\boldsymbol{u}_{\perp}>=\Re e[-j\boldsymbol{U}^{\tau}\boldsymbol{I}^{*}]=\mathrm{Jm}[\boldsymbol{U}^{\tau}\boldsymbol{I}^{*}]. \quad (17)$$

Powers (15) and (17) are connected by complex power – SP of 3-complexes of voltage and current

$$\dot S=\boldsymbol{U}^{\tau}\boldsymbol{I}^{*}=\mathrm{Re}[\boldsymbol{U}^{\tau}\boldsymbol{I}^{*}]+j\,\mathrm{Jm}[\boldsymbol{U}^{\tau}\boldsymbol{I}^{*}]=P+jQ. \quad (18)$$

At the sinusoidal mode at *symmetrical* load the equation of powers is correct

$$P^2+Q^2=\|\boldsymbol{i}\|\cdot\|\boldsymbol{u}\|\cdot \quad (19)$$

Equivalent conductivities of load current. At the sinusoidal mode 3-complexes of current and voltage permit to determine equivalent conductivities of current in the section <*A*, *B*, *C*>

$$\dot Y_m=G_m-jB_m=\frac{\dot I_m}{\dot U_m},\ m\in\{a,b,c\} \quad (20)$$

and represent a 3-complex of 3-phase current in the matrix form

$$\boldsymbol{I}=\begin{bmatrix}\dot U_a\dot Y_a\\ \dot U_b\dot Y_b\\ \dot U_c\dot Y_c\end{bmatrix}=\begin{bmatrix}\dot Y_a & 0 & 0\\ 0 & \dot Y_b & 0\\ 0 & 0 & \dot Y_a\end{bmatrix}\begin{bmatrix}\dot U_a\\ \dot U_b\\ \dot U_c\end{bmatrix}=\hat Y\boldsymbol{U} \quad (21)$$

by using a diagonal matrix

$$\hat Y=diag\{\dot Y_a,\dot Y_b,\dot Y_c\}. \quad (22)$$

For a 4-wire circuit with a star-type load equivalent conductivities (20) in the section <*A*, *B*, *C*> equal to conductivities of phase loads.

Active power and power of shift are adequately represented by quadratic forms of the 3-complex of voltage

$$P = \mathrm{Re}[\boldsymbol{U}^{\tau}\hat{Y}^{*}\boldsymbol{U}^{*}],\ Q = \mathrm{Jm}[\boldsymbol{U}^{\tau}\hat{Y}^{*}\boldsymbol{U}^{*}]. \quad (23)$$

Active power (power of shift) depends only on conductivities of active (reactive) load elements

$$P = \sum\nolimits_m G_m |\dot{U}_m|^2,\ Q = \sum\nolimits_m B_m |\dot{U}_m|^2. \quad (24)$$

Losses of total 3-phase current per one Ω

$$\|\boldsymbol{i}\|^2 = \mathrm{Re}[\boldsymbol{I}^{\tau}\boldsymbol{I}^{*}] = \sum\nolimits_m (G_m^2 + B_m^2)|\dot{U}_m|^2. \quad (25)$$

Active and reactive current. For 3-D curve of sinusoidal current (9) it is correct

$$\boldsymbol{i}(t) = \sqrt{2}\Re e[\hat{Y}\boldsymbol{U}e^{j\omega t}],\ \boldsymbol{I} = \hat{Y}\boldsymbol{U}. \quad (26)$$

Algebraic form of complex equivalent conductivities (20) permits to resolute the diagonal matrix (22)

$$\hat{Y} = \hat{G} - j\hat{B}, \quad (27)$$

$$\hat{G} = diag\{G_a, G_b, G_c\},\ \hat{B} = diag\{B_a, B_b, B_c\} \quad (28)$$

and divide 3-complex of current into two components associated with active and reactive load elements

$$\boldsymbol{I} = \boldsymbol{I}_A + \boldsymbol{I}_R,\ \boldsymbol{I}_A = \hat{G}\boldsymbol{U},\ \boldsymbol{I}_R = -j\hat{B}\boldsymbol{U} = \hat{B}\boldsymbol{U}_{\perp}. \quad (29)$$

Resolution of 3-D curve of current (26)

$$\boldsymbol{i}(t) = \boldsymbol{i}_A(t) + \boldsymbol{i}_R(t) \quad (30)$$

into active and reactive current

$$\boldsymbol{i}_A(t) = \sqrt{2}\Re e[\hat{G}\boldsymbol{U}e^{j\omega t}],\ \boldsymbol{i}_R(t) = \sqrt{2}\Re e[\hat{B}\boldsymbol{U}_{\perp}e^{j\omega t}] \quad (31)$$

is orthogonal in the space of 3-D curves (4).

Because of the quantity

$$\boldsymbol{I}_A^{\tau}\boldsymbol{I}_R^{*} = (\hat{G}\boldsymbol{U})^{\tau}\left(-j\hat{B}\boldsymbol{U}\right)^{*} = j\sum\nolimits_m U_m^2 G_m B_m \quad (32)$$

is pure imaginary then 3-D curves (31) are orthogonal

$$<\boldsymbol{i}_A, \boldsymbol{i}_R> = \mathrm{Re}[\boldsymbol{I}_A^{\tau}\boldsymbol{I}_R^{*}] = 0 \ \Rightarrow\ \boldsymbol{i}_A \perp \boldsymbol{i}_R. \quad (33)$$

Because of orthogonality of the resolution (29) for losses per one Ω the Pythagoras equality is correct

$$\|\boldsymbol{i}\|^2 = \|\boldsymbol{i}_A\|^2 + \|\boldsymbol{i}_R\|^2. \quad (34)$$

Losses of active and reactive current

$$\|\boldsymbol{i}_A,\|^2 = \mathrm{Re}[\boldsymbol{I}_A^{\tau}\boldsymbol{I}_A^{*}] = \sum\nolimits_m G_m^2 |\dot{U}_m|^2, \quad (35)$$

$$\|\boldsymbol{i}_R,\|^2 = \mathrm{Re}[\boldsymbol{I}_R^{\tau}\boldsymbol{I}_R^{*}] = \sum\nolimits_m B_m^2 |\dot{U}_m|^2 \quad (36)$$

determine losses of total current (25). Here

$$\|\boldsymbol{i}_A\|^2 \le \|\boldsymbol{i}\|^2,\ \|\boldsymbol{i}_R\|^2 \le \|\boldsymbol{i}\|^2.$$

Active current guarantees EE supply with active power of total current (24)

$$<\boldsymbol{u}, \boldsymbol{i}_A> = \mathrm{Re}[\boldsymbol{U}^{\tau}\boldsymbol{I}_A^{*}] = \mathrm{Re}[\boldsymbol{U}^{\tau}\hat{G}\boldsymbol{U}^{*}] =$$

$$= \sum\nolimits_m G_m |\dot{U}_m|^2 = <\boldsymbol{i}, \boldsymbol{u}> = P. \quad (37)$$

Reactive current guarantees EE transmission of power of shift of total current (24)

$$<\boldsymbol{i}_R, \boldsymbol{u}_{\perp}> = \mathrm{Re}[-j\boldsymbol{U}^{\tau}\boldsymbol{I}_R^{*}] = \mathrm{Jm}[\boldsymbol{U}^{\tau}\hat{B}\boldsymbol{U}^{*}] =$$

$$= \sum\nolimits_m B_m |\dot{U}_m|^2 = <\boldsymbol{i}, \boldsymbol{u}_{\perp}> = Q. \quad (38)$$

In the resolution (30) active (reactive) current is caused by *summarily* symmetry and asymmetry of active (reactive) load elements.

Balanced current component. A sinusoidal mode is *balanced* if 3-complexes of current and voltage (10) are collinear (parallel $\boldsymbol{I} \| \boldsymbol{U}$) [7, 8]

$$\boldsymbol{I} \| \boldsymbol{U} \ \Leftrightarrow\ \boldsymbol{I} = \beta\boldsymbol{U}\ (\dot{\beta} = \beta' + j\beta'',\ \beta \ne 0). \quad (39)$$

A mode is *really* balanced [7, 8] if $Jm[\beta] = \beta'' = 0$. If the load is symmetrical then the mode is balanced at any unbalanced voltage.

For an unbalanced mode the 3-complex of components of current balanced with 3-phase voltage equals to projection of 3-complex of voltage in the space $C^{(3)}$

$$\boldsymbol{I}_S = (\boldsymbol{I}^{\tau}\boldsymbol{\upsilon}^{*})\boldsymbol{\upsilon} = \frac{(\boldsymbol{I}^{\tau}\boldsymbol{U}^{*})\boldsymbol{U}}{|\boldsymbol{U}|^2}. \quad (40)$$

Hereinafter:

$$\boldsymbol{\upsilon} = [\dot{\upsilon}_a\ \ \dot{\upsilon}_b\ \ \dot{\upsilon}_c]^{\tau},\ |\boldsymbol{\upsilon}|^2 = \upsilon_a^2 + \upsilon_b^2 + \upsilon_c^2 = 1 \quad (41)$$

is the ort of the 3-complex of voltage

$$\boldsymbol{U} = |\boldsymbol{U}|\boldsymbol{\upsilon},\ \dot{U}_m = U\dot{\upsilon}_m\ (m \in \{a, b, c\}). \quad (42)$$

In terms of conductivities of the 3-complex of balance current (40)

$$\boldsymbol{I}_S = \frac{(\boldsymbol{I}^{\tau}\boldsymbol{U}^{*})\boldsymbol{U}}{|\boldsymbol{U}|^2} = \underbrace{(S^{*}/U^{2})}_{\dot{\mathsf{y}}_{\mathsf{s}}} \cdot \boldsymbol{U} = \dot{\mathsf{y}}_{\mathsf{s}}\boldsymbol{U}. \quad (43)$$

Hereinafter:

$$\dot{\mathsf{y}}_{\mathsf{s}} = S^{*}/U^{2} = \dot{Y}_a\upsilon_a^2 + \dot{Y}_b\upsilon_b^2 + \dot{Y}_c\upsilon_c^2 \quad (44)$$

is the equivalent complex conductivity of the balanced current component;

$$S^{*} = (\boldsymbol{U}^{\tau}\boldsymbol{I}^{*})^{*} = \boldsymbol{I}^{\tau}\boldsymbol{U}^{*} = \boldsymbol{U}^{\tau}\hat{Y}\boldsymbol{U}^{*}$$

is the complex conjugate power.

In terms of the ort of the 3-complex of voltage (42) the active and reactive power have equivalent form of representation:

$$P = \mathrm{Re}[\dot{S}] = \boldsymbol{U}^{\tau}\hat{G}\boldsymbol{U}^{*} = U^2\sum\nolimits_m G_m\upsilon_m^2; \quad (45)$$

$$Q = \mathrm{Jm}[\dot{S}] = \boldsymbol{U}^{\tau}\hat{B}\boldsymbol{U}^{*} = U^2\sum\nolimits_m B_m\upsilon_m^2. \quad (46)$$

Equivalent complex conductivity (44) of 3-D curve of balance current

$$\boldsymbol{i}_s(t) = \sqrt{2}\Re e[\dot{\mathsf{y}}_{\mathsf{s}}\boldsymbol{U}e^{j\omega t}],\ \boldsymbol{I}_s = \dot{\mathsf{y}}_{\mathsf{s}}\boldsymbol{U} \quad (47)$$

in all phases is the same and equal to weighted average sum of equivalent complex phase conductivities (20). Weighting factors are determined by the ort of the 3-complex of voltage (42).

If voltage is symmetric with direct sequence (DS) then

$$\boldsymbol{\upsilon} = (1/\sqrt{3})[1\ \ \alpha^{*}\ \ \alpha]^{\tau},\ \upsilon_a^2 = \upsilon_b^2 = \upsilon_c^2 = 1/3, \quad (48)$$

where $\alpha = e^{j120^0} = -1/2 + j\sqrt{3}/2$.

If the load is unbalanced

$$\dot{\mathsf{y}}_{\mathsf{s}} \ne \dot{Y}_a,\ \dot{\mathsf{y}}_{\mathsf{s}} \ne \dot{Y}_b,\ \dot{\mathsf{y}}_{\mathsf{s}} \ne \dot{Y}_b, \quad (49)$$

then the mode is unbalanced at any voltage

The complex conductivity of the balance current (47)

$$\dot{\mathsf{y}}_{\mathsf{s}} = \mathsf{g}_{\mathsf{s}} - j\mathsf{b}_{\mathsf{s}}, \quad (50)$$

determines conductivities associated with symmetry of active and reactive load elements

$$\mathsf{g}_{\mathsf{s}} = G_a\upsilon_a^2 + G_b\upsilon_b^2 + G_c\upsilon_c^2; \quad (51)$$

$$\mathsf{b}_{\mathsf{s}} = B_a\upsilon_a^2 + B_b\upsilon_b^2 + B_c\upsilon_c^2. \quad (52)$$

These conductivities equal to weighted average sums of phase conductivities. If the load is unbalanced then

$$\mathsf{g}_s \neq G_a,\ \mathsf{g}_s \neq G_b,\ \mathsf{g}_s \neq G_c; \quad (53)$$

$$\mathsf{b}_s \neq B_a,\ \mathsf{b}_s \neq B_b,\ \mathsf{b}_s \neq B_c. \quad (54)$$

Conductivities (51, 52) characterize the symmetry of active and reactive load elements by phases for the 3-phase voltage.

3-complex (43) of the balanced component has two components: active and reactive

$$\boldsymbol{I}_{sA} = \mathsf{g}_s \boldsymbol{U},\ \boldsymbol{I}_{sR} = -j\mathsf{b}_s \boldsymbol{U} = \mathsf{b}_s \boldsymbol{U}_\perp \quad (56)$$

and guarantees resolution of the balanced current

$$\boldsymbol{i}_s(t) = \boldsymbol{i}_{sA}(t) + \boldsymbol{i}_{sR}(t) \quad (57)$$

into components associated with active and reactive load elements:

$$\boldsymbol{i}_{sA}(t) = \sqrt{2}\Re e[\boldsymbol{I}_{sA} e^{j\omega t}] = \sqrt{2}\Re e[\mathsf{g}_s \boldsymbol{U} e^{j\omega t}], \quad (58)$$

$$\boldsymbol{i}_{sR}(t) = \sqrt{2}\Re e[\boldsymbol{I}_{sR} e^{j\omega t}] = \sqrt{2}\Re e[\mathsf{b}_s \boldsymbol{U}_\perp e^{j\omega t}]. \quad (59)$$

3-D curves (58) и (59) are orthogonal because

$$< \boldsymbol{i}_{sA}, \boldsymbol{i}_{sR} > = \mathrm{Re}[j \sum\nolimits_m U_m^2 \mathsf{g}_s \mathsf{b}_s] = 0. \quad (60)$$

Because of orthogonality of the resolution (57) for current component the Pythagoras equality is correct

$$\boldsymbol{i}_{sA}(t) \perp \boldsymbol{i}_{sR}(t) \quad \Rightarrow \quad I_{sA}^2 + I_{sR}^2 = I_s^2; \quad (61)$$

$$I_{sA}^2 = \mathsf{g}_s^2 U^2,\ I_{sR}^2 = \mathsf{b}_s^2 U^2.$$

From (58) it follows

$$< \boldsymbol{u}, \boldsymbol{i}_{sA} > = \mathrm{Re}[\boldsymbol{U}^\tau \boldsymbol{I}_{sA}^*] = \mathrm{Re}[\boldsymbol{U}^\tau \mathsf{g}_s \boldsymbol{U}^*] = P. \quad (62)$$

Because of balanced active current is *really* parallel with voltage ($\boldsymbol{I}_{sA} \| \boldsymbol{U} \ \Rightarrow \ \boldsymbol{I}_{sA} = \mathsf{g}_s \boldsymbol{U}$) it guarantees EE supply of active power (62) with minimal losses [7]

$$\| \boldsymbol{i}_{sA} \| \leq \| \boldsymbol{i}_A \| \leqslant \| \boldsymbol{i} \|. \quad (63)$$

Here $P = < \boldsymbol{u}, \boldsymbol{i}_{sA} > = \| \boldsymbol{u} \| \cdot \| \boldsymbol{i}_{sA} \|$.

Balanced reactive current guarantees EE supply of power of shift

$$< \boldsymbol{u}_\perp, \boldsymbol{i}_{sR} > = \mathrm{Re}[-j\boldsymbol{U}^\tau \boldsymbol{I}_{sR}^*] = < \boldsymbol{u}_\perp, \boldsymbol{i} > = Q. \quad (64)$$

Because of balanced reactive current is *really* parallel with voltage $\boldsymbol{I}_{sR} \| \boldsymbol{U}_\perp \ \Rightarrow$ it guarantees EE supply of reactive power of shift with minimal losses $\| \boldsymbol{i}_{sR} \| \leq \| \boldsymbol{i}_R \| \leqslant \| \boldsymbol{i} \|$. Here

$$| Q | = | < \boldsymbol{u}_\perp, \boldsymbol{i}_{sR} > | = \| \boldsymbol{u} \| \cdot \| \boldsymbol{i}_{sR} \|. \quad (65)$$

Unbalanced current and asymmetry of load conductivities. At the unbalanced mode the unbalanced component of the 3-complex of current (unbalance current) is determined as an orthogonal complement to the balanced component (40)

$$\boldsymbol{I}_D = \boldsymbol{I} - \boldsymbol{I}_S,\ (\boldsymbol{I}_D \perp \boldsymbol{I}_S). \quad (66)$$

Unbalanced component (66) can be represented by using vector product in the space of 3-complexes $C^{(3)}$ [7, 8].

From (21) and (47) it follows

$$\boldsymbol{I}_D = \boldsymbol{I} - \boldsymbol{I}_S = \hat{Y}\boldsymbol{U} - \dot{\mathsf{y}}_s \boldsymbol{U} = \underbrace{(\hat{Y} - \dot{\mathsf{y}}_s)}_{\hat{\mathsf{y}}_D} \boldsymbol{U} = \hat{\mathsf{y}}_D \boldsymbol{U}. \quad (67)$$

The matrix form of the 3-complex of unbalance current

$$\boldsymbol{I}_D = \hat{\mathsf{y}}_D \boldsymbol{U} = \begin{bmatrix} \dot{\mathsf{y}}_{Da} & 0 & 0 \\ 0 & \dot{\mathsf{y}}_{Db} & 0 \\ 0 & 0 & \dot{\mathsf{y}}_{Dc} \end{bmatrix} \begin{bmatrix} \dot{U}_a \\ \dot{U}_b \\ \dot{U}_c \end{bmatrix}. \quad (68)$$

Uses a complex diagonal matrix

$$\hat{\mathsf{y}}_D = diag\{\dot{\mathsf{y}}_{Da}, \dot{\mathsf{y}}_{Db}, \dot{\mathsf{y}}_{Dc}\} \quad (69)$$

of equivalent conductivities of the unbalance current

$$\dot{\mathsf{y}}_{Dm} = \dot{Y}_m - \dot{\mathsf{y}}_s,\ m \in \{a,b,c\}. \quad (70)$$

If the voltage is symmetric to DS then (48) and

$$\dot{\mathsf{y}}_{Dm} = (2\dot{Y}_m - \sum\nolimits_{k \neq m} \dot{Y}_k) \big/ 3,\ m \in \{a,b,c\}. \quad (71)$$

Complex conductivities (70) characterize dissipation by phases of load conductivities regarding balance conductivity. Unbalance (asymmetry) determines the unbalanced current

$$\boldsymbol{i}_u(t) = \sqrt{2}\Re e[\boldsymbol{I}_D e^{j\omega t}], \quad (72)$$

which is orthogonal to voltage

$$< \boldsymbol{u}, \boldsymbol{i}_u > = \mathrm{Re}[\boldsymbol{U}(\ \hat{\mathsf{y}}_D \boldsymbol{U})^*] = \mathrm{Re}[U^2 \sum\nolimits_m \upsilon_m^2 (\dot{Y}_m - \dot{\mathsf{y}}_s)] =$$

$$= \mathrm{Re}[U^2 (\underbrace{\sum\nolimits_m \upsilon_m^2 \dot{Y}_m}_{\dot{\mathsf{y}}_s}) - \dot{\mathsf{y}}_s)] = 0. \quad (73)$$

Here from (67) the resolution follows

$$\boldsymbol{I} = \boldsymbol{I}_S + \boldsymbol{I}_D,\ \boldsymbol{i}(t) = \boldsymbol{i}_s(t) + \boldsymbol{i}_u(t). \quad (74)$$

Dissipation (unbalance) by phases of separately active and reactive load elements

$$\mathsf{g}_{Dm} = G_m - \mathsf{g}_s,\ \mathsf{b}_{Dm} = B_m - \mathsf{b}_s,\ m \in \{a,b,c\} \quad (75)$$

is represented by diagonal matrices of conductivities of active and reactive load elements:

$$\hat{\mathsf{g}}_D = diag\{\mathsf{g}_{Da}, \mathsf{g}_{Db}, \mathsf{g}_{Dc}\},$$

$$\hat{\mathsf{b}}_D = diag\{\mathsf{b}_{Da}, \mathsf{b}_{Db}, \mathsf{b}_{Dc}\}.$$

Unbalance by phases (asymmetry of phase conductivities) separately of active and reactive load elements determines resolution of 3-complex of unbalance current into two components

$$\boldsymbol{I}_D = \boldsymbol{I}_{DA} + \boldsymbol{I}_{DR}, \quad (76)$$

$$\boldsymbol{I}_{DA} = \hat{\mathsf{g}}_D \boldsymbol{U} = [\mathsf{g}_{Da} \dot{U}_a \quad \mathsf{g}_{Db} \dot{U}_b \quad \mathsf{g}_{Dc} \dot{U}_c]^\tau, \quad (77)$$

$$\boldsymbol{I}_{DR} = -j\hat{\mathsf{b}}_D \boldsymbol{U} = -j[\mathsf{b}_{Da} U_a \quad \mathsf{b}_{Db} U_b \quad \mathsf{b}_{Dc} U_c]^\tau. \quad (78)$$

The resolution of the unbalanced current is correct

$$\boldsymbol{i}_u(t) = \boldsymbol{i}_{uA}(t) + \boldsymbol{i}_{uR}(t), \quad (79)$$

where $\boldsymbol{i}_{uA}(t) = \sqrt{2}\Re e[\boldsymbol{I}_{DA} e^{j\omega t}] = \sqrt{2}\Re e[\hat{\mathsf{g}}_D \boldsymbol{U} e^{j\omega t}]$, (80)

$$\boldsymbol{i}_{uR}(t) = \sqrt{2}\Re e[\boldsymbol{I}_{DR} e^{j\omega t}] = \sqrt{2}\Re e[\hat{\mathsf{b}}_D \boldsymbol{U}_\perp e^{j\omega t}] \quad (81)$$

are the components determined by asymmetry of active and reactive load elements.

3-D curves (80) and (81) are orthogonal because

$$< \boldsymbol{i}_{uA}, \boldsymbol{i}_{uR} > = \mathrm{Re}[\boldsymbol{I}_{DA}^\tau \boldsymbol{I}_{DR}^*] = \mathrm{Re}[j \sum\nolimits_m U_m^2 \mathsf{g}_{Dm} \mathsf{b}_{Dm}] = 0.$$

Because of orthogonality of the resolution (79) the Pythagoras equality is correct

$$\boldsymbol{i}_{uA}(t) \perp \boldsymbol{i}_{uR}(t) \quad \Rightarrow \quad I_{DA}^2 + I_{DR}^2 = I_D^2, \quad (82)$$

$$I_{DA}^2 = U^2 (\upsilon_a^2 \mathsf{g}_{Da}^2 + \upsilon_b^2 \mathsf{g}_{Db}^2 + \upsilon_c^2 \mathsf{g}_{Dc}^2), \quad (83)$$

$$I_{DR}^2 = U^2 (\upsilon_a^2 \mathsf{b}_{Da}^2 + \upsilon_b^2 \mathsf{b}_{Db}^2 + \upsilon_c^2 \mathsf{b}_{Dc}^2). \quad (84)$$

So, for the resolution of current two dichotomous factors are used:

- the first factor is determined by activity and reactivity of load elements;
- the second factor is determined by symmetry and asymmetry of load elements by phases.

Resolution of 3-phase current and power equation of unbalanced mode. Combination of values of two factors classifying the load:

- «activity/reactivity» – the first factor)

$$\boldsymbol{i} = \boldsymbol{i}_A + \boldsymbol{i}_R ;$$

- («symmetry/asymmetry» – the second factor)

$$\boldsymbol{i} = \boldsymbol{i}_s + \boldsymbol{i}_u ,$$

permitted to obtain four mutually orthogonal components of 3-phase current

$$\boldsymbol{i}_{sA}, \quad \boldsymbol{i}_{uA}, \quad \boldsymbol{i}_{sR}, \quad \boldsymbol{i}_{uR},$$

which guarantee resolution into four mutually orthogonal 3-phase current components

$$\boldsymbol{i} = \boldsymbol{i}_A + \boldsymbol{i}_R = \underbrace{(\boldsymbol{i}_{sA} + \boldsymbol{i}_{uA})}_{\boldsymbol{i}_A} + \underbrace{(\boldsymbol{i}_{sR} + \boldsymbol{i}_{uR})}_{\boldsymbol{i}_R}. \qquad (85)$$

Because of current resolution (85) is orthogonal then identity (equation of losses per one Ω) is correct

$$\| \boldsymbol{i} \|^2 = \| \boldsymbol{i}_{sA} \|^2 + \| \boldsymbol{i}_{uA} \|^2 + \| \boldsymbol{i}_{sR} \|^2 + \| \boldsymbol{i}_{uR} \|^2 . \qquad (86)$$

Multiplication of equation (86) by square of rms of voltage $\| \boldsymbol{u} \|^2$ gives the equation for powers of sinusoidal unbalanced mode

$$S_T^2 = P^2 + Q^2 + D_G^2 + D_B^2 . \qquad (87)$$

Here:

$$S_T = \| \boldsymbol{i} \| \cdot \| \boldsymbol{u} \| \qquad (88)$$

is the total power;

$$P = \| \boldsymbol{i}_{sA} \| \cdot \| \boldsymbol{u} \| = < \boldsymbol{i}, \boldsymbol{u} > \qquad (89)$$

is the active balance power determined by symmetry of active load elements;

$$| Q | = \| \boldsymbol{i}_{sR} \| \cdot \| \boldsymbol{u}_{\perp} \| = | < \boldsymbol{i}, \boldsymbol{u}_{\perp} > | \qquad (90)$$

is the reactive balance power determined by symmetry of active load elements;

$$D_G = \| \boldsymbol{i}_{uA} \| \cdot \| \boldsymbol{u} \| \qquad (91)$$

is the unbalance power determined by asymmetry of active load elements;

$$D_G = \| \boldsymbol{i}_{uR} \| \cdot \| \boldsymbol{u} \| \qquad (92)$$

is the unbalance power determined by asymmetry of reactive load elements;

Power equation (87) generalizes the equation for the sinusoidal unbalanced mode [7]

$$I^2 \cdot U^2 = P^2 + Q^2 + D_u^2 , \qquad (93)$$

because of $D_u^2 = D_G^2 + D_B^2$.

Practical value of the received orthogonal decomposition of current and power equations is the ability to use them not only for separated measurement and recording of inactive components of TP but also to solve the compensation problem at sinusoidal unbalanced mode.

Conclusions. For a 3-phase 4-wire network with a sinusoidal unbalanced mode at asymmetric voltage a 4-component orthogonal decomposition of the 3-phase current is obtained. Components having a clear power sense independently classify the load condition. The resulting decomposition expands the CPC theory to 4-wire circuits with unbalanced voltage imbalance by resolution of the unbalance current into two components determined by the asymmetry of the active and reactive load elements.

REFERENCES

1. *1459-2010 IEEE Standard definitions for the measurement of electric power quantities under sinusoidal, nonsinusoidal, balanced, or unbalanced conditions*. **doi: 10.1109/ieeestd.2010.5439063**.

2. Czarnecki L.S. Orthogonal decomposition of the currents in a 3-phase nonlinear asymmetrical circuit with a nonsinusoidal voltage source. *IEEE Transactions on Instrumentation and Measurement*, 1988, vol.37, no.1, pp. 30-34. **doi: 10.1109/19.2658**.

3. Ferrero A., Superti-Furga G. A new approach to the definition of power components in three-phase systems under nonsinusoidal conditions. *IEEE Transactions on Instrumentation and Measurement*, 1991, vol.40, no.3, pp. 568-577. **doi: 10.1109/19.87021**.

4. Lev-Ari H., Stankovic A.M. A decomposition of apparent power in polyphase unbalanced networks in nonsinusoidal operation. *IEEE Transactions on Power Systems*, 2006, vol.21, no.1, pp. 438-440. **doi: 10.1109/tpwrs.2005.860903**.

5. Czarnecki L.S., Haley P.M. Unbalanced power in four-wire systems and its reactive compensation. *IEEE Transactions on Power Delivery*, 2015, vol.30, no.1, pp. 53-63. **doi: 10.1109/tpwrd.2014.2314599**.

6. Czarnecki L.S., Bhattarai P.D. Currents' physical components (CPC) in three-phase systems with asymmetrical voltage. *Przegląd Elektrotechniczny*, 2015, no.6, pp. 40-47. **doi: 10.15199/48.2015.06.06**.

7. Sirotin Iu.A. Vectorial instantaneous power and energy modes in three-phase circuits. *Tekhnichna elektrodynamika – Technical electrodynamics*, 2013, no.6, pp. 57-65. (Rus).

8. Sirotin Iu.A. Non-pulsed mode of supply in a three-phase system at asymmetrical voltage. *Przeglad Elektrotechniczny*, 2013, no.7, pp. 54-58.

Received 29.02.2016

Iu.A. Sirotin, Doctor of Technical Science, Professor,
National Technical University «Kharkiv Polytechnic Institute»,
21, Frunze Str., Kharkiv, 61002, Ukraine,
e-mail: yuri_sirotin@ukr.net

How to cite this article:
Sirotin Iu.A. Orthogonal components of the three-phase current at asymmetrical active-reactive load in 4-wire circuit. *Electrical engineering & electromechanics*, 2016, no.3, pp. 62-66. doi: 10.20998/2074-272X.2016.3.10.

UDC 621.311.171 **doi: 10.20998/2074-272X.2016.3.11**

Ye.I. Sokol, O.G. Gryb, S.V. Shvets

NETWORK CENTRISM OPTIMIZATION OF EXPEDITIOUS SERVICE OF ELEMENTS OF THE POWER SUPPLY SYSTEM

Purpose. Development of precision selection criteria of options of technical realization of effective active and adaptive system of expeditious service of elements of a power supply system in the conditions of network-centric management. Methodology. In development of power supply systems their evolution from the elementary forms using elementary network technologies and models of interactions in power to more irregular shapes within the concept of Smart Grid with elements of network-centric character is observed. This direction is based on Internet-technologies of the last generation, and realize models of power activity which couldn't be realized before. Results. The number of possible options of active and adaptive system of expeditious service of elements of a power supply system is usually rather big and it is difficult to choose the acceptable option by direct search. Elimination of admissible options of the technical realization constructed on the principles of a network centrism means application of the theory of multicriteria optimization from a position of discrete programming. The basis of procedure of elimination is made by algorithm of an assessment of system by criterion of accuracy. Originality. The case of an assessment of the precision characteristic of system at restrictions for the set accuracy is connected with need of decomposition of requirements of all system in general and on separate subsystems. For such decomposition the ratios connecting the accuracy of functioning of a separate subsystem with variations of parameters of all system, and also with precision characteristics of subsystems of the lower levels influencing this subsystem are received. Practical value. In the conditions of the network-centric organization of management of expeditious service of elements of a power supply system elimination of options of subsystems when using precision criterion allows to receive the maximum number of essentially possible options of system of service taking into account the accepted service strategy. References 8.

Key words: **network-centric managements, precision criterion, expeditious service, element of technical realization, output variable of a subsystem.**

В статье уделено внимание вопросам использования сетецентрического подхода при формировании активно-адаптивной системы оперативного обслуживания элементов энергосистемы в условиях идеологии Smart Grid. Определен точностной критерий отсева вариантов технической реализации этой системы, реализующей концепцию «обслуживания на основе отклика». Библ. 8.

Ключевые слова: **сетецентрическое управления, точностной критерий, оперативное обслуживание, элемент технической реализации, выходная переменная подсистемы.**

Introduction and problem definition. Today in Ukraine there is a growing interest in the rapidly developing in the last decade throughout the world toward science and technology innovation transform electric power based on the new Smart Grid concept. State structures in most countries consider Smart Grid as an ideology of national power development programs, energy companies – as a base for sustainable innovative modernization of its activity [1-3].

At the same time, a number of problems of improving the power grid management, taking into account the recent experience of energy reforming are developed not enough [4]. The development of an integrated concept of the formation of adaptive control structure and power system information and intellectual bases of increase of efficiency of management techniques in the framework of a customer-oriented approach in the Smart Grid concept is an important and urgent issue of reforms in the energy sector of Ukraine.

Analysis of last investigations and publications. Smart Grid technology helps to create a next-generation power grid, which will allow power companies to effectively manage the production and consumption of electricity. Smart Grid is a system delivering electricity from generating energy enterprises to consumers, with an integrated communication and information technologies and providing improved transparency of the energy system, high-quality customer service and providing environmental benefits [5].

Despite the concept of smart grid can be interpreted in different ways, it is obvious that an intelligent communications network is the basis of smart grid. Enterprises of power industry are investing in communications networks to improve the situational awareness of the resources for the purpose of power system automation, integration of systems and control [6].

Intellectual energy value lies in the fact that electric power companies will be able to «smooth out» the need for electricity in times of peak load, eliminate the use of hot spares and reduce the need for long-term investment in additional generation companies, as well as reduce the need for other investments, such as system reorganization to improve performance [7].

Platform for advanced energy systems constitute intellectual elements that are at the level of the digital technologies that electric power companies were added to the traditional analog and modern infrastructure of the energy system.

In modern power systems most acute problems are of reliability, safety and efficiency of power plants on the basis of the organization of operational management. The aim of this process is the uninterrupted supply of electricity to consumers of adequate quality, including the task of daily schedules of power plants, maintenance of current conditions, the output of the equipment to be repaired and the elimination of the emergency power system conditions [8]. Development of optimization methods will solve the important problem of optimal organization of the system of operational maintenance and management of its energy system as a component of the structure of operational management within the customer-oriented approach Smart Grid concept.

The goal of investigations is the development of precision criteria for the selection of technical options for the effective implementation of the active-adaptive grid system of operational service elements in a network-centric control.

Main materials of investigations. In the development of power systems observed their evolution from the simplest forms, using basic networking technologies and replicate traditional models of information interactions in the energy sector, to more complex forms within the Smart Grid concept with elements of network-centric nature. This direction is based on the latest generation of Internet technologies, and implements models of energy-related activities, which previously could not be realized. Existing scientific developments in this area have not yet formed an integrated security model of functioning of a multi-level set of software and hardware complexes of operational dispatch and automatic power systems with the flexibility to manage intellectual elements (active-adaptive) network with increasing automation of volume and an increase in the quantitative and qualitative collection of characteristics, handling, storage, distribution information.

With regard to energy network centrism is used as a term associated with the operational management of the power grid in a single information and communication management space, we consider the union of dissimilar objects act as a system, and a discrete manner how some segments of unified management of distributed network. In this case, network centrism is the organizing principle of the operational control system power supply system, which allows to realize the mode of situational awareness due to the formation and maintenance of the same for all tiers of an integrated management, contextual information environment and inclusion in the process of continuous updating of the greatest possible number of primary sources of information.

Network-centric approach to the construction of information system in the power industry should be based on the creation of equal geographically distributed nodes that perform different functions, and allows users to work with applications and databases through a browser from any location and from any device connected to global telecommunication networks. Network-centric system should allow to bind to a single system interface and database management, monitoring and development control decisions for the use of various software applications regardless of location of objects and subjects of management.

Ukrainian information system requires a higher level of structural and parametric elements of the organization and the energy system should be developed based on the principles of functioning of large systems. However, this requires the restructuring not only the merging of local power system elements, but also the entire global information network (a set of distributed energy facilities).

The solution of the problem is complicated by the presence of weak and at the same time, extensive information management connections over large areas, which limits the ability to collect and analyze large data flows. That is, in our country, its regions and cities require technical and organizational support for a new level of structural and parametric elements of the organization of energy systems, including taking into account the promising development.

Taking the above into consideration, within the framework of improving the structural and parametric organization of energy systems based on active-adaptive electric networks as the primary network infrastructure, new electric power it is necessary to provide:

- creation of a single adaptive management information network within the intellectual electric power system of Ukraine, in order to achieve the sustainable development of electric power strategic indicators;
- the development, integration and access to industry databases based on the information gathered and the introduction of smart electricity grids;
- development and implementation of information monitoring which allows you to plan and allocate resources to the tasks, and provide control over the achievement of results, taking into account the territorial management priorities;
- determination of conditions, the general principles of the energy market regulation techniques based on «Smart Grid – Opportunities», providing high efficiency of state regulation and market self-regulation – based on intelligent electrical power system of Ukraine with the active-adaptive grid power systems that solve the problem the introduction of the new market organization-economic nature, including new formats of energy consumer actions;
- implementation of feedback mechanisms between the government regulation and energy companies on the basis of a fundamentally new class of intelligent distributed management environments based on Smart Grid and related organizational change of management techniques.

The specific implementation of the principle of network centrism in structural-parametric elements of the

organization of power systems provides the fulfillment of certain conditions. The first condition is, above all, the presence of the stable type of communication from the head of any rank in any place, wherever he may be at the moment. The second condition – it should be possible to access information on the current response of the energy system changes its state under the influence of various factors. The next condition is the possibility of replay for analysis guidelines and to take the necessary decisions for displaying the information received in a variety of applications. In a word, the state of the power system information should be presented in a form suitable for analysis, recognition, transmission, distribution and storage.

Network-centric management system with the development of the technical component of the overall process is constantly being improved and developed. It should be noted that the network-centric management system in its entirety, but there is only elements of the system, but they are constantly being improved.

Specificity of the organization of operational management of energy systems implies an adaptive operational service. Among the activities of operational services should be allocated grid complex of works on maintenance of the required mode of operation of the power elements, the production of switches, inspection equipment, preparation for production of repair, maintenance of equipment.

The implementation of network-centric energy system of governance will build adaptive operational services based on the concept of «service system on the basis of response» (SSR). Implementation of the SSR concept aims to service a particular object (digital substation, power lines, power system status monitoring subsystem elements, etc.) located in a particular area and at a particular time, and which currently require operational services in accordance with the response of the energy system.

Technical implementation of effective active-adaptive grid system of operational maintenance (SOM) built on the principles of network centrism based on the supremacy of communication systems that enable real-time to receive and transmit information packets huge variety of customers, including centralized and distributed transmission. The peculiarity of this system lies in the fact that the information in the system hangs, and it allows you to access it without additional time.

A management system implemented in the SOM should be based on developed and implemented in the practice of software products on the intellectual level, the so-called common design models (tasks) combined in a single system.

These components are the basis for formulation of the problem for the development of network-centric, and SOM is the cornerstone of the network centrism. In a single population in the synthesis of SOM are executive digital elements, means of communication, ways and forms of SOM.

The embodiment of a network-centric concept of the SSR in the proposed ESR is inextricably linked with the use of unmanned aerial vehicle (UAV) – quadrocopters. This is dictated by the rapid development of various power equipment diagnostic methods, such as the power and the switching and control equipment and protection in connection with the high cost of direct and indirect losses as a result of accidents.

The development of modern methods of diagnosis allows a high degree of probability to determine the actual condition of the equipment and to predict its change in the near future. However, modern diagnostic equipment is very expensive, which hinders its complete set of each object. It should be noted that the proper organization of work can significantly reduce of diagnostic costs.

An example of such an organization could be the implementation of a special SOM, being composed of UAVs to carry out thermal imaging inspection of substation equipment, optical inspection supporting-rod and hanging insulation, examination of technical condition of transformers and auto-transformers, and a number of other works.

Presence of UAV determines ways of formation of administrative decisions regarding the structure of the power system to adapt to the results of SOM activities of the SSR concept. Screening valid options involves the use of the theory of multi-criteria optimization with discrete programming position. The number of options is usually quite large and select the appropriate solution by brute force is rather difficult. We define the basic provisions of the procedure for constructing options dropout SOM which implements the management decisions adopted within the framework of the SSR.

The basis of this procedure is evaluating options of SOM algorithm according to the criterion of accuracy. In our case it is the concept of precision is very important in management decisions as well as the use of drones as a source of information about the state of the power system elements introduces some degree of uncertainty.

Accuracy of SOM operation as a whole will be judged by the values of deviations of output variables from the set of software subsystems values of the n-th level calculated in accordance with the equations of state at the time $t_n + 1 = T$:

$$\Delta y_{nh}^{h\alpha}(v_i) = \left| y_{nh}^{h\alpha}(v_i)_T - y_{nh(0)}^{h\alpha}(T) \right|,$$

$$(h \in I_n, \alpha = 1, ..., \alpha_{nh}^h),$$

where $y_{nh}^{h\alpha}(v_i)_T$ is the value of the α-th component of the output variable of the h-th subsystem of the n-th level of SOM at time T for variant $v_i \in V$; $y_{nh(0)}^{h\alpha}(T)$ is the given program value of the output variable of the subsystem of the n-th level of SOM; $\Delta y_{nh}^{h\alpha}(v_i)$ is the value of deviation of the output variable of the subsystem of the n-th level of SOM.

Here, the set of technical implementation options of the designed SOM is determined as:

$$V = \{v_i\} = \prod_{i=1}^{M} V_i \,.$$

The values of the output variables subsystems of the *n*-th level of SOM depend on the types of control laws defined by the SSR strategy; of the accuracy characteristics of elements of the technical implementation of an appropriate control law, defines a set of I_n (for $h \in I_n$)) subsystems of the *n*-th level of SOM; output variables $y_{n-k} = (t_n)$ of subsystems of *n*-*k*-th levels $\forall k \in K_{nh}$. Variables $y_{n-k} = (t_n)$ also depend on the accuracy characteristics of the elements of the technical implementation of the control law of the subsystem of the *n*-*k*-th level of output variables of the previous level of SOM. Overall, therefore, the accuracy of the whole system depends on the operation of all subsystems levels, i.e. on a variety of the set *V*.

Two cases of estimation of the system accuracy characteristic are possible: the first one – when it is necessary to find a variant of the system $v_i \in V$ minimizing the value $\Delta y_{nh}^{h\alpha}(v_i)$, the second one – when this value should not exceed the given one:

$$\Delta y_{nh}^{h\alpha}(v_i) \le \varepsilon_{nh}^{h\alpha}, \quad (h \in I_n, \alpha = 1, ..., \alpha_{nh}^{h}), \qquad (1)$$

where $\varepsilon_{nh}^{h\alpha}$ is a non-negative value that characterizes the degree of closeness of α-th output coordinates of the *h*-th subsystem of the *n*-th level of SOM and its program value.

In more detail, consider the second case, as typically specified in the design constraints on some variables output subsystem components that operate at the last time interval.

We assume that each *q*-th type of element of the SOM technical realization is characterized by nominal value of the parameter p_q^0 and a set $\Delta p_{q(\zeta_q)}$ $(\zeta_q \in 1, ..., \zeta_q^0)$ of possible variants of this parameter determined by different modifications of the set $E_q(\Delta p_q) = \{\Delta p_{q(\zeta_q)} \; \forall \zeta_q \in 1, ..., \zeta_q^0\}$. Then, a table of given errors will correspond to the separate variant of the SOM realization:

$$\left\{ \begin{array}{c} \Delta p_{1(1)}, ..., \Delta p_{1(\zeta_1)}, ..., \Delta p_{1(\zeta_1^0)} \\ ..... \\ \Delta p_{q(1)}, ..., \Delta p_{q(\zeta_q)}, ..., \Delta p_{q(\zeta_q^0)} \\ ..... \\ \Delta p_{m(1)}, ..., \Delta p_{m(\zeta_m)}, ..., \Delta p_{m(\zeta_m^0)} \end{array} \right\}.$$

We determine the vector of parameters of dimension $q_{il(\zeta_l)}$ as

$$p_{il(\zeta_l)} = \{p_q^0 \pm \Delta p_q \; \forall q \in I_{il(\zeta_l)}\},$$

corresponding to elements of the SOM technical realization of the set $I_{il(\zeta_l)}$ for the control low $u_{il(\zeta_l)}$.

We write solution of the system of differential equations for the *l*-th subsystem of the *i*-th level in the form:

$$y_{il}^{j}(t, v_j^{il}) = F_{il(\zeta_l)}^{j}(u_{il(\zeta_l)}(t), p_{il(\zeta_l)}, y_{il(0)}^{j}) \quad (k \in K_{il}, q \in I_{i-k}^{l}), \qquad (2)$$

where v_j^{il} is the part of variant $v_j \in V$ on which the value of the output variable of the *l*-th subsystem of the *i*-th level depends; $y_{il(0)}^{j\alpha} = y_{i-k,q}^{l\lambda}(t_i)$ $(k \in K_{il})$ are the initial conditions for the initial differential equations which are values of output variables of the subsystem of the $i-k$ -th levels $\forall k \in K_{il}$ connected by the *l*-th subsystem of the *i*-th level $(\alpha = 1, ..., \alpha_{il}^{j})$; $F_{il(\zeta_l)}^{j}$ is vector function whose components are continuous functions of their arguments belonging to the class of discrete optimization problems.

Vector function $F_{il(\zeta_l)}^{j}$ components have non-zero first derivatives in a neighborhood of the point $(y_{i-k,q}^{l}(t_i), p_{il(\zeta_l)(0)})$ defined by the nominal values of parameters and initial conditions. It should be of a variety of possible options of the SOM $v_i \in V$ creation which are characterized as forms of control laws in each of the subsystems, as well as errors in the technical implementation of the elements, select those that meet criteria (1).

Direct construction of all variants of the set *V* with the assessment of their accuracy criterion (1) makes it necessary to integrate the system of initial differential equations and obtain solutions of the type (2) for all subsystems. This is due to a large amount of calculation, which does not allow to select the appropriate version of the system in the given timeframe. In this connection there is need to develop prior dropout rules both types of control laws in accordance with the SSR strategy and elements of the technical implementation of the SOM. This is due to the need for the decomposition of requirements on the system as a whole, determined by the relation (1), to the requirements for individual subsystem type:

$$\Delta y_{il}^{j\alpha} = \left| y_{il}^{j\alpha}(v_j^{il})\,|_{t_{i+1}} - y_{il(0)}^{j\alpha}(t+1) \right| \le \varepsilon_{il}^{j\alpha}, \qquad (3)$$

where $\varepsilon_{il}^{j\alpha}$ is the closeness of the α-th component of the output variable of the *l*-th subsystem of the *i*-th level; $y_{il}^{j\alpha}(v_j^{il})\,|_{t_{i+1}}$ is determined from the equations describing behavior of the *l*-th subsystem of the *i*-th level.

For such a decomposition is necessary to obtain relations between the accuracy of the functioning of a separate subsystem with variations SSR parameters as well as lower levels of accuracy characteristics of subsystems that affect this subsystem.

In order to output variables of each *l*-th subsystem of the *i*-th level described by a vector function whose components are continuously differentiable convex or

concave function defined on a set of parameters $p_{il(\zeta_l)}$ and initial conditions $y^j_{il(0)}$ that satisfy the constraints of the form (3), enough to vector deviation parameters and initial conditions of the nominal values

$$p_{il(\zeta_l)(0)} = \{p^q_{il(\zeta_l)(0)}\} \quad (q = 1, \dots, q_{il(\zeta_l)}),$$

$$y^j_{il(0)} = \{y^{j\alpha}_{il(0)}\} \quad (\alpha = 1, \dots, \alpha^j_{il}),$$

meet inequalities

$$\Delta p^q_{il(\zeta_l)} = \left| p^q_{il(\zeta_l)} - p^q_{il(\zeta_l)(0)} \right| \le \varepsilon^q_{il(\zeta_l)}; (q = 1, \dots, q_{il(\zeta_l)}),$$

$$\Delta y^{j\alpha}_{il} = \left| y^{j\alpha}_{il} - y^{j\alpha}_{il(0)} \right| \le \varepsilon^{j\alpha}_{il}; (\alpha = 1, \dots, \alpha^j_{il}),$$

where $\varepsilon^q_{il(\zeta_l)}; (q = 1, \dots, q_{il(\zeta_l)})$ и $\varepsilon^{j\alpha}_{il}; (\alpha = 1, \dots, \alpha^j_{il})$ – belong the region:

$$D_{il(\zeta_l)} = \bigcap_{\alpha=1}^{\alpha^j_{il}} D^{\alpha}_{il(\zeta_l)},$$

in which $D^{\alpha}_{il(\zeta_l)}$ is the convex domain of the space of variables $\Delta p_{il(\zeta_l)}$ and $\Delta y^p_{i-k,q}$ formed by the intersection $2^{\alpha^j_{il}+q_{il(\zeta_l)}}$ of subspaces:

$$\sum_{q\in J_{il(\zeta_l)}} \frac{\Delta p_q}{\delta^{\alpha q}_{il(\zeta_l)}} + \sum_{q\in I^l_{i-k}} \sum_{\lambda=1}^{\alpha^l_{i-k,q}} \frac{\Delta y^{l\lambda}_{i-k,q}}{\delta^{\alpha\lambda}_{il(\zeta_l)}} \le 1,$$

$$\sum_{q\in J_{il(\zeta_l)}} \frac{\Delta p_q}{\gamma^{\alpha q}_{il(\zeta_l)}} + \sum_{q\in I^l_{i-k}} \sum_{\lambda=1}^{\alpha^l_{i-k,q}} \frac{\Delta y^{l\lambda}_{i-k,q}}{\gamma^{\alpha\lambda}_{il(\zeta_l)}} \le 1. \qquad (4)$$

Here

$$\delta^{\alpha r}_{il(\zeta_l)} = \begin{cases} \widetilde{\delta}^{\alpha r}_{il(\zeta_l)}, & if\ y^{\alpha}_{r(+)} \le y^{j\alpha}_{il(0)} + \varepsilon^{j\alpha}_{il}, \\ \widetilde{\gamma}^{\alpha r}_{il(\zeta_l)} = \dfrac{\varepsilon^{j\alpha}_{il}\ \widetilde{\delta}^{\alpha r}_{il(\zeta_l)}}{y^{j\alpha}_{il(0)} - y^{\alpha}_{r(+)}}, \\ if\ y^{\alpha}_{r(+)} > y^{j\alpha}_{il(0)} + \varepsilon^{j\alpha}_{il}, \end{cases} \qquad (5)$$

And value $\gamma^{\alpha r}_{il(\zeta_l)}$ is determined as:

$$\gamma^{\alpha r}_{il(\zeta_l)} = \begin{cases} -\delta^{\alpha r}_{il(\zeta_l)}, & if\ y^{\alpha}_{r(-)} \le y^{j\alpha}_{il(0)} + \varepsilon^{j\alpha}_{il}, \\ \dfrac{\varepsilon^{j\alpha}_{il}\ \widetilde{\delta}^{\alpha r}_{il(\zeta_l)}}{y^{\alpha}_{r(-)} - y^{j\alpha}_{il(0)}}, & if\ y^{\alpha}_{r(-)} > y^{j\alpha}_{il(0)} + \varepsilon^{j\alpha}_{il}, \end{cases} \qquad (6)$$

$$\widetilde{\delta}^{\alpha r}_{il(\zeta_l)} = -\frac{\varepsilon^{j\alpha}_{il}}{h^{\alpha r}_{il}}, \qquad (7)$$

$$y^{\alpha}_{r(+)} = y^{j\alpha}_{il}(p_{1(0)}, \dots, p_{r-1(0)}, p_r + \widetilde{\delta}^{\alpha r}_{il(\zeta_l)}, p_{r+1(0)}, \dots, y^j_{il(0)}\ \forall\ r \in 1, \dots, q_{il(\zeta_l)} + \alpha^j_{il}, \qquad (8)$$

$$y^{\alpha}_{r(-)} = y^{j\alpha}_{il}(p^l_{1(0)}, y^{j1}_{il(0)}, \dots, y^{j,r-1}_{il(0)}, y^{jr}_{il(0)} - \widetilde{\delta}^{\alpha r}_{il(\zeta_l)}, y^{j,r+1}_{il(0)}, \dots)\ \forall\ r \in 1, \dots, q_{il(\zeta_l)} + \alpha^j_{il}, \qquad (9)$$

$$h^{\alpha r}_{il} = \left. \frac{\partial y^{j\alpha}_{il}}{\partial p^r} \right|_0 \ \forall\ r \in 1, \dots, q_{il(\zeta_l)} + \alpha^j_{il}. \qquad (10)$$

Systems of inequalities (4) are constructed by successively replacing the first inequality of δ value on the value of γ firstly in one member, then in two members, etc. By the value $y^{\alpha}_{r(+)}$ we indicated values of the output variable when the values of the parameters or initial conditions are increased by the value $\widetilde{\delta}^{\alpha r}_{il(\zeta_l)}$, and $y^{\alpha}_{r(-)}$ are reduced by the same value. By $h^{\alpha r}_{il}$ we indicated functions of sensitivity of output variables for parameters and initial conditions in nominal points.

The area of permissible variations of initial conditions and parameters we consider in positive orthant (due to the symmetrical shape of restrictions on assignment variations of initial conditions and parameters). It is defined by the inequalities (4) and can be written as:

$$D_{il(\zeta_l)} = \bigcap_{\alpha=1}^{\alpha^j_{il}} D^{\alpha}_{il(\zeta_l)},$$

where

$$D^{\alpha}_{il(\zeta_l)} : \sum_{q\in J_{il(\zeta_l)}} \frac{\Delta p^q_{il(\zeta_l)}}{a^{\alpha q}_{il(\zeta_l)}} + \sum_{\lambda=1}^{\alpha^j_{il}} \frac{\Delta y^{j\lambda}_{il}}{a^{\alpha\lambda}_{il(\zeta_l)}} \le 1,$$

$$a^{\alpha r}_{il(\zeta_l)} = \min\{|\ \delta^{\alpha r}_{il(\zeta_l)}\ |, |\ \gamma^{\alpha r}_{il(\zeta_l)}\ |\}; (r = 1, \dots, q_{il(\zeta_l)} + \alpha^j_{il}),$$

and values $\delta^{\alpha r}_{il(\zeta_l)}$ and $\gamma^{\alpha r}_{il(\zeta_l)}$ are determined by relations (5), (6).

On the basis of presented relationships we form the dropout condition of SOM options for the acting SSR.

If the control law $u_{i-k,q(\zeta_l)}$ of the q-th subsystem of the i-k-th level at nominal values of the parameters leads to the variations of the output variables $\Delta y^l_{i-k(\zeta_l)}$ which do not belong to the domain:

$$D^{(0)}_{il} = \bigcup_{\zeta_l=1}^{\xi_{il}} D_{il(\zeta_l)},$$

at minimal variations of parameters of control lows $u_{il(\zeta_l)} \in U_{il}$, i.e.:

$$\Delta y^l_{i-k(\zeta_l)} \notin D^{(0)}_{il} = \bigcup_{\zeta_l=1}^{\xi_{il}} D_{il(\zeta_l)}\ |_{\Delta p_{il(\zeta_l)\min}}, \qquad (11)$$

it will not form a system of options with control laws from the set U_{il} satisfying the inequality (3).

Conclusions. Thus, at conditions of network-centric organizations of management of operational services of the power system screening options of subsystems of the i-k-th level when checking the condition (11) allows you to obtain the maximum number of principally possible SOM creation variants taking into account adopted SSR by narrowing the set of technical implementation of the l-th subsystem of the i-th level.

REFERENCES

1. Kobets B.B., Volkov I.O. Smart Grid – Conceptual provisions. *Energorynok – Energy Market*, 2010. no.3(75), pp. 67-72. (Rus).

2. Shidlovskii A.K., Vypanasenko S.I., Vorohov L.P. *Tendentsiyi rozvytku enerhetyky Ukrayiny* [Trends in Energy Ukraine]. Donetsk, National Mining University Publ., 2005. 104 p. (Ukr).

3. Kirilenko O.V., Denysyuk S.P., Rybina O.B., Batalov A.G. Features Integration of IPS Ukraine into the European system UCTE. *Tekhnichna elektrodynamika. Tem. vypusk «Silova elektronika i energoefektivnist» – Technical electrodynamics. Thematic issue «Power electronics & energy efficiency»*, 2006, vol.1, pp. 63-68. (Ukr).

4. Bojtsov Y.A., Vasiljev A.P. The solution of a problem of rational architecture of system of operative service of electrical networks. *Izvestiia vysshikh uchebnykh zavedenii. Problemy energetiki – Proceedings of the higher educational institutions. Energy sector problems*, 2008, no.1-2, pp. 56-63. (Rus).

5. Burmistrov V.N., Drogunov S.V. Perspective innovative directions of development of power. *Elektrika – Electrics*, 2011, no.5, pp. 9-12. (Rus).

6. Massel L.V., Ivanov R.A. Possibility of application of situational awareness in energy research. *Proceedings of the Workshop on Computer Science and Informational Technologies (CSIT-2010)*, Russia, Moscow – St.Petersburg, 13-19 September, 2010. Vol.1, Ufa State Aviation Technical University, 2010. pp. 185-187.

7. News and priorities of energy: Digest. *Novyny enerhetyky – News energy*, 2005, no.9, p. 50. (Ukr).

8. Titov N.N. *Povyshenie nadezhnosti i kachestva funktsionirovaniia avtomatizirovannykh sistem dispetcherskogo upravleniia elektroenergeticheskimi sistemami* [Increase of reliability and quality of functioning of the automated systems of dispatching management of electrical power systems]. Kharkiv, Fact Publ., 2013. 200 p. (Rus).

Received 29.03.2016

Ye.I. Sokol[1]*, Doctor of Technical Science, Professor, Corresponding Member of the National Academy of Science of Ukraine,*
O.G. Gryb[1]*, Doctor of Technical Science, Professor,*
S.V. Shvets[2]*, Candidate of Technical Science, Associate Professor,*
[1] National Technical University «Kharkiv Polytechnic Institute», 21, Frunze Str., Kharkiv, 61002, Ukraine.
[2] O.M. Beketov National University of Urban Economy in Kharkiv,
17, Marshal Bazhanov Str., Kharkiv, 61002, Ukraine,
phone +380 67 7680838, e-mail: se_sx@bk.ru

How to cite this article:
Sokol Ye.I., Gryb O.G., Shvets S.V. Network centrism optimization of expeditious service of elements of the power supply system. *Electrical engineering & electromechanics*, 2016, no.3, pp. 67-72. doi: 10.20998/2074-272X.2016.3.11.

Матеріали приймаються за адресою:
Кафедра "Електричні апарати", НТУ "ХПІ", вул. Фрунзе, 21, м. Харків, 61002, Україна
Електронні варіанти матеріалів по e-mail: a.m.grechko@mail.ru

Довідки за телефонами: +38 050 653 49 82 Клименко Борис Володимирович
+38 067 359 46 96 Гречко Олександр Михайлович

Передплатний індекс: 01216